Model Based Pavement-Vehicle Interaction Simulation for Life Cycle Assessment of Pavements

April 2012

Mehdi Akbarian
Franz-Josef Ulm

Concrete Sustainability Hub
Massachusetts Institute of Technology
77 Massachusetts Avenue
MIT Room 1-372
Cambridge MA 02139

Massachusetts Institute of Technology

CSH concrete sustainability hub

EXECUTIVE SUMMARY

Problem

Responsible for about a third of the annual energy consumption and greenhouse gas (GHG) emissions, the U.S. transportation Network needs to attain a higher level of sustainability. This is particularly true for the roadway Network and the design of pavements in it. Improving sustainability of this network necessitates a fundamental understanding of pavements and their interaction with the users, vehicles. Vehicle fuel consumption required to overcome resisting forces due to pavement-vehicle interaction (PVI) is an essential part of life-cycle assessment (LCA) of pavement systems. These PVIs are intimately related to pavement structure and material properties.

While various experimental investigations have revealed potential fuel consumption differences between flexible and rigid pavements, there is high uncertainty and high variability in the evaluated impact of pavement deflection on vehicle fuel consumption. This is mainly due to the level of accuracy required for onsite measurements of fuel consumption, and the lack of a fundamental understanding of the relationship between PVI and pavement structural and material properties.

Approach

This research adopts the perspective that a mechanistic model which links pavement structural and material properties to fuel consumption can contribute to closing the knowledge gap of PVI in pavement LCA. With this goal in mind a first-order mechanistic pavement model is considered; a Bernoulli-Euler beam on viscoelastic foundation subjected to a moving load. Based on the model, scaling relationships are developed between the input parameters of top layer and subgrade moduli, pavement thickness, and loading conditions, with their impact on PVI and vehicle fuel consumption. The strength of these scaling relationships and their ability to guide pavement design are presented through examples.

An original calibration-validation method is established through wave propagation, using Falling Weight Deflectometer (FWD) time history data from FHWA's Long Term Pavement Performance program (LTPP). Statistical analyses of model parameters are performed on pavement material properties (top layer and subgrade moduli), structural properties (thickness), and loading conditions; obtained from model calibration and the LTPP datasets for 5643 FWD points, representing the U.S. roadway Network. These distributions are used as inputs to Monte Carlo simulations to determine the impact of flexible and rigid pavement deflection on passenger car and truck fuel consumption within the roadway Network.

Main Findings

From the Monte-Carlo simulations it is shown that rigid pavements within the Network behave better than flexible ones in regard to PVI due to higher stiffness. A comparison of the deflection induced PVI on flexible and rigid pavements with independent field data provides a reality check of the order of magnitude estimates of fuel consumption, as determined by the model. Moreover,

distributions of model based change in fuel consumption are used in a comparative partial LCA of flexible and rigid pavements. It is shown that the impact of deflection induced PVI (at 95% confidence intervals) becomes increasingly important for high volume flexible roadways and can surpass GHG emissions due to construction and maintenance of the roadway system in its lifetime.

Impact

The presented mechanistic model and the developed scaling relationships provide a link between pavement design criteria and their impact on PVI. Through the model, the level of importance of each parameter and their potential influence on fuel consumption and ultimately within a LCA is determined. As such a model matures to include more aspects of PVI, it can be implemented into design procedures and tools such as the mechanistic-empirical pavement design guide (MEPDG) to enhance pavement design for reduction of PVI related emissions within the Network.

KEYWORDS

Pavement-Vehicle Interaction (PVI); fuel consumption; pavement deflection; life cycle assessment (LCA); pavements; greenhouse gases (GHGs); global warming potential (GWP)

ACKNOWLEDGMENTS

This research was carried out by the CSHub@MIT with sponsorship provided by the Portland Cement Association (PCA) and the Ready Mixed Concrete (RMC) Research & Education Foundation. The authors are grateful to industry reviewers as well as third-party technical reviewers namely Prof. Lev Khazanovich, Prof. Karim Chatti, and Jean-Michel Piau, whose comments and suggestions significantly improved this report.

Contents

List of Figures

List of Tables

Part I

General Presentation

Chapter 1

Introduction

1.1 Industrial Context

The construction, operation, and maintenance of the United States roadway system are responsible for substantial energy and resource consumption. The two primary types of pavements are concrete and asphalt pavements, which together make up approximately 13.7 million lane kilometers (8.5 million lane miles) of paved public roads in the United States [17]. In addition to the need for continually maintaining public roads, this network has been growing each decade, requiring substantial investment for maintenance and new construction. This vast network has major environmental and economic impacts for the Nation and the planet.

The cumulative environmental impact of the road network is unknown, though significant greenhouse gases (GHG) are released during the construction and operation of pavements. Annually, 320 million metric tons of raw materials go into the construction, rehabilitation, and maintenance of this system [23]. The current system of paved roads in the United States handles a volume of traffic on the order of five trillion vehicle-kilometers per year, or about 13 billion vehicle-kilometers per day [48]. Due to high energy demand, road transport contributed the most GHGs of any transport mode in 2007, accounting for 83% of emissions from the transportation sector and 27% of all GHG emissions in the United States [15].

Due to the high environmental and economic impact of pavements, there is growing interest in the ability to rigorously quantify the performance of pavements. The design and operation of pavements in future decades will likely follow a similar path toward greater concern for sus-

tainability, and several "green" rating systems are currently under development for pavements (e.g., [20], [18]).

Improving the sustainability of pavements requires a better understanding of how this infrastructure impacts the natural environment. Products and services have impacts throughout their life, beginning with materials extraction and production to construction, operation and maintenance, and finally ending with a waste management strategy. Conventional environmental assessments often overlook use phase related emissions due to the lack of a scientific understanding and the high uncertainties involved, leading to conclusions based on incomplete results. Hence, modeling of pavement use phase elements requires further research to capture their impacts on the environment.

1.2 Research Objective and Approach

An important element within the use phase of pavements is coherently related to users of these systems, vehicles, and their emissions throughout the life time of the pavement. Pavement-vehicle interaction (PVI) describes the effect of pavement structural and surface properties on vehicle fuel consumption. While the mechanics of PVI are not well understood, previous research has shown that this is a potentially important part of the pavement life cycle, especially for high-traffic roadways [38]. Various empirical studies have looked at the impact of pavement deflection on fuel consumption; however, their main focus has been on a binary material view of asphalt versus concrete pavement, with no consideration of the relationship between pavement deflection and its structure and material behavior [2], [10], [22], [30], [45], [46], [51], [53].

Even though the effect of PVI on vehicle fuel consumption is small, its impact within a full pavement life cycle can be significant due to the large number of vehicles that travel over pavements. The change in vehicle fuel consumption between pavement structures due to PVI becomes increasingly important for high volume traffic roadways and can surpass energy consumption and emissions due to construction and maintenance of the roadway system in its lifetime. In general, roughness and deflection of a pavement are considered as the main contributors to pavement vehicle interaction [38]. This research focuses on latter phenomenon: the impact of deflection on PVI's relation to fuel consumption and ultimately to GHG emissions.

This research uses a mechanistic approach to draw a relationship between pavement structural and material properties with its deflection, and creates a link between pavement properties and the impact of PVI on fuel consumption. To achieve this goal, this study makes use of a simplified model to predict pavement deflection, and performs a model calibration and validation for pavement deflection values, estimates fuel consumption caused by the deflection basin, and compares the results to that of existing field data.

1.3 Report Outline

This report is divided into three parts. Part I reviews existing work that has been performed with regard to the impact of pavement deflection on fuel consumption of vehicles, and describes their strengths and shortcomings. Part II considers the relationship between deflection with structural and material properties from the perspective of Dimensional Analysis, describes the methodology used to predict pavement deflection due to an external load, and performs a calibration-validation of the model against Falling Weight Deflectometer (FWD) experimental data collected through the Long Term Pavement Performance program (LTPP) of the Federal Highway Administration (FHWA). In part III of this report, a scaling relationship is developed between pavement deflection and change in Instantaneous Fuel Consumption (IFC) of vehicles. The IFC is calculated through empirical relationships for a range of LTPP pavement sections, and the impact of the calculated change in fuel consumption is evaluated within a full Life Cycle Assessment (LCA) of pavements.

1.4 Research Significance

To fill in the existing knowledge gaps within the use phase of a pavement's life cycle assessment, this work proposes a new modeling approach to PVI which moves away from empirical relationships and defines a baseline for changes in fuel consumption of pavement structures in function of the relevant material and geometrical design parameters. The model is calibrated and validated, and predicts changes in fuel consumption comparable to previously performed empirical studies. Moreover, this study presents the impact of PVI within a pavement life cycle assessement and provides a framework for a model-based LCA to guide pavement structural

design to reduce environmental emissions.

Chapter 2

Literature Review

With increasing fuel prices and environmental concerns over the past few decades, agencies along with researchers have been studying the impact of internal and external factors on vehicle fuel consumption. In 1982, Zaniewski et al. [53] published a study on vehicle operating costs, fuel consumption, and pavement type and condition factors as one of the first studies on the impacts of pavements on vehicle fuel consumption. Ever since, more studies have refined their findings, but mainly through empirical approaches. This chapter reviews some of the major empirical studies performed and discusses the predictive shortcomings of empirical approaches of pavement-vehicle interaction; which motivates the later development of a new approach.

2.1 Introduction

The US road network is a combination of asphalt (flexible), concrete (rigid), and an interlay of asphalt and concrete (composite) pavements. Various studies have looked at the impact of each pavement type on vehicle fuel consumption, mainly focusing on flexible and rigid pavements. The existing literature has established that a link exists between pavement type and quality with fuel consumption. For instance, Zaniewski et al. [53] suggested the extreme example that it would require much more fuel to drive 100 kilometers at the same speed over a gravel road than over a newly paved road. Though less dramatic, measurements (as presented in Table 2-8) have revealed potential fuel consumption differences between flexible and rigid pavements. This change in fuel consumption is solely attributed to the pavement types tested, overlooking

any of the structural (pavement thickness) and material (stiffness, subgrade) properties of each pavement design.

A main shortcoming of the empirical approach to the impact of PVI on fuel consumption is the measurement precision required for the relatively small change in fuel consumption proposed. While the cumulative fuel consumption difference between pavement types can be large when measured over an entire service life, the impact for a single vehicle is quite small. For instance, a study by Taylor and Patten [46] suggests a maximum fuel consumption difference between flexible and rigid pavements of 0.007 liters per vehicle-kilometer for trucks. Measurements at this scale will be highly influenced by external factors including local temperatures (surface, air, tire, etc.), tire pressure, vehicle suspension dynamics, vehicle speed, and other variables. Small shifts in these conditions could lead to fuel consumption changes of the same order as any pavement-type differences. Similarly, a change in tire pressure by 7 kPa (1 psi) can entail a change in fuel consumption of 0.005 liters per vehicle-kilometer [34]. In order to effectively isolate the influence of pavement type and structure on vehicle fuel consumption, all competing factors must be precisely controlled and accounted for in a given study. A recent report by the Lawrence Berkeley National Laboratory reviewed the existing literature and determined that although there is strong evidence suggesting a difference between different pavement structures, the aggregate research is often conflicting and inconclusive [39]. The authors conclude that a comprehensive mechanical model needs to be developed before structure-related PVI can be quantitatively included in a LCA.

2.2 HDM-4 Model for Estimating Fuel Consumption

The vehicle fuel consumption is proportional to the resistive forces acting on the vehicle. These forces are rolling resistance, gradient, inertia, curvature, and aerodynamic forces. The rolling resistance force (due to the pavement-vehicle interaction) is greatly influenced by pavement conditions, so that a 3 m/km reduction in a pavement's International Roughness Index (IRI)[1] would lead to a 10% decrease in rolling resistance, which in turn would result in 1-2% reduction in fuel consumption [51]. Various models are available for estimating the vehicle operating cost

[1] International Roughness Index (IRI) is obtained from measured longitudinal road profiles with units of slope (m/km, in/mi). For more detail see Page 24.

(VOC) of which the World Bank's Highway Design and Maintenance Standards Model (HDM) versions HDM-3 and HDM-4 are highly adopted. The HDM-4 VOC model has benefited from previous research in different countries, and is adopted by developing and developed countries. The model adopted is based on the ARFCOM mechanistic model [33] with alteration to the engine speed, engine drag, and the accessories power, as presented by Zabaar and Chatti [51].

The general form of the model is conceptually expressed as:

$$\text{IFC}=f(P_{tr}, P_{accs}+P_{eng}) = \max(\alpha, \xi * P_{tot} * (1 + d_{Fuel})) \tag{2.1}$$

where

IFC= instantaneous fuel consumption (mL/s),

P_{tot}= total power,

P_{tr}= power required to overcome traction forces (kW),

P_{accs}= power required for engine accessories (i.e. fan belt, alternator; kW),

P_{eng}= power required to overcome internal engine friction (kW),

α= fuel consumption at idling (mL/s),

ξ= engine efficiency (mL/kW/s),

d_{Fuel}= excess fuel consumption caused by congestion.

The total power required includes traction power, engine drag, and vehicle accessories, and can be calculated by two methods depending on whether the traction power is positive or negative. In turn the traction power is a function of gradient, inertial, curvature, aerodynamic and rolling resistance forces. The rolling resistance forces are in direct relationship with pavement conditions, tire parameters, and vehicle characteristics, and have great influence on vehicle fuel consumption. For instance, water or snow presence on the road increase rolling resistance and fuel consumption. Table 2-1 and Table 2-2 summarize the equations and submodels of the HDM-4 fuel consumption model, and Table 2-3 to 2-7 present the required parameters for these models.

The rolling resistance force F_r, applied to a vehicle through pavement-vehicle interaction, represents pavement deflection through the Benkelman beam rebound deflection parameter (DEF) and pavement roughness through the International Roughness Index (IRI). The Benkel-

Name	Description	Unit
Total power (P_{tot})	$P_{tot} = \frac{P_{tr}}{\text{edt}} + P_{accs} + P_{eng}$ $P_{tr} > 0$ uphill/level $P_{tot} = edtP_{tr} + P_{accs} + P_{eng}$ $P_{tr} < 0$ downhill	kW
edt	Drive-train efficiency factor	
Engine and accessories power ($P_{eng.accs} = P_{eng} + P_{accs}$)	$P_{eng.accs}$ =KPea$*P_{\max} * (P_{accs_al} + (P_{accs_a0} - P_{accs_al})) * \frac{\text{RPM-RPMIdle}}{\text{RPM100-RPMIdle}}$	kW
KPea	Calibration factor (Table 2-4)	
$P_{\max}$	Rated engine power	kW
P_{accs_al}	$P_{accs\_al} = \frac{-b \pm \sqrt{b^2 - 4*a*c}}{2*a}$	kW
	$\begin{cases} a = \xi_b * \text{ehp} * \text{KPea}^2 * P_{\max} * \frac{100 - \text{PctP}_{eng}}{100} \\ b = \xi_b * \text{KPea} * P_{\max} \\ c = -\alpha \end{cases}$	
ξ_b	Engine efficiency depends on the technology type (gasoline versus diesel)	mL/kW/s
ehp	Engine horsepower	hp
α	Fuel consumption at idling	mL/s
P_{accs_a0}	Ratio of engine and accessories drag to rated engine power when traveling at 100 km/hr	
PctP_{eng}	Percentage of the engine and accessories power used by the engine	%
Engine speed	RPM=a0+a1*SP+a2*SP^2+a3*SP^3 SP=max(20,V)	RPM
V	Vehicle speed	m/s
$a0$ to $a3$	Model parameter (Table 2-3)	
RPM100	Engine speed at 100 km/hr	RPM
RPMIdle	Idle engine speed	RPM
Traction power (P_{tr})	$P_{tr} = \frac{v(F_a + F_g + F_c + F_r + F_i)}{1{,}000}$	kW
F_a	Aerodynamic forces (Table 2-2)	N
F_g	Gradient forces (Table 2-2)	N
F_c	Curvature forces (Table 2-2)	N
F_r	Rolling resistance forces (Table 2-2)	N
F_i	Inertial forces (Table 2-2)	N
Note: ξ_b= engine efficiency, dependent on the technology type (gasoline versus diesel); SP= maximum between 20 km/h and the vehicle speed.		

Table 2.1: HDM-4 Fuel Consumption Model.

Name	Description	Unit
Aerodynamic forces (F_a)	$Fa = 0.5 * \rho * CDmult * CD * AF * v^2$	N
CD	Drag coefficient	
CDmult	CD multiplier	
AF	Frontal area	m^2
ρ	Mass density of the air	kg/m^3
v	vehicle speed	m/s
Gradient forces (F_g)	$F_g = M*GR*g$	N
M	Vehicle weight	kg
GR	Gradient	radians
g	Gravity	m/s^2
Curvature forces (F_c)	$F_c = \max(0, \frac{(\frac{M*v^2}{R} - M*g*e)^2}{Nw*Cs} * 10^{-3})$	N
R	Curvature radius	m
Superelevation (e)	$e = \max(0,0.45\text{-}0.68*\text{Ln}(R))$	m/m
Nw	Number of wheels	
Tire stiffness (Cs)	$Cs=KCS*[a0+a1*\frac{M}{Nw}+a2*(\frac{M}{Nw})^2]$	
KCS	Calibration factor	
a0 to a2	Model parameter (Table 2-5)	
Rolling resistance (F_r)	$F_r = CR2 * FCLIM * (b11 * Nw + CR1 * (b12 * M + b13 * v^2))$	N
CR1	Rolling resistance tire factor	
Rolling resistance parameters ($b11$, $b12$, $b13$)	$\begin{cases} b11=37*Dw \\ b12=\begin{cases} 0.067/Dw & \text{old tires} \\ 0.064/Dw & \text{latest tires} \end{cases} \\ b13=0.012*Nw/Dw^2 \end{cases}$	
Rolling resistance surface factor (CR2)	$=Kcr2[a0+a1*Tdsp+a2*IRI+a3*DEF]$	
Kcr2	Calibration factor (Table 2-4)	
$a0$ to $a3$	Model coefficient (Table 2-6)	
Tdsp	Texture depth using sand path method	mm
IRI	International roughness index	m/km
DEF	Benkelman beam rebound deflection	mm
Climate factor (FCLIM)	FCLIM = 1+0.003+PCTDS+0.002*PCTDW	
Inertial forces (Fi)	$F_i = M * (a0 + a1 * \arctan(\frac{a2}{v^3})) * a$	
a0 to a2	Model parameter (Table 2-7)	
Note: Dw = diameter of wheels (m), PCTDS = percent driving in snow conditions, and PCTDW = percent driving in wet conditions		

Table 2.2: HDM-4 Traction Forces Model.

	Engine speed coefficients			
Vehicle type	a0	al	a2	a3
Small car	720.05	0.868	0.2006	-0.0007
Medium car	720.05	0.868	0.2006	-0.0007
Large car	720.05	0.868	0.2006	-0.0007
Light delivery car	589.6	-0.5145	0.0168	0.0019
Light goods vehicle	589.6	-0.5145	0.0168	0.0019
Four wheel drive	982.37	3.6701	-0.1331	0.0019
Light truck	550.08	-3.0722	0.3798	-0.0018
Medium truck	720.05	0.868	0.2006	-0.0007
Heavy truck	550.08	-3.0722	0.3798	-0.0018
Articulated truck	799.6	-5.3791	0.2077	0.00006
Mini bus	799.6	-5.3791	0.2077	0.00006
Light bus	799.6	-5.3791	0.2077	0.00006
Medium bus	799.6	-5.3791	0.2077	0.00006
Heavy bus	799.6	-5.3791	0.2077	0.00006
Coach	799.6	-5.3791	0.2077	0.00006

Table 2.3: Engine Speed Parameters [52].

Vehicle Type	Kcr2	Kpea
Medium car	0.5	0.25
SUV	0.58	0.56
Light truck	0.99	0.61
Van	0.67	0.49
Articulated truck	1.1	0.35

Table 2.4: Model Calibration Factors [52].

	$\leqslant$2500 Kg		>2500 kg	
Coefficient	Bias	Radial	Bias	Radial
a0	30	43	8.8	0
al	0	0	0.088	0.0913
a2	0	0	-0.0000225	-0.0000114
Kcs	1	1	1	1

Table 2.5: Parameters for Cs Model [4].

		⩽2500 Kg				>2500 kg			
Surface class	Surface type	a0	al	a2	a3	a0	al	a2	a3
Bituminous	AM or ST	0.5	0.02	0.1	0	0.57	0.04	0.04	1.34
Concrete	JC or GR	0.5	0.02	0.1	0	0.57	0.04	0.04	0
Unsealed	GR	1	0	0.075	0	1	0	0.075	0
Unsealed	-	0.8	0	0.1	0	0.8	0	0.1	0
Block	CB, BR or SS	2	0	0	0	2	0	0	0
Unsealed	SA	7.5	0	0	0	7.5	0	0	0

Table 2.6: Parameters for CR2 Model [4].

	Effective mass ratio model coefficient		
	a0	al	a2
Small car	1.14	1.01	399
Medium car	1.05	0.213	1260.7
Large car	1.05	0.213	1260.7
Light delivery car	1.1	0.891	244.2
Light goods vehicle	1.1	0.891	244.2
Four wheel drive	1.1	0.891	244.2
Light truck	1.04	0.83	12.4
Medium truck	1.04	0.83	12.4
Heavy truck	1.07	1.91	10.1
Articulated truck	1.07	1.91	10.1
Mini bus	1.1	0.891	244.2
Light bus	1.1	0.891	244.2
Medium bus	1.04	0.83	12.4
Heavy bus	1.04	0.83	12.4
Coach	1.04	0.83	12.4

Table 2.7: Parameters for Effective Mass Ratio Model [4].

Pavement Condition	Characteristic Deflection (mm)
Excellent	0.45-0.75
Good	0.75-1.10
Fair	1.10-1.50
Poor	1.50-2.00
Very poor	>2.00

Table 2.8: The Benkelman beam deflection's representation of pavement conditions [21].

man beam, developed by the Western Association of State Highway Organizations (WASHO) in 1952, is a simple lever arm that is used to measure the pavement surface rebound as a truck is moved. The beam is used with a truck loaded to 80 kN (18,000 lb) on a single axle with dual tires and a tire pressure of 480 to 550 kPa (70-80 psi). The tip of the beam is placed between the dual tires; and as the truck moves away, the pavement surface rebound is measured. The Benkelman beam deflection (in millimeters) can describe a pavement's structural properties, conditions, and stiffness. Moreover, it can be used to calculate the pavement's structural number (SN) through various methods. Table 2-8 summarizes the relationship between pavement condition and the Benkelman beam deflection results.

Today, the Falling Weight Deflectometer (FWD) testing method is highly adopted for measurements of a pavement's dynamic response, and relationships between DEF and FWD measurements are available for different locations and different practices [21].

The impact of roughness is included in the HDM-4 model through the International Roughness Index (IRI) as a resistive force to the vehicle's motion. As seen in Table 2-2, the impact of DEF (mm) and IRI (m/km) is carried through the equation of rolling resistance surface factor (CR2) to the rolling resistance force F_r (N). The impact of each force is considered through traction power P_{tr} which adds up with P_{assc} and P_{eng} to obtain the total power P_{tot} required by the vehicle. By calculating P_{tot}, the instantaneous fuel consumption (IFC) of a vehicle is calculated.

2.3 Empirical studies

The impact of pavements on vehicle fuel consumption is due to two main effects: pavement deflection and pavement roughness. The main contributors to PVI resistive forces are dependent

Study	Year	Vehicle Type	Speed (km/hr)	IRI Value (m/km) (in/mi)	Increased Fuel Consumption (liter/100km)	Source
Zaniewski	1982	Trucks	16–110	1–6.7 (63-422)	0	[53]
Zaniewski	1982	Cars	16–110	1–6.7 (63-422)	0	[53]
De Graaff	1999	Trucks	90	-	-0.2-0.2	[10]
NRC I	2000	Trucks	100	1–3.5 (63-220)	4.0–4.3	[45]
NRC I	2000	Trucks	60	1–3.5 (63-220)	1.6–1.7	[45]
NPC	2002	Trucks	80	-	0.04–.24	[30]
NRC II	2002	Trucks	100	1–3.5 (63-220)	1.4–2.3	[22]
NRCII	2002	Trucks	60	1–3.5 (63-220)	1.4–2.2	[22]
NRC III	2006	Trucks	100	1 (63)	0–0.7	[46]
NRC III	2006	Empty Trucks	100	1 (63)	0–0.4	[46]
NRC III	2006	Full Trucks	60	1 (63)	0–0.5	[46]
NRC III	2006	Cars	100	1 (63)	-0.1-0.3	[46]
U Texas	2009	Cars	60	2.7–5.1 (170-321)	0.4–0.9	[2]
Michigan SU	2010	Cars	60	-	0	[51]
Michigan SU	2010	Trucks	60	-	1	[51]

Table 2.9: List of major studies on the effect of pavement type on fuel consumption of vehicles. Increased fuel consumption on an asphalt pavement, compared to a concrete pavement.

on material and structural properties of a pavement system along with that of the vehicle. The impact of pavement deflection on fuel consumption has been empirically studied; however, the sole link between pavement deflection and these studies is the pavement type–flexible versus rigid. Table 2-9 summarizes the scope and results of studies performed on the the change in fuel consumption due to pavement type. Figure 2-1 graphically presents the values from each study, showing that a change in fuel consumption due to pavement type exists. However, there is high uncertainty and high variability within the suggested values. Even though these studies aimed to capture the impact of pavement deflection on fuel consumption, neither the pavement structure and material, nor the pavement response were included in the analyses. The major and common criteria of vehicle type was reported in all studies.

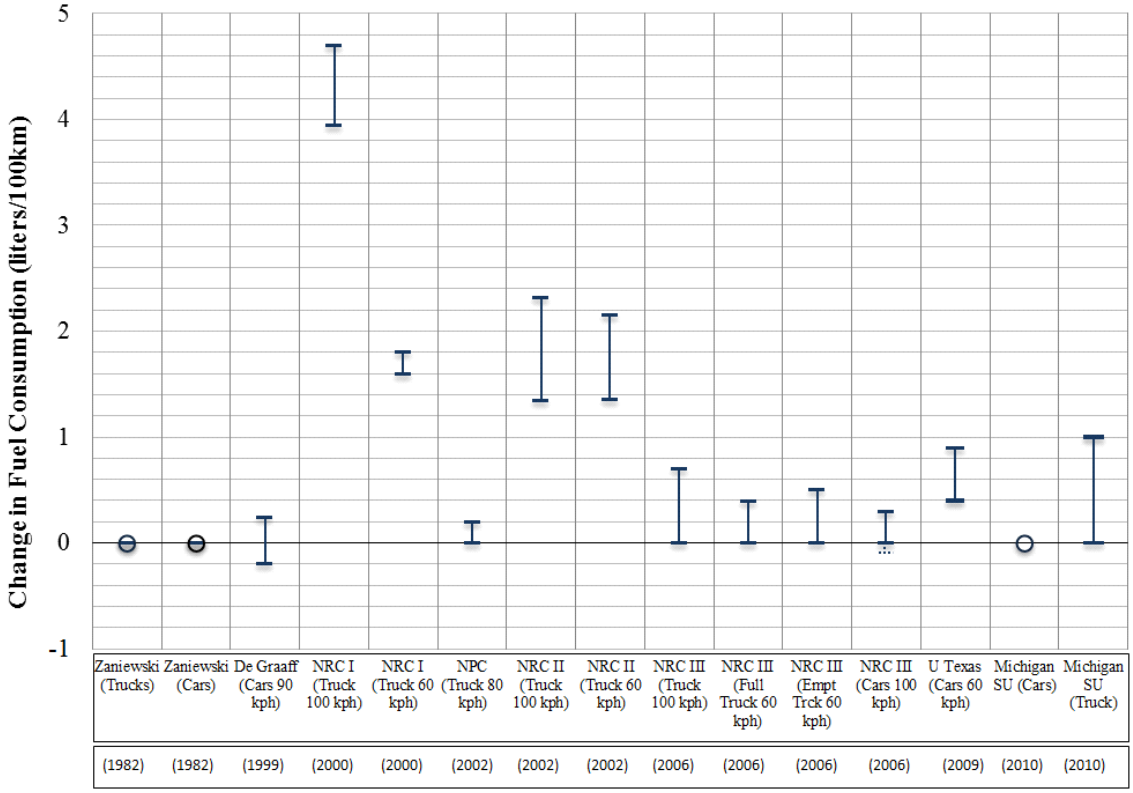

Figure 2-1: Values reported by previous studies on the effect of pavement type on fuel consumption of vehicles in liters/100km (gal/100mi). Change in fuel consumption on an asphalt (flexible) pavement compared to a concrete (rigid) pavement.

The impact of pavement roughness on fuel consumption has been studied extensively from an empirical perspective. Pavement roughness, represented by the International Roughness Index (IRI), is obtained from the longitudinal road profile. It is calculated using a quarter-car vehicle math model, whose response is accumulated to yield a roughness index with units of slope, m/km, in/mi. This index was originally developed to determine if and when repairs and maintenance are needed [40]. In 2010, Zaabar and Chatti [51] investigated the impact of pavement roughness on fuel consumption for five different vehicle classes (medium car, SUV, van, light truck, articulated truck) at IRI values of 1-5 m/km (63-315 in/mi). The change in vehicle fuel consumption suggested by Zabaar and Chatti [51] per a change of 1 m/km in IRI is presented in Figure 2-2. The findings of this study were used to calibrate the HDM-4 Model

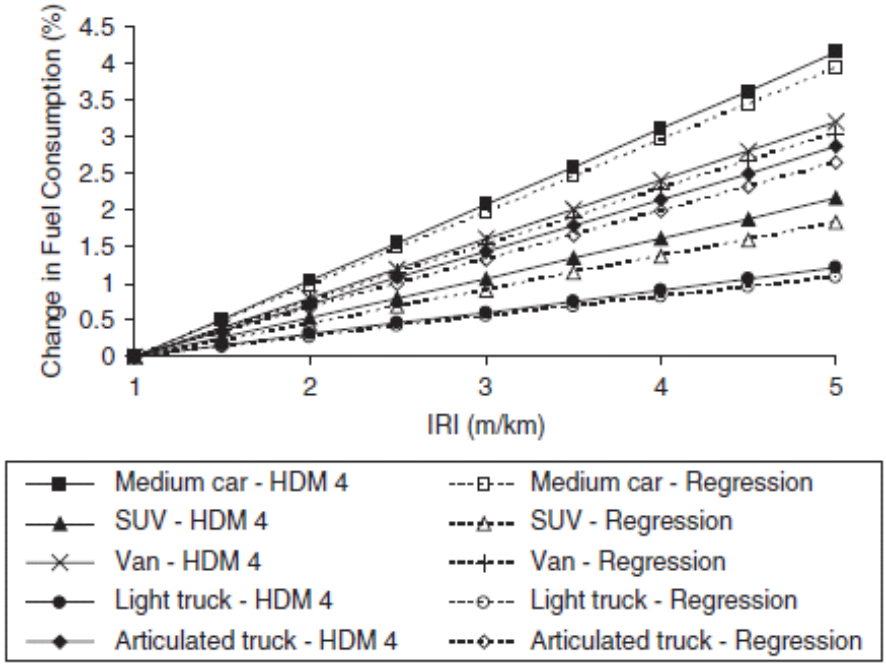

Figure 2-2: Effect of pavement roughness on fuel consumption [51].

for Estimating Fuel Consumption.

The main empirical studies of the impact of pavement type on fuel consumption listed in Table 2-9 are reviewed briefly below with a follow up on the common limitations of these studies and generally of the empirical approach to PVI.

2.3.1 Zaniewski et al., 1982

The pioneering study on pavement-vehicle interaction is due to Zaniewski et al. [53] who in 1982 looked at the impact of various factors that influence vehicle fuel consumption such as speed, grade, curves, pavement condition, and pavement type. The authors performed fuel consumption readings on eight vehicles, four automobiles and four trucks, of different size classes. The tests were done at 10 mph increments from speed of 10 mph to 70 mph on 12 pavement sections. The pavement sections were selected so that roughness and grade scales would be equal across different pavement surface types.

Rather than defining differences in pavements based on their structural and material prop-

erties, this study looked at the impact of pavement type (asphalt, Portland cement concrete, and gravel) on fuel consumption. This was done through measuring fuel consumption for each of the individual combinations of speed and section, to determine any significant changes to fuel consumption. The authors found changes in fuel consumption between asphalt and concrete pavements of up to 20%. However, there were no statistically significant differences at the 95% confidence level between the paved sections.

2.3.2 NRC II, 2002

The G.W. Taylor Consulting as part of the National Research Council of Canada (NRC) reanalyzed data collected in a preliminary study (NRC I) between 1999 and 2000 [45] and published the second phase of the NRC studies [22]. The goal of this reanalysis was to draw a relationship between changes in fuel consumption of a semi-trailer tank truck and vehicle data (speed, fuel flow, wind speed, temperature), road roughness data, and roadway grade. Multivariate linear regression analysis was used to investigate the effect of pavements on fuel consumption; the variables accounted for in this study were fuel consumption, vehicle load, pavement temperature, International Roughness Index (IRI), road grade, and vehicle speed.

This study found that fuel consumption on asphalt and composite pavements are higher than that of a concrete pavement by 4.1-4.9% and 2.7-3.2%, respectively. Also, the authors determined that with an increase in pavement temperature, fuel consumptions on asphalt and composite pavements increase, suggesting a high impact from the temperature dependent behavior of asphalt binder. One of the unique findings of this study is the intertwined impact of roughness and pavement type on fuel consumption. This study determines that on a pavement with an IRI of over 2.2 m/km (139 in/mi) the impact of pavement type cannot be detected due to the momentum effects caused by higher roughness.

2.3.3 NRC III, 2006

Unlike the NRC II study, where previously collected data on a semi-trailer tank truck was reanalyzed, the third study by Taylor and Patten [46] used a semi-trailer truck and a passenger car to determine fuel consumption changes on concrete, asphalt, and composite pavements. The tests were conducted in five climatic conditions of winter, spring, summer cool, summer hot,

and fall at speeds of 60 km/hr (37 mph) and 100 km/hr (62 mph). Also, three weight classes were investigated by loading and unloading the trailer to determine the impact of vehicle weight on fuel consumption.

This study employed a multiple regression analysis where the fuel consumption rate was related to the International Roughness Index (IRI), the grade, the applied load, the pavement temperature, along with the vehicle speed, and air speed.

Compared to the NRC II study in 2002, the authors suggest smaller changes in fuel consumption on an asphalt and a composite pavements compared to a concrete pavement. The authors report a change in fuel consumption of 0.8-1.8% and 0.8-3.1% for asphalt and composite pavement compared to that of a concrete pavement respectively. These results are for highway speed traffic at 100 km/hr. Also, this study reports that the fuel consumption of a passenger car (2002 Pontiac Grand Prix) is 2.9% higher on an asphalt pavement with respect to a concrete pavement in winter, and is 2.3% lower on a composite pavement compared to a concrete pavement.

2.3.4 U Texas, 2009

To better understand the impact of pavement type on fuel consumption of passenger vehicles at city speeds, Ardekani and Sumitsawan [2] used two pairs of asphalt and concrete pavements with identical gradient and roughness measurements to perform their study. They performed fuel consumption measurements for two driving conditions of constant speed of 48 km/hr (30 mph) and acceleration from stand still. The authors controlled the vehicle mass, tire pressure, fuel type, ambient temperature, humidity, wind speed and direction to eliminate unwanted effects of these factors.

The authors found that passenger vehicles use significantly less fuel on concrete pavements compared to asphalt pavements, both under constant speed and acceleration scenarios. Their reported values for change in fuel consumption are anywhere between 7-20% increase in fuel consumption.

However, one of the overlooked issues of this study is their choice of pavement sections for conducting the experiments. The pavements used have an International Roughness Index (IRI) of 2.7 m/km (170 in/mi) to 5.1 m/km (321 in/mi), categorizing them as very rough pavement

sections. As shown by Taylor et al. in the NRC II study [22], the accuracy of fuel measurement systems highly decrease on pavements with IRI values greater than 2.2 m/km (139 in/mi) due to the impact of roughness on vehicle dynamics. The results of this study disagree with the findings of Zaniewski et al. in 1982 [53], NRC III in 2006 [46], and Michigan SU in 2010 [51]. In fact, in contrast to [51] and [53], Ardekani and Sumitsawan find an impact on fuel consumption of passenger vehicles related to pavement type; an impact much greater than what is suggested by [46] for these vehicles.

2.3.5 Michigan SU, 2010

In a study to calibrate the HDM-4 model for estimating the effects of pavements on fuel consumption, Zaabar and Chatti [52] also performed tests to determine the impact of pavement type on fuel consumption. The authors made use of five vehicles (passenger car, van, SUV, light truck, articulated truck) at speeds of 56 km/hr (35 mph), 72 km/hr (45 mph) and 88 km/hr (55 mph). They determined that only a change in fuel consumption of light and articulated trucks in summer conditions and at low speed could be detected between pavement types. They report a detected change in fuel consumption between an asphalt and a concrete pavement of 5% under these conditions. The reported change in fuel consumption due to pavement type is presented in Figure 2-3, while the impact of roughness on fuel consumption is shown in Figure 2-2.

2.3.6 General Limitations

All the empirical studies listed in Table 2-9 and reviewed above miss to account for pavement structural and material properties. These properties have a significant impact on the longivity and response of the pavement to vehicle loads. The sole pavement attribute in these studies is flexible versus rigid. Given the diversity of pavement systems, such a categorization does not allow a generalization of the results. Moreover, these studies are unable to control many internal and external factors of vehicle fuel consumption, such as wind speed, engine efficiency, constant vehicle speed, surface, air, tire temperature, etc., which lead to unreliable and at times unrepeatable tests. The impact of roughness and temperature on fuel consumption readings lead to some limitations of empirical studies due to equipment and setup deficiencies. The

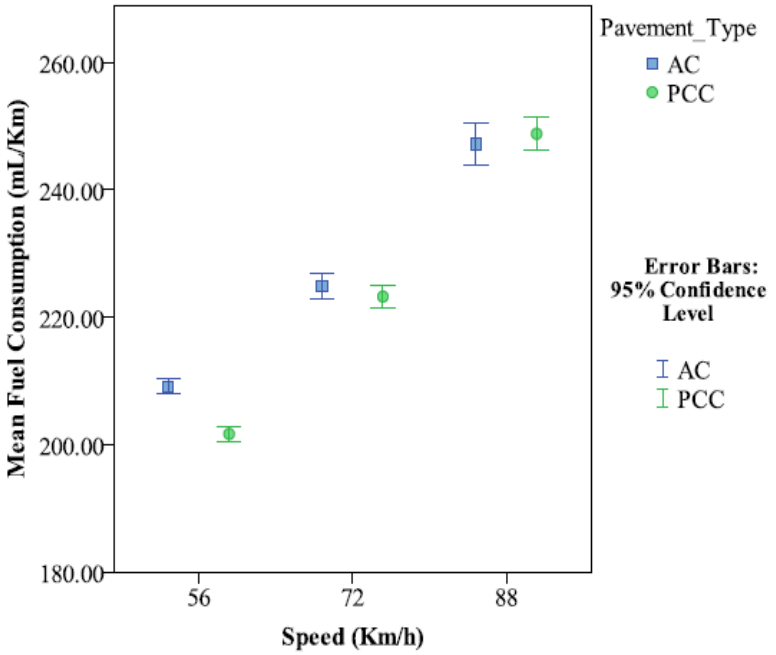

(a)

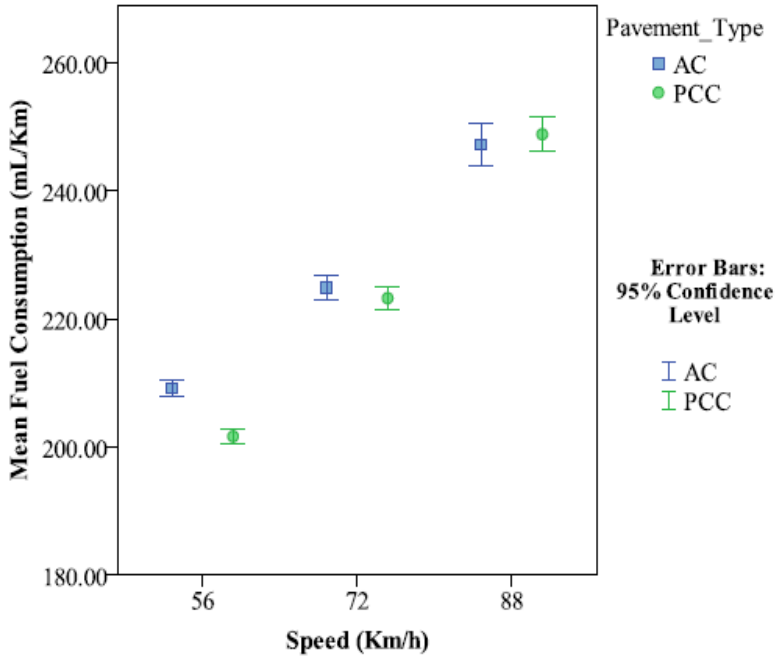

(b)

Figure 2-3: Mean and standard deviation of fuel consumption for different pavement types and speeds. (a) articulated truck, (b) light truck [52].

lack of control over many fuel consumption factors along with variations in pavement designs, materials, and conditions, vehicle speeds, vehicle types, temperature variations, etc. would call for a vast empirical study that collects sufficient data to create a relationship between fuel consumption and the aforementioned factors. Such a study would need to feed into a VOC system (i.e. HDM-4) to calibrate the models as well as provide the required coefficients with higher accuracy. So far, a comprehensive study has not been performed and none in the literature attempt to provide such a relationship or present an understanding of the measured changes in fuel consumption. Due to the limitations and high cost of such a study, a mechanistic model is required to relate fuel consumption with pavement structural and material properties, along with vehicle speeds and loads that is capable of handling variations representative of those that exist in the road transportation network.

2.4 Chapter Summary

The review of the existing studies provides evidence that pavement type has an effect on fuel consumption of vehicles. However, lack of correlation between pavement structural and material properties (pavement design, or pavement response to deflection tests) with fuel consumption lead to high uncertainty and variability in the results. These studies show the importance of small changes in fuel consumption of vehicles. However, when compared they suggest inconclusive results on the magnitude of this impact. One of the main reasons for variations in the results is the different conditions under which the tests were performed: vehicle types, pavement structures, differences in grades, speed, etc.

The shortcomings of the existing data and knowledge determines the focus of our investigation. In order to avoid environmental and vehicle influences on PVI, this work adopts a first-order mechanistic model for different pavement types to focus on pavement structure and material characteristics to determine PVI. These characteristics are then related to the changes they induce on fuel consumption through the HDM-4 model calibrated by Zabaar and Chatti [51].

Part II

PVI Model, Calibration, Validation

Chapter 3

PVI Model

The available field database on fuel consumption related to PVI for different pavement systems exhibit a high level of uncertainty varying by at least an order of magnitude, and is void of any structural and material properties of the particular pavement systems tested. Here we adopt the perspective that a mechanistic model which links pavement structural and material properties to fuel consumption can contribute to closing the uncertainty gap of PVI in LCA of pavements. In order to understand the impact of deflection on vehicle fuel consumption, this chapter introduces the quantities involved through a dimensional analysis and presents the deflection model for pavement response predictions, depending on the relevant mechanical and geometrical properties.

3.1 Model

The focus of the pavement vehicle interaction model is a first-order estimation of deflection-induced fuel consumption. Neglecting roughness effects, irreversible deformation (cracking, rutting etc.), a model is thus required that captures the dynamic response of a road pavement to moving loads on the surface.

There are several methods for modeling the dynamic response of a road pavement to moving loads. The pavement can be modeled as a beam, a plate, or the top layer of a multilayer soil system. The substructure can also be modeled as a system of elastic springs with dashpots, or a homogeneous or layered half-space. There are also various methods of modeling the pavement

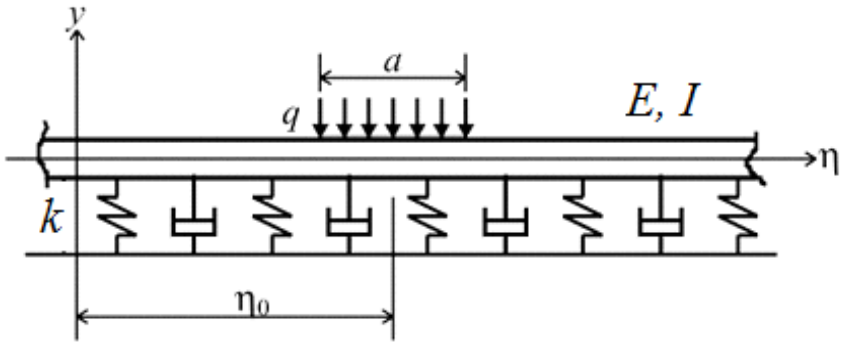

Figure 3-1: Schematic representation of a beam on damped elastic foundation under line load.

material behavior: elastic, viscoelastic, water-saturated poroelastic or inelastic. The loads are either presented as concentrated loads, or distributed loads with a finite width. These conditions define the model and the predicted response, under certain material and structural conditions. The pavement deflection response can be calculated through analytical or numerical methods such as the Finite Element Method (FEM), or the Boundary Element Method (BEM). Beskou and Theodorakopoulos [5] review various models and solution strategies in more detail.

Among the variety of existing models we choose the beam on a viscoelastic foundation model (Figure 3-1) with the tire represented as a line load, in which the beam represents the pavement and the spring and dashpot bedding the subgrade response. This model, though simple, continues to gain traction in pavement engineering due to its ability to provide quantitative means to investigate the main factors that influence the elastic deformation of pavement systems subjected to various moving loads (see e.g. [41]-[44]). Moreover, this model allows the derivation of scaling relations between structural and material quantities to better understand their impacts, as developed later on.

3.2 Bernoulli-Euler Beam on Viscoelastic Foundation

The beam on an elastic foundation represents various properties of a pavement. It draws a relationship between pavement material properties of top layer elastic modulus E, mass per unit length m, and subgrade modulus k, along with the structural property of moment of

inertia I, with deflection y under an external load $q(x,t)$. By assuming a moving coordinate system η on the load (vehicle wheel) a relationship between deflection under (and at distances away from) the load can be calculated.

The governing differential equation for an infinite beam on an elastic foundation in fixed Cartesian coordinates {x,y} at time t is:

$$d\frac{\partial^4 y\,(x,t)}{\partial x^4} + m\frac{\partial^2 y\,(x,t)}{\partial t^2} = q\,(x,t) - f\,(x,t) \tag{3.1}$$

where $d = EI$ is the rigidity of the beam, E is Young's modulus of elasticity, I is the moment of inertia of the beam, m is the unit mass per length of the beam; while $q(x,t)$ and $f\,(x,t)$ are applied external loads and restoring forces from the substrate, respectively. The latter's expression classically assumes a linear pressure response and damping such that:

$$f\,(x,t) = ky + c\,(\partial y/\partial t) \tag{3.2}$$

where k (of pressure/width dimension) is called the modulus of subgrade reaction, and c (of pressure$\times$times/width dimension) stands for the subgrade viscosity. For a load moving in the x direction with a constant velocity V and amplitude ($f = \text{const}$), it is commode to introduce a moving co-ordinate system, $\eta = x - Vt$, and rewrite Eq. (3.1) in the following form [24]:

$$d\frac{\partial^4 y}{\partial \eta^4} + mV^2\frac{\partial^2 y\,(\eta)}{\partial \eta^2} + k\;y\,(\eta) - cV\frac{\partial y\,(\eta)}{\partial \eta} = q(\eta) \tag{3.3}$$

To fully appreciate the forthcoming developments, it is useful to perform a dimensional analysis of the governing equation. The key output of the model is the beam deflection y, which depends on the following quantities:

$$y = f(q, k, \eta, d, c, V, m) \tag{3.4}$$

The exponent matrix in a LMT base system reads:

	$[y]$	$[q]$	$[k]$	$[\eta]$	$[d]$	$[c]$	$[V]$	$[m]$
$[L]$	1	0	-1	1	3	0	1	-1
$[M]$	0	1	1	0	1	1	0	1
$[T]$	0	-2	-2	0	-2	-2	-1	0

(3.5)

The rank of the matrix is k=3. Knowing that the relationship between pavement deflection y and external load q is linear we apply the Π-theorem and write:

$$\left[\frac{y(\eta)}{q(\eta)}\right] = L^1 M^{-1} T^2 = [k]^\alpha [d]^\beta [m]^\gamma \tag{3.6}$$

From the relationship in Eq. (3.6) the values of α, β, and γ are determined as such:

$$\begin{aligned} L \quad & (-1)\alpha + (3)\beta + (-1)\gamma = 1 \\ M \quad & (1)\alpha + (1)\beta + (1)\gamma = -1 \\ T \quad & (-2)\alpha + (-2)\beta + (0)\gamma = 2 \end{aligned} \tag{3.7}$$

where $\alpha = -1$, $\beta = 0$, and $\gamma = 0$. Hence:

$$\Pi = \left(\frac{y(\eta)k}{q(\eta)}\right) = \mathcal{F}\left(\Pi_1, \Pi_2, \Pi_3\right) \tag{3.8}$$

To calcualte the three solution invariants (Π_1, Π_2, Π_3), dimensions of each parameter in Eq. (3.5) is used. Here, calculation of Π_1 is described. From Eq. (3.5) dimension of V is written as:

$$[V] = L^1 M^0 T^{-1} = [k]^\alpha [d]^\beta [m]^\gamma \tag{3.9}$$

where

$$\begin{aligned} L \quad & (-1)\alpha + (3)\beta + (-1)\gamma = 1 \\ M \quad & (1)\alpha + (1)\beta + (1)\gamma = 0 \\ T \quad & (-2)\alpha + (-2)\beta + (0)\gamma = -1 \end{aligned} \tag{3.10}$$

Solving for α, β, and γ reads:

$$[V] = [k]^{1/4} [d]^{1/4} [m]^{-1/2} \tag{3.11}$$

The first invariant $\Pi_1 = \bar{V}$ is determined so that:

$$\Pi_1 = \bar{V} = \frac{V}{k^{1/4} d^{1/4} m^{-1/2}} = \frac{V}{(d/k)^{1/4} (k/m)^{1/2}} \tag{3.12}$$

The same method is used to identify the three solution invariants, namely:

$$y(\eta) = \frac{q}{k} \times \Pi \left(\overline{\eta} = \frac{\eta}{(d/k)^{1/4}}; \zeta = \frac{c}{c_{crit}}; \overline{V} = \frac{V}{V_{os}} \right) \tag{3.13}$$

We recognize the familiar scaling of the deflection solution with the Winkler foundation length–scale[1], $L_s \sim (d/k)^{1/4}$; the subgrade damping ratio, ζ, that is the ratio of the damping coefficient c to the critical damping coefficient of the substrate, $c_{crit} = 2\sqrt{mk}$; and the velocity ratio relative to the oscillation velocity $V_{os} = (d/k)^{1/4} (k/m)^{1/2}$, where $(k/m)^{1/2}$ is (close to a multiplying constant) the subgrade eigenfrequency. Using these quantities in the governing equations yields:

$$\frac{\partial^4 y(\overline{\eta})}{\partial \overline{\eta}^4} + \overline{V}^2 \frac{\partial^2 y(\overline{\eta})}{\partial \overline{\eta}^2} + y(\eta) - 2\zeta \overline{V} \frac{\partial y(\overline{\eta})}{\partial \overline{\eta}} = \frac{q}{k} \tag{3.14}$$

Consider then a Fourier transform w.r.t. $\overline{\eta}$ such that $G\left[y^{(n)}(\overline{\eta})\right] = (i\xi)^n G[y(\overline{\eta})]$. The dynamic displacement response can be obtained using the inverse Fourier transform so that:

$$y(\overline{\eta}) = \frac{q}{k} \times \overline{Y}(\overline{\eta}); \overline{Y}(\overline{\eta}) = \frac{1}{2\pi} \int_{-\infty}^{+\infty} \frac{\overline{Q}(\overline{\eta})}{\xi^4 - \overline{V}^2 \xi^2 + 1 - 2i\zeta \overline{V} \xi} e^{i\xi\overline{\eta}} d\xi \tag{3.15}$$

where a moving load of constant amplitude is assumed, and ξ is defined as the transformed field of $\overline{\eta}$ (moving space). $\overline{Y}(\overline{\eta})$ is the normalized deflection profile, while $Q(\overline{\eta})$ is the transformed load, and $\overline{Q}(\overline{\eta})$ its normalized expression defined respectively by:

$$Q(\overline{\eta}) = \frac{q}{k} \times \overline{Q}(\overline{\eta}); \ \overline{Q}(\overline{\eta}) = \int_{-a/\left(2(d/k)^{1/4}\right)}^{+a/\left(2(d/k)^{1/4}\right)} e^{i\xi\overline{\eta}} d\overline{\eta} \tag{3.16}$$

with a the loading width corresponding to the tire contact length as shown in Figure 3-1. If frequency-independent linear hysteretic damping (material damping) is considered, an expression $2i\zeta$ is often added to expression (3.15) so that the normalized deflection profile reads

[1] The characteristic wavelength of the Bernoulli-Euler beam on viscoelastic foundation, width of the deflection basin, is calculated as $L_s = (4d/k)^{1/4}$.

[24]:

$$\overline{Y}\left(\overline{\eta}\right) = \frac{1}{2\pi}\int_{-\infty}^{+\infty} \frac{\overline{Q}\left(\overline{\eta}\right)}{\xi^4 - \overline{V}^2\xi^2 + \ 1 + 2i\zeta\left(1 - \overline{V}\xi\right)} e^{i\xi\overline{\eta}} d\xi \tag{3.17}$$

It is generally accepted that most of the energy dissipation in soils takes place through hysteretic damping (internal friction) rather than through viscous behavior. The energy loss due to hysteretic damping is cyclic and is frequency independent [24], [41]-[44]. Since the pavement subgrade is composed of soil deposits, frequency-independent linear hysteretic damping is considered for the foundation. Therefore, the viscous damping term is eliminated and Eq. (3.17) is written as:

$$\overline{Y}\left(\overline{\eta}\right) = \frac{1}{2\pi}\int_{-\infty}^{+\infty} \frac{\overline{Q}\left(\overline{\eta}\right)}{\xi^4 - \overline{V}^2\xi^2 + \ 1 + 2i\zeta} e^{i\xi\overline{\eta}} d\xi \tag{3.18}$$

The impact of damping on the pavement response and its relationship with the pavement-vehicle interaction is further discussed in the next chapter.

3.3 Solution Strategy

The governing equation of a beam on a frequency independent damped elastic foundation can be solved either numerically or analytically as shown by Kim & Roesset (2003) [24] and Sun (2001) [42]. In this section, the approach of Sun [42] is used to solve this equation analytically, where the theorem of residue is employed. Eq. (3.18) is used to calculate the pavement response. To evaluate this integral analytically, poles of the integrand are identified by:

$$\xi_0 = 0 \tag{3.19}$$

$$\xi_1 = \sqrt{\frac{\overline{V}^2 + \sqrt{\overline{V}^4 - 4(1+2i\zeta)}}{2}} \tag{3.20}$$

$$\xi_3 = \sqrt{\frac{\overline{V}^2 - \sqrt{\overline{V}^4 - 4(1+2i\zeta)}}{2}} \tag{3.21}$$

$$\xi_2 = -\xi_1;\ \xi_4 = -\xi_3 \tag{3.22}$$

Every pole and its order are isolated and given in closed form. The theorem of residue is then applied to represent the generalized integral in form of a contour integral in the complex plane [24]. The contour is presented in Figure 3-2.

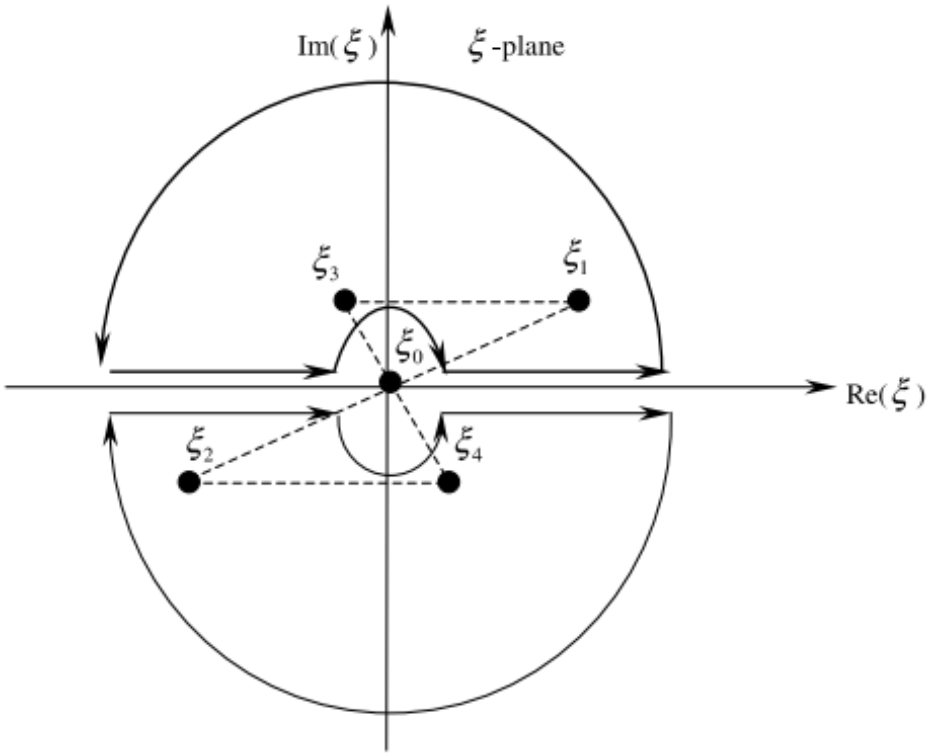

Figure 3-2: Representative contour for the integral [42].

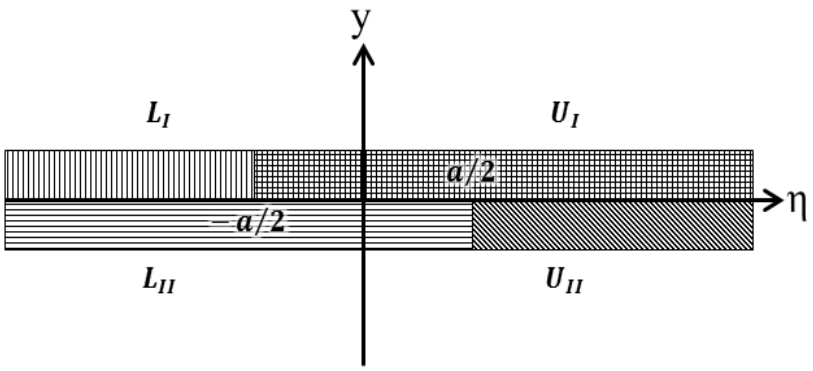

Figure 3-3: Representation of the pavement and location dominance for Eq. (3.24) to (3.27).

In order to simplify the final solution, we let $\bar{a} = a/(2(d/k)^{(1/4)})$ in Eq. (3.16), and the solution to Eq. (3.18) is obtained from:

$$\begin{gathered} p.v.\int_{-\infty}^{+\infty} \frac{e^{i\xi(\overline{\eta}-\overline{a})}-e^{i\xi(\overline{\eta}+\overline{a})}}{\xi i(\xi^4-\overline{V}^2\xi^2+(1+2i\zeta))}d\xi = \\ \frac{2\pi i}{d}\sum_{\mathrm{Im}\,\xi_j>0}\mathrm{Res}\{\frac{e^{i\xi(\overline{\eta}-\overline{a})}-e^{i\xi(\overline{\eta}+\overline{a})}}{\xi i\prod_{j=0}^{4}(\xi-\xi_j)}\}+\frac{\pi i}{d}\sum_{\mathrm{Im}\,\xi_j=0}\mathrm{Res}\{\frac{e^{i\xi(\overline{\eta}-\overline{a})}-e^{i\xi(\overline{\eta}+\overline{a})}}{\xi i\prod_{j=0}^{4}(\xi-\xi_j)}\} \end{gathered} \tag{3.23}$$

where p.v. indicates the principal value of the integrand, and Im represents the imaginary part of the complex variable ξ_j. Eq. (3.23) can be expanded as:

$$U_I = \frac{2\pi i}{d}\{\frac{e^{i\xi_2(\overline{\eta}+\overline{a})}}{2\xi_2^2(\xi_2^2-\xi_4^2)}+\frac{e^{i\xi_4(\overline{\eta}+\overline{a})}}{2\xi_4^2(\xi_4^2-\xi_2^2)}\}+\frac{\pi i}{d}\{\frac{1}{\xi_2^2\xi_4^2}\} \tag{3.24}$$

$$U_{II} = \frac{2\pi i}{d}\{\frac{e^{i\xi_2(\overline{\eta}-\overline{a})}}{2\xi_2^2(\xi_2^2-\xi_4^2)}+\frac{e^{i\xi_4(\overline{\eta}-\overline{a})}}{2\xi_4^2(\xi_4^2-\xi_2^2)}\}+\frac{\pi i}{d}\{\frac{1}{\xi_2^2\xi_4^2}\} \tag{3.25}$$

$$L_I = \frac{2\pi i}{d}\{\frac{e^{-i\xi_2(\overline{\eta}+\overline{a})}}{2\xi_2^2(\xi_2^2-\xi_4^2)}+\frac{e^{-i\xi_4(\overline{\eta}+\overline{a})}}{2\xi_4^2(\xi_4^2-\xi_2^2)}\}+\frac{\pi i}{d}\{\frac{1}{\xi_2^2\xi_4^2}\} \tag{3.26}$$

$$L_{II} = \frac{2\pi i}{d}\{\frac{e^{-i\xi_2(\overline{\eta}-\overline{a})}}{2\xi_2^2(\xi_2^2-\xi_4^2)}+\frac{e^{-i\xi_4(\overline{\eta}-\overline{a})}}{2\xi_4^2(\xi_4^2-\xi_2^2)}\}+\frac{\pi i}{d}\{\frac{1}{\xi_2^2\xi_4^2}\} \tag{3.27}$$

where $U_{I,II}$ and $L_{I,II}$ represent the principal values of the integrand for locations away from the center point ($\eta = 0$) as shown in Figure 3-3. Moreover, a is the total loaded zone per Figure 3-1.

Using the values from Eq. (3.24) through Eq. (3.27) for $U_{I,II}$ and $L_{I,II}$ the final solution can be obtained using a Heaviside step function $H[n] = \begin{cases} 0, & n < 0 \\ 1, & n > 0 \end{cases}$ as:

$$\overline{Y}(\overline{\eta}) = \frac{-\bar{Q}}{2\pi i}\{H[\bar{\eta}-\bar{a}]*(U_{II}-U_I)-H[\bar{a}-\bar{\eta}]*H[\bar{a}+\bar{\eta}]*(U_1+L_{II})+H[-(\bar{\eta}+\bar{a})]*(L_1-L_2)\} \quad (3.28)$$

3.4 Model Output Example

Using the solution strategy presented above, the model response for different input parameters is presented in the next two chapters. For illustration only, we consider the following input parameters as suggested by Kim and Roesset [24] and used by Sun and Luo [44] and Beskou and Theodorakopoulos [5]: d=2.3 kN.m^2, k=68.9 MPa, m=48.2 kg/m, q=-70 kN/m, a=0.075 m, V=9.525 m/s, and ζ=0, where the negative sign of q means that the load direction is opposite to the y direction shown in Figure 3-1. Using these parameters the model response is shown in Figure 3-4. This Figure shows the model's deflection response at distances away from the loading zone; distance zero represents the tire location. The predicted model deflection corresponds to the results obtained by Kim and Roesset [24], Sun and Luo [44], and Beskou and Theodorakopoulos [5]; showing that the model implementation is correct.

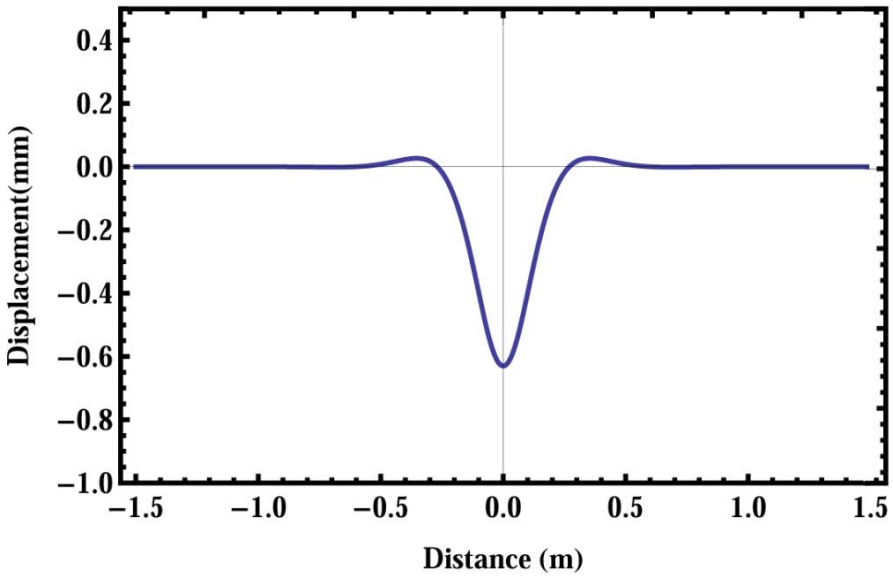

Figure 3-4: Deflected shape from model response for ζ=0, $\bar{V}$=18.09; d=2.3 kN.m^2, k=68.9 MPa, m=48.2 kg/m, q=-70 kN/m, a=0.075 m, and V=9.525 m/s.

3.5 Chapter Summary

In this chapter, a first-order mechanistic pavement model, the Bernoulli-Euler beam on a viscoelastic foundation subjected to a moving load was chosen to determine pavement deflection. This model is an idealized representation of the dynamic interaction of pavements and vehicles, but proves to be effective for the purpose of understanding and evaluating, in first order, the relationship between material and structural elements within PVI and their impact on fuel consumption. The main model parameters that affect pavement deflection, hence PVI's impact on fuel consumption, are:

- E the top layer Young's modulus of elasticity;
- k the modulus of subgrade;
- h the pavement thickness;
- Q the applied load.

The impact of these parameters on pavement deflection and fuel consumption are discussed from a scaling relationship standpoint, later in Chapters 5 and 6. Also the effect of the damping term ζ and its importance are discussed later. We now have an operational model to calculate deflection for given pavement structural and material properties. This will ultimately enable us to estimate the impact of pavement deflection on fuel consumption.

Chapter 4

Calibration & Validation

In order to apply the deflection model to the pavement-vehicle interaction phenomenon, the model needs to be calibrated and validated. Calibration and validation of the deflection model is performed against Falling Weight Deflectometer (FWD) time history data recorded by the Long-Term Pavement Performance program (LTPP) of the Federal Highway Administration [28]. For the purpose of this study, all available FWD datasets have been selected from pavements designed to carry highway traffic.

4.1 Description of Test

The Long-Term Pavement Performance (LTPP) program, a current division of the Federal Highway Administration (FHWA), initiated data collection on pavements in 1987. Two of the primary objectives of this program are to improve pavement prediction and design models, achieved through extensive data collection on pavement response to loads. This program makes use of Falling Weight Deflectometer (FWD) data to measure pavement deflection response to a load of known magnitude. This method provides pavement engineers with an indicator of the structural capacity, material properties, and the expected longevity of the pavement. There are approximately 2,500 sections within the LTPP monitored network [32].

Measurement accuracy and consistency are important factors in FWD measurements. Aside from the pavement cross-sectional properties (layer thickness, material type, material quality, and subgrade quality), major influencing factors on the pavement response during testing in-

clude:

- Environmental factors: layer temperature, moisture;
- Pavement discontinuities: cracks, joints;
- Variations in pavement structure.

These factors can have different influences on rigid and flexible pavements. For example, the stiffness of flexible pavements (asphalt top layer modulus) is highly temperature dependent, so that deflection values measured by the FWD test are greater during summer than winter time. Also, pavement discontinuities (cracks, joints, air voids, etc.) will generally lead to higher deflections than a pavement section without such defects. Variations in pavement structure, along with equipment and operational errors are inevitable but are minimized by trained FWD operators [32].

4.1.1 FWD Experiment Setup

In the Falling Weight Deflectometer test a load is applied to the pavement, and deflection is measured at various distances away from the loading point using geophones with the corresponding time from application of the load. Figure 4-1 shows an illustration of the FWD testing trailer; point D0 in this figure is the loading location where a load is dropped on a rubber buffer, and D1 through D6 are location of geophones for this setup. For each measurement, the loading time along with the progression of deflection in time for each geophone is recorded. The line of influence illustratively shows how deep the impact from the load penetrates and that the maximum deflection is under the load plate. Here, the experimental procedure is briefly discussed.

Deflection Sensor Spacing

The LTPP falling weight deflectometer test uses nine deflection sensors placed radially away from the center of the load. The location of each sensor is predefined to simplify data collection, decrease testing time, and minimize errors in sensor spacing. Figure 4-2 schematically shows sensor spacing and location for the 9 deflection sensors used throughout LTPP.

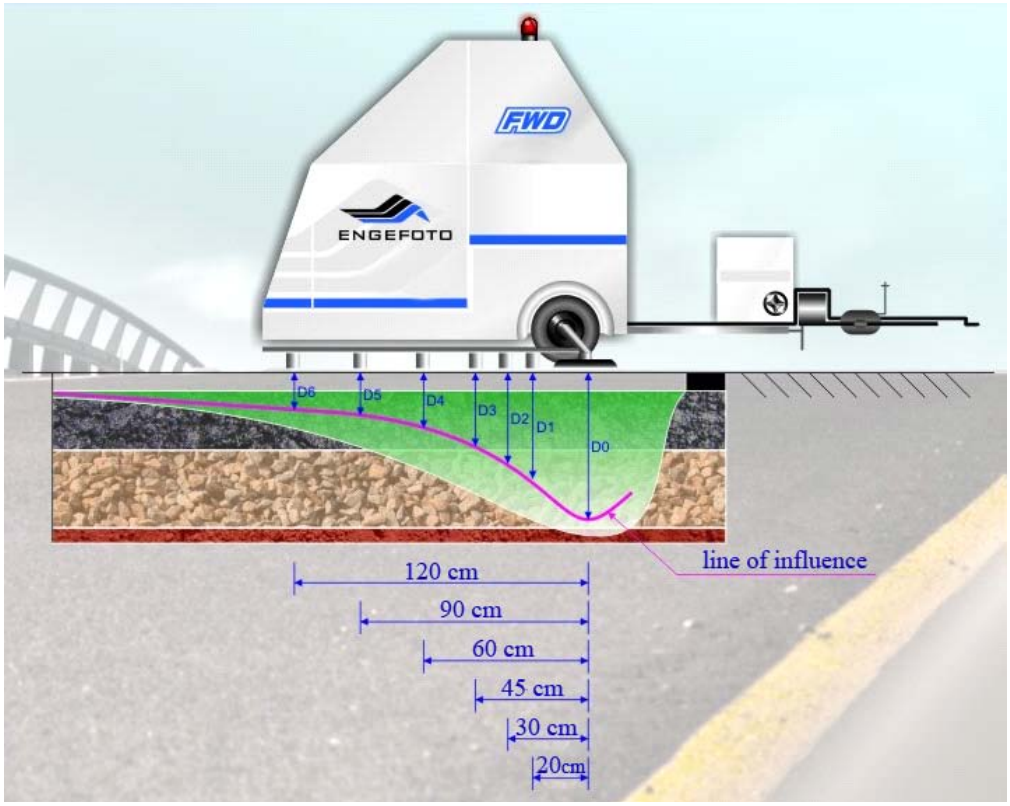

Figure 4-1: Illustration of the Falling Weight Deflectometer device [14].

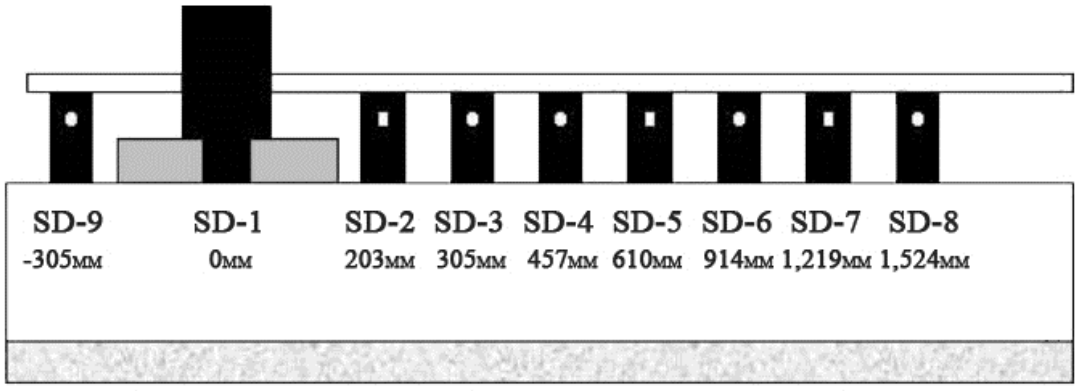

Figure 4-2: Fixed sensor configuration for LTPP FWD testing [32].

Drop Height	Target Load (kN)	Acceptable Range (kN)
1	26.7 (6.0 kips)	24.0 to 29.4 (5.4 to 6.6 kips)
2	40.0 (9.0 kips)	36.0 to 44.0 (8.1 to 9.9 kips)
3	53.4 (12.0 kips)	48.1 to 58.7 (10.8 to 13.2 kips)
4	71.2 (16.0 kips)	64.1 to 78.3 (14.4 to 17.6 kips)

Table 4.1: Load drop seqence for flexible pavements [32].

Drop Height	Target Load (kN)	Acceptable Range (kN)
2	40.0 (9.0 kips)	36.0 to 44.0 (8.1 to 9.9 kips)
3	53.4 (12.0 kips)	48.1 to 58.7 (10.8 to 13.2 kips)
4	71.2 (16.0 kips)	64.1 to 78.3 (14.4 to 17.6 kips)

Table 4.2: Load drop sequence for rigid pavements [32].

Load Drop Heights and Magnitude

The induced impulse load and the measured load from the FWD testing machine are influenced by the pavement stiffness and temperature of the rubber buffer. Increase in the rubber buffer's temperature results in a decrease in stiffness, and hence a decrease in the applied load. Therefore, the induced load from the same drop height can vary from pavement to pavement. To overcome shortcomings in the experiment, the LTPP manual [32] suggests load levels from each drop height be verified. The load drop sequence and magnitude differ for flexible and rigid pavements. There are four drop heights and load levels with an acceptable range for flexible pavement tests, as presented in Table 4-1. For rigid pavement tests, three drop heights, target loads, and acceptable load ranges are defined in the LTPP manual [32], as shown in Table 4-2.

Field Measurements

During an FWD test, LTPP operators collect field data for further analysis and research purposes. The data collected during the deflection testing procedure includes pavement surface and gradient temperature, pavement distress, along with crack and joint width.

After setting up the experiment and conducting the test, deflection values at each geophone along with the deflection time history are recorded. From this data, time history graphs are produced, which show the load and deflection progression versus time at distances away from the load. A sample FWD time history is presented in Figure 4-3. The first line in the graph represents the loading versus time and each of the remaining lines represents deflection at a

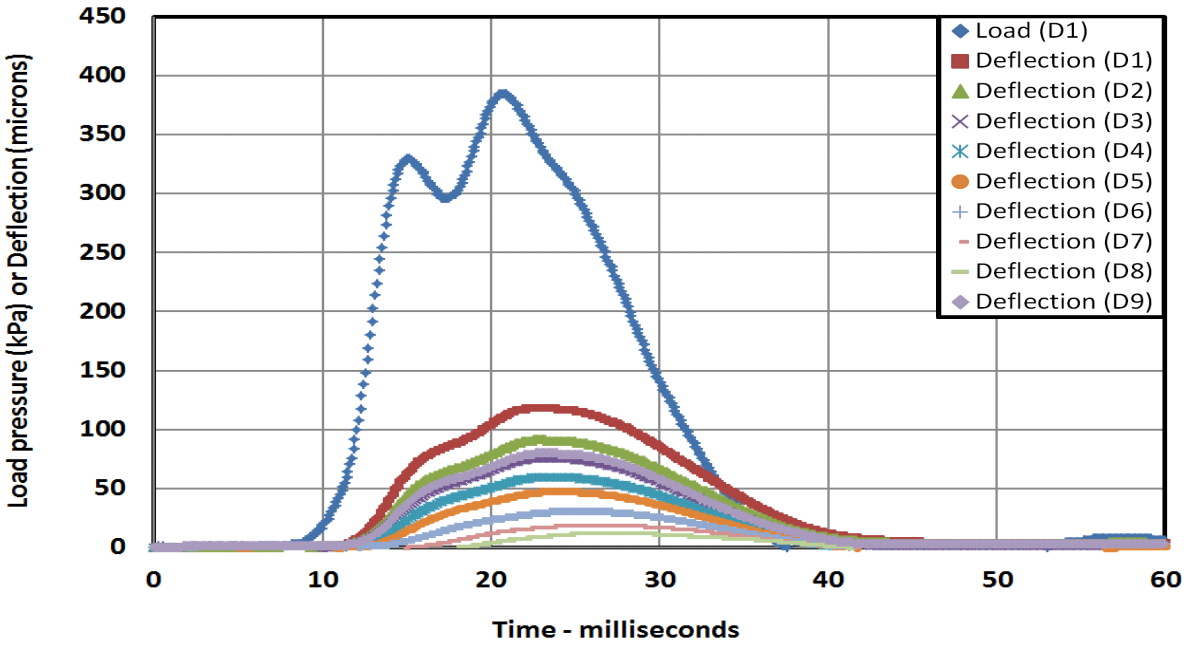

Figure 4-3: Sample FWD time history obtained from field experiments by the LTPP program of FHWA, section 345K02A1 [28].

certain time at various distances (D) away from the loading zone. The distance D corresponds to the values provided in Figure 4-2.

4.2 Description of Databases

Approximately 2,500 unique sections are monitored by the LTPP program throughout their lifetime. Data collected from these sections are organized and distributed through FHWA's Standard Data Release (SDR). The latest version, SDR 25, was made available in January of 2011 containing pavement perfomance data, FWD peak deflections, pavement designs and maintenance schedules, and other valuable information. Due to the large volume of the FWD time history datasets (42.4 GB), they are not included with the SDRs but are available upon request.

The FWD time history databases are recorded with different file extensions and different accuracies. Table 4-3 summarizes the available time history formats, their content, and the

File extension	Content	Data collection frequency (micro-seconds)
*.FWD	Containing both peak deflection data and time history data	200
*.F25	Containing peak deflection data only	200
*.HXT	ASCII files containing converted binary encoded time history data	100
*.DDX	ASCII files converted from MS Access files containing peak and time-history data	100

Table 4.3: Summary of FWD file types and data collection frequencies [32].

data collection frequency.

In total there are roughly 60,000 data files collected over time from the 2,500 LTPP sections. However, FWD time histories with the highest data quality are required for higher accuracy. This study makes use of the file extensions *.DDX and *.HXT which contain 10,094 data files. The steps that were taken to ensure the quality, consistency, and the applicability of the data files for this study are briefly explained here:

- Duplicate *.DDX and *.HXT files were removed from further analysis.
- Since this study only focuses on flexible and rigid pavements, composite pavement data files were removed from further analysis.
- Data files corresponding to non-highway sections were removed from further analysis.
- Since FHWA performs internal quality checks on all datasets and provides quality indicators, only data files with a RECORD_STATUS of E were selected for this study (C, D, and E are the main quality indicators, where C is the worst and E is the best) [27].

After reviewing the data files, 1,079 time history data files corresponding to rigid pavements and 4,564 data files for flexible pavement were selected for further analysis.

4.3 Calibration

Currently, most pavement engineers discard about 99% of the pavement response data captured from FWD tests, as only the peak deflections are used and the time histories are discarded

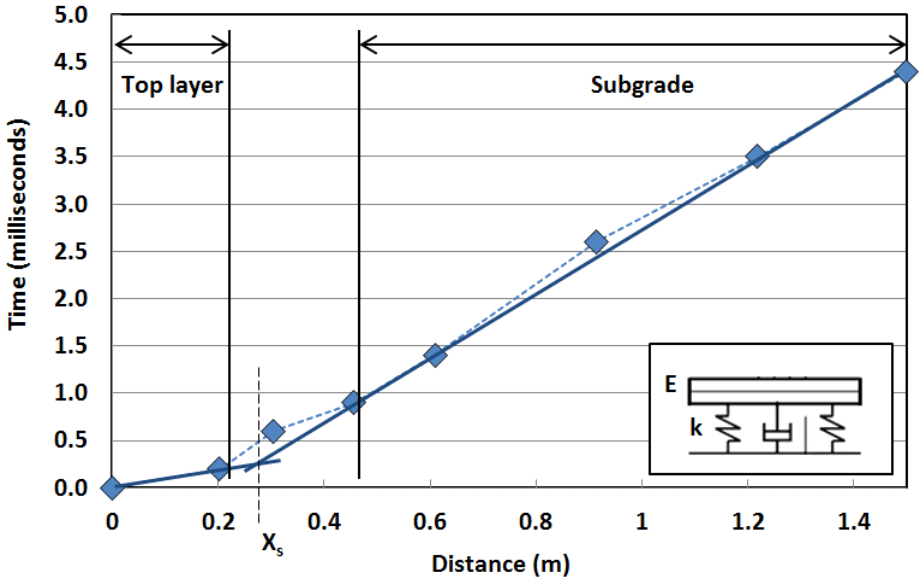

Figure 4-4: Wave propagation in the upper layer and the subgrade of a pavement along with the signal arrival time at various distances for an asphalt pavement, section 345K02A1.

[36]. These peak deflections are used to back calculate the elastic moduli of pavements and subgrade based on the number of layers and their thicknesses, assuming the materials to behave linear elastic. Of the various back calculation software available, FHWA suggests the use of MODCOMP4 to determine the material properties from the collected databases [49]. This software uses the deflection basin profile and iteratively calculates the elastic moduli of each pavement layer with known thicknesses, so that the calculated and measured deflections are within an acceptable range.

Here, we propose an alternative route that separates the calibration step from the validation step. Calibration is achieved by considering the wave propagation that follows the falling weight drop, and which is measured in the FWD as discrete values of arrival time at certain distances. A typical example is displayed in Figure 4-4, as further discussed here below.

4.3.1 Seismic Refraction vs. FWD Test Data

The employment of geophones in an array and an energy source in the FWD test (see Section 4.1.1) is a hallmark of seismic refraction as commonly employed in in the fields of engineering

geology, geotechnical engineering and exploration geophysics. While the main features of the FWD test are quite similar, there are some fundamental differences which make it difficult to employ the standard methods of seismic refraction analysis to the FWD test. In fact, while seismic refraction methods and the FWD test have in common that seismic waves have differing velocities in different types of layers, seismic refraction is based on the principle that the waves are refracted when they cross the boundary between different types (or conditions) of layers. This refraction though, only occurs if each layer has increasing velocity, so that a head wave forms which is registered at the surface [1]. This principle is depicted in Figure 4-5. That is, the seismic refraction method cannot detect a low velocity layer below a high velocity layer, which is the typical case of an asphalt or concrete pavement layer on a softer subgrade. Thus, the main difference between classical seismic refraction and the FWD test is that the initial velocity in short distances from the energy source (inverse of the slope in Figure 4-4) is substantially greater than the velocity registered in larger distances (inverse of second slope in Figure 4-4). This calls for some further considerations to explain the particular shape of the Time–Distance curve in the FWD test.

4.3.2 Background: Wave Propagation

The propagation of body waves is dependent on the material properties of the medium through which the vibrations travel as compressional and shear waves. Compressional waves (also known as pressure, primary, or P-waves) are the fastest traveling of all seismic waves, where the particle motion is extension and compression along the propagating direction. In seismic refraction, it is typically these P-waves which first reach the boundaries in between two different materials. Provided that the deeper layer has a higher stiffness, and thus a higher velocity, the wave refracts along the boundary, and returns to the surface to impact the detectors (geophones). As already noted this is not the case for pavement structures, with a subgrade stiffness several orders of magnitude smaller than the top-layer stiffness. In such systems, a headwave does not form, and it is thus likely that the P-wave continues traveling downward, with minimal defraction at the boundary. In this scenario, the wave measured at the surface in terms of the arrival time of the signal may be understood as a shear wave (also known as secondary, transverse, or S-wave), which is slower than the P-wave, and for which particle motion occur

perpendicular to the propagating direction [1]. For a homogeneous isotropic material, the shear velocity relates to the shear modulus μ and the density ρ by:

$$V_s^2 = \frac{\mu}{\rho} = \frac{E}{2\,(1+\nu)\,\rho} \tag{4.1}$$

where E is the Young's modulus, and ν the Poisson's ratio.

Eq. (4.1) strictly holds for a homogenous material of same stiffness properties and density. For instance, provided that the wave front is contained within the top-layer, the first slope in Figure 4-4 provides a means to determine the pavement stiffness:

$$D < X_s : V_1 = V_s \Rightarrow E = 2\,(1+\nu)\,\rho V_s^2 \tag{4.2}$$

where X_s is the crossover distance, where the change of slope in the wave arrival time – distance plot (See Figure 4-4).

On the other hand, for distances far beyond this crossover distance, a second slope indicates the existence of a second velocity of lower value. If we assume that the wave for this regime is mainly contained in the subgrade, with little refraction at the interface, the influence of the top-layer on the S-wave propagation becomes negligible, and one can attribute the second velocity to the subgrade velocity:

$$D \gg X_s : V_2 = V_s \Rightarrow k = 2\,(1+\nu)\,\rho V_s^2 \tag{4.3}$$

To illustrate our purpose, consider that the effective stiffness and density sensed by the propagating wave is given by a mixture rule, so that:

$$z > h : \frac{\rho_2 V_s^2}{\mu_2} = \frac{\mu_1/\mu_2\,(h/z) + 1 - h/z}{\rho_1/\rho_2\,(h/z) + 1 - h/z} \tag{4.4}$$

where μ_1/μ_2 is the shear modulus contrast between top layer and subgrade, and ρ_1/ρ_2 the associated density contrast. While certainly too rough to capture the specific wave shape that occurs in the FWD test, relation (4.4) nevertheless shows that as the wave propagates deeper into the subgrade, mechanical homogenization leads to reducing the effect of the top layer on the shear velocity measured at the surface. If we replace the velocity in (4.4) by

the distance–to–arrival time ratio D/t, we find that the particular shape of the wave arrival time – distance plot, can be explained by mechanical homogenization; as illustrated in Figure 4-6. In any case, for large values of $D \gg X_s$ for which $h/z \ll 1$, we recover Eq. (4.3) as an asymptotic case. While a refined modeling of the actual wave propagation would allow a refinement of the transition between the two velocity regimes, we shall employ Eqs. (4.2) and (4.3) as two asymptotic cases, for small distances and large distances, respectively. Roesset et al. [35] also developed procedures for estimating the modulus of subgrade directly from deflection time histories of FWD tests under the following assumptions: uniform subgrade, minor impact of pavement layers on the Rayleigh wave velocity of the subgrade, deep bedrock resulting in little interference with the Rayleigh wave propagation, negligible near field effects, negligible difference between Rayleigh wave and shear wave velocities, and that the offset time between far sensors represent subgrade properties. These assumptions also hold true for the procedure in Eqs. (4.2) and (4.3)[1].

Figure 4-7 shows, in more detail, the occurrence of peak deflections at distances away from the loading point through time from Figure 4-3. Plotting the arrival time of wave signals corresponding to the maximum deflection at each offset (Figure 4-7) versus the distance of these points from the loading zone creates two main slopes: at $D < X_s$, relating to the elastic modulus E of the top layer and at $D > X_s$, for the subgrade modulus k.

4.3.3 Application to Data

Rather than discarding the deflection time histories and performing a back calculation, the full FWD database can be used to determine the pavement material moduli from the wave propagation perspective. From these databases, wave speeds through the pavement are calculated, where the material moduli are proportional to the square of the wave velocity [36] (Eqs. (4.2) and (4.3)).

The peak deflection velocity (Figure 4-7) can be measured with good precision from the FWD time histories. This velocity corresponds to the S-wave velocity V_s, and can be used to

[1]The Raleigh wave velocity V_r and the shear wave velocity V_s are close, so that in case of plane wave propagation $V_r = 0.93V_s$ and for axi-symmetric wave propagation $V_r = 0.81V_s$ [35], [8]. Here, we assume that the 7% (plane waves) and 19% (axi-symmetric waves) difference in velocity ratios is negligible, given that the same methodology is used for calculation of E and k for both flexible and rigid pavements.

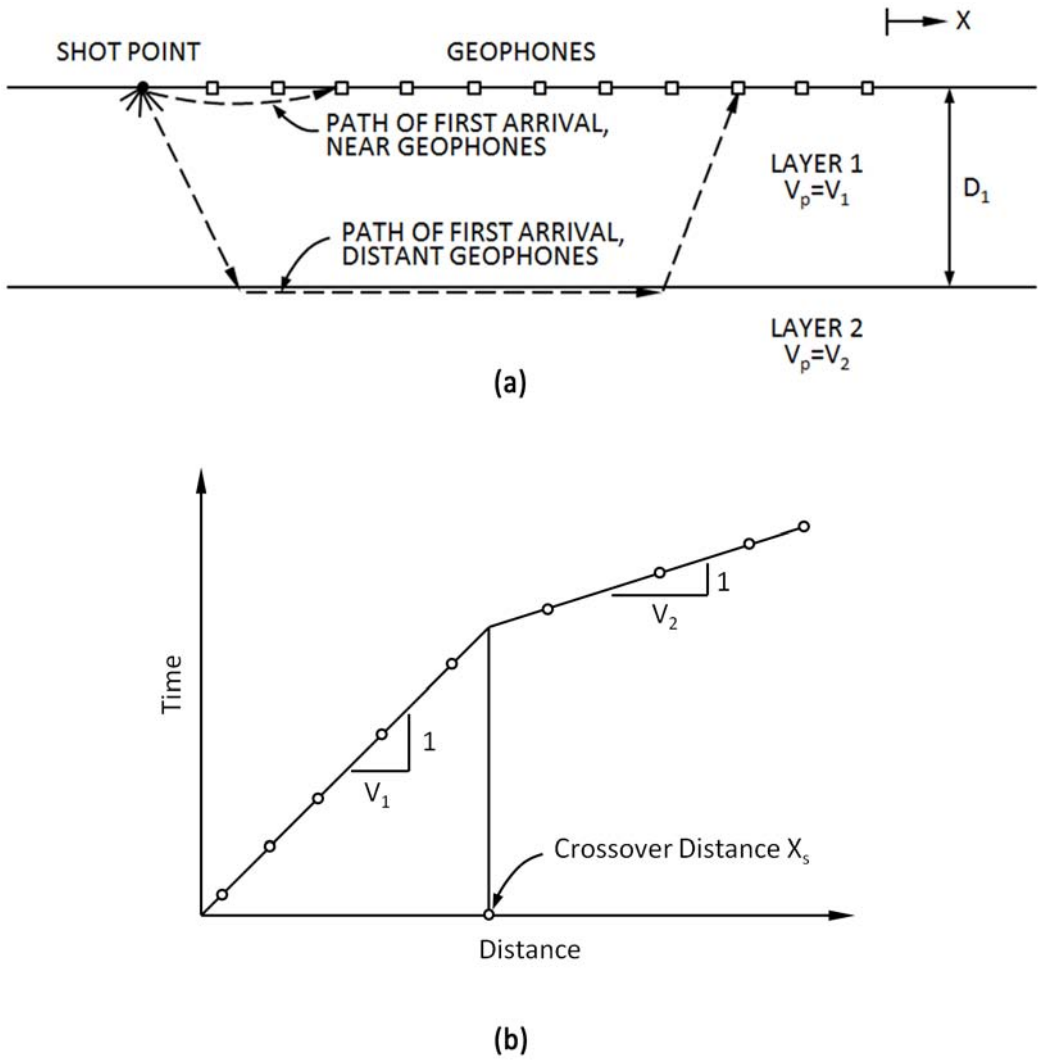

Figure 4-5: (a) Schematic of seismic refraction in a two layered medium. (b) Arrival time-distance plot for $V_2 > V_1$ [1]. Contrast this test with typical FWD measurements, Figure 4-4.

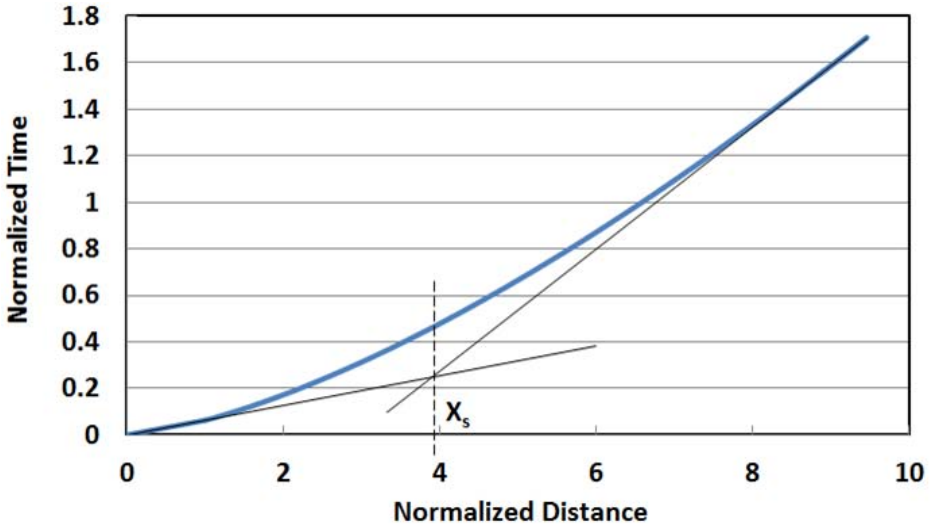

Figure 4-6: Wave arrival time versus distance plot due to mechanical homogenization, explaining the particular shape of FWD test results; results for $\mu_1/\mu_2 = 500$; $\rho_1/\rho_2 = 1.2$.

determine the surface layer elastic modulus (E) and the subgrade modulus (k) using Eq. (4.2) and Eq. (4.3).

In order to verify the calibration method, there is a need to compare E and k values calculated from Eq. (4.2) and Eq. (4.3) with E and k values reported by the Federal Highway Administration. FHWA released back calculated E and k values until SDR version 20, which was released in 2005. However, the back calculation procedure was only applied to FWD data collected by 1/8/1998 and the higher quality data, *.HXT and *.DDX, are available since 3/29/1999. Therefore, in order to compare our calculated moduli values with those reported by FHWA, the latest data files from FHWA and the oldest data files from the FWD time histories were selected for the LTPP sections that did not receive major rehabilitations (overlay, diamond grinding, etc.) between the back calculation date and the next FWD time history measurements. In total, 37 sections were selected for verifying the calculation method.

Values of E and k, obtained from Eq. (4.2) and Eq. (4.3) correspond closely to the E and k values reported by FHWA, and are presented in Table 4-4 and Figure 4-8. The good agreement shows the relevance of the developed wave-propagation for calibration of material properties from FWD tests. The main advantage, yet, of our method is that it provides an access to

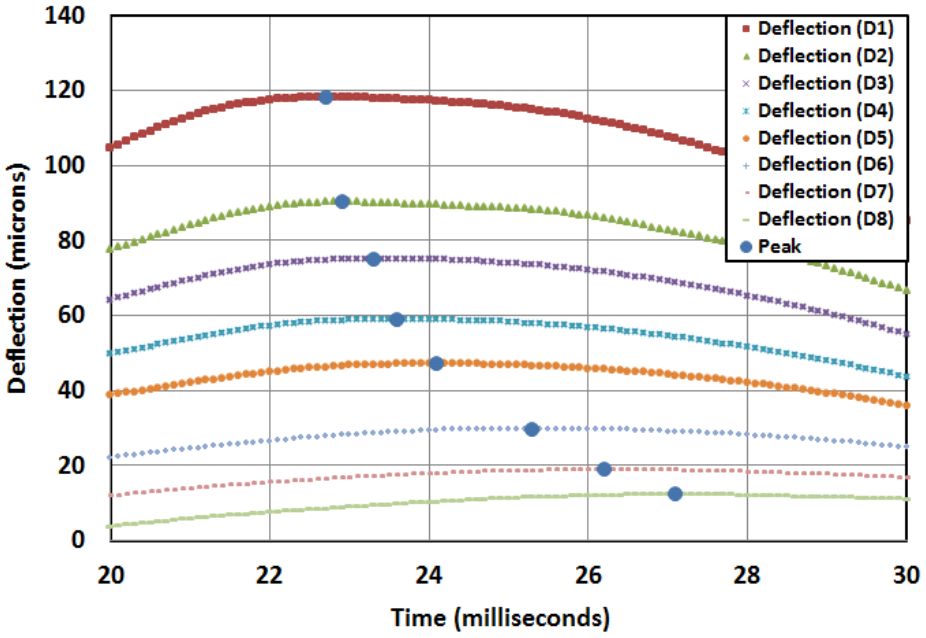

Figure 4-7: Peak deflections from Figure 4-4 showing wave progression through time, section 345K02A1.

these properties independent of deflection. In return, deflection can be used to validate the determined properties.

4.4 Validation

After having calibrated the model to determine top layer and subgrade moduli, validation of the deflection model is carried out against deflection values from the FWD tests at various distances away from the loading point.

Figure 4-9 shows the FWD experimental deflection values versus the predicted model deflection values for the damped and un-damped cases for all datasets. Damping is used as the sole free parameter to improve the model prediction of deflection, as deflection without damping is typically overestimated. The value of damping is calculated by minimizing the difference between the predicted deflection under load, $y(0)$, and the experimental measurement for deflection at this point within a range of $0 < \zeta < 0.4$. It is observed that the experimental deflection

Section ID	Calibration model				FHWA [28]			
	E		k		E		k	
	MPa	psi	MPa	psi	MPa	psi	MPa	psi
40121	19328	2.80E+06	195	2.83E+04	18947	2.75E+06	212	3.07E+04
40122	15813	2.29E+06	57	8.27E+03	16866	2.45E+06	71	1.03E+04
40120	14411	2.09E+06	89	1.29E+04	17466	2.53E+06	95	1.38E+04
40118	26549	3.85E+06	235	3.41E+04	27100	3.93E+06	212	3.07E+04
40116	14898	2.16E+06	68	9.86E+03	15848	2.30E+06	88	1.28E+04
40123	12610	1.83E+06	138	2.00E+04	14050	2.04E+06	158	2.29E+04
40115	13428	1.95E+06	37	5.37E+03	13472	1.95E+06	48	6.96E+03
40124	14019	2.03E+06	82	1.19E+04	13350	1.94E+06	91	1.32E+04
40119	17077	2.48E+06	122	1.77E+04	18344	2.66E+06	122	1.77E+04
40117	20251	2.94E+06	168	2.44E+04	20725	3.01E+06	180	2.61E+04
4A430	29551	4.29E+06	109	1.58E+04	32800	4.76E+06	125	1.81E+04
4A410	39171	5.68E+06	141	2.05E+04	39675	5.75E+06	154	2.23E+04
40213	31906	4.63E+06	70	1.02E+04	32900	4.77E+06	79	1.15E+04
170605	26083	3.78E+06	120	1.74E+04	26850	3.89E+06	126	1.83E+04
87B330	4102	5.95E+05	228	3.31E+04	4439	6.44E+05	247	3.58E+04
87B320	3707	5.38E+05	94	1.36E+04	5005	7.26E+05	110	1.60E+04
484142	31432	4.56E+06	183	2.65E+04	38289	5.55E+06	259	3.76E+04
67493	34894	5.06E+06	212	3.07E+04	37993	5.51E+06	244	3.54E+04
537409	19226	2.79E+06	70	1.02E+04	21045	3.05E+06	92	1.33E+04
533014	23651	3.43E+06	103	1.49E+04	24180	3.51E+06	126	1.83E+04
493011	34489	5.00E+06	232	3.36E+04	34910	5.06E+06	298	4.32E+04
274040	28232	4.09E+06	100	1.45E+04	30998	4.50E+06	113	1.64E+04
190217	29489	4.28E+06	158	2.29E+04	34522	5.01E+06	155	2.25E+04
190213	25362	3.68E+06	125	1.81E+04	29152	4.23E+06	138	2.00E+04
323013	25483	3.70E+06	156	2.26E+04	28516	4.14E+06	182	2.64E+04
533011	24633	3.57E+06	112	1.62E+04	31742	4.60E+06	124	1.80E+04
260221	21300	3.09E+06	180	2.61E+04	26962	3.91E+06	175	2.54E+04
260213	25671	3.72E+06	125	1.81E+04	29034	4.21E+06	154	2.23E+04
200201	29247	4.24E+06	154	2.23E+04	33294	4.83E+06	159	2.31E+04
833802	29157	4.23E+06	110	1.60E+04	32855	4.77E+06	136	1.97E+04
200205	34136	4.95E+06	126	1.83E+04	35466	5.14E+06	191	2.77E+04
200208	24939	3.62E+06	217	3.15E+04	30192	4.38E+06	249	3.61E+04
170605	26064	3.78E+06	170	2.47E+04	30094	4.36E+06	185	2.68E+04
40216	29236	4.24E+06	196	2.84E+04	30716	4.45E+06	245	3.55E+04
40218	20363	2.95E+06	201	2.92E+04	22029	3.20E+06	235	3.41E+04
40220	17090	2.48E+06	281	4.08E+04	20198	2.93E+06	321	4.66E+04
40223	26216	3.80E+06	265	3.84E+04	29968	4.35E+06	288	4.18E+04

Table 4.4: Comparison of top layer and subgrade modulus values from model calibration using falling weight deflectometer time histories and from Federal Highway Administration reported data [28].

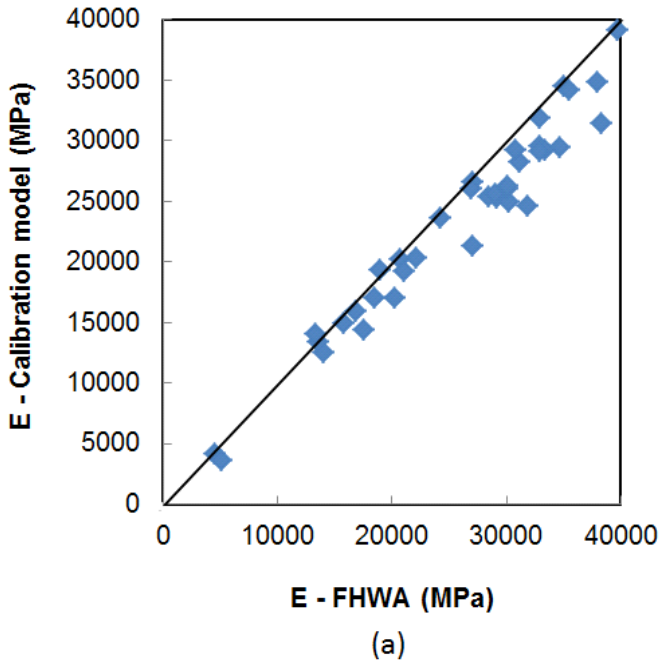

(a)

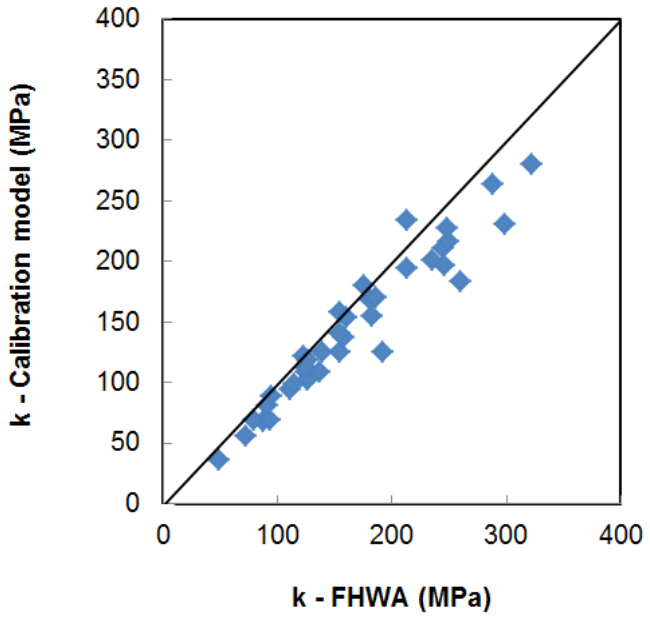

(b)

Figure 4-8: Comparison of top layer modulus E and subgrade modulus k values obtained from calibration model and from the LTPP reported data [28].

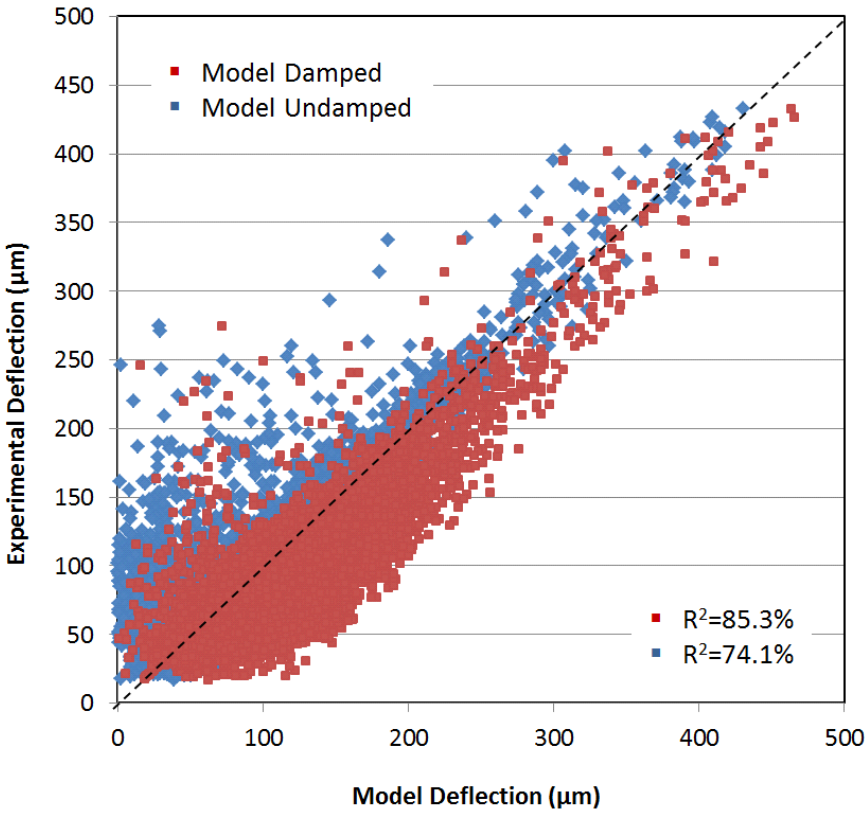

Figure 4-9: Model validation: measured experimental versus model predicted deflection values for damped and undamped cases.

and predicted values from the model are in very good agreement for both the damped and undamped systems, but are refined in the case of the damped subgrade. Thus, a combination of the calibration wave propagation model with the validation deflection model provides a means to extract all model material parameters from the FWD tests.

Figures 4-10 and 4-11 present the modeled and measured deflection basins for a concrete and an asphalt pavement section. The solid lines are the model output for the deflection basins of the undamped case; the dashed lines represent the model prediction of deflection for the damped case; and the red circles are that of the FWD test recorded deflections. It is observed that the model predictions match the experimental deflection to an acceptable accuracy for both the damped and undamped cases.

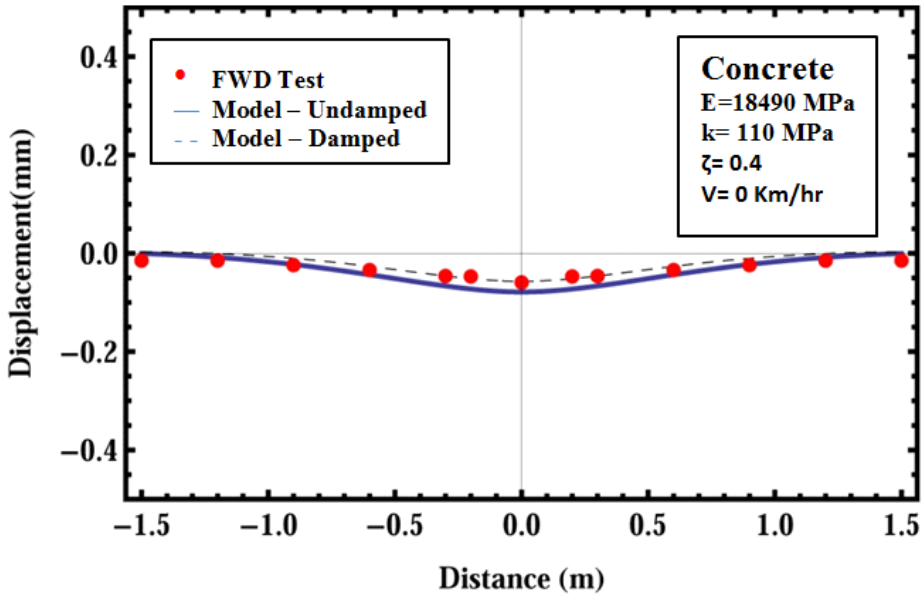

Figure 4-10: FWD test versus model prediction of the deflection basin for a concrete section.

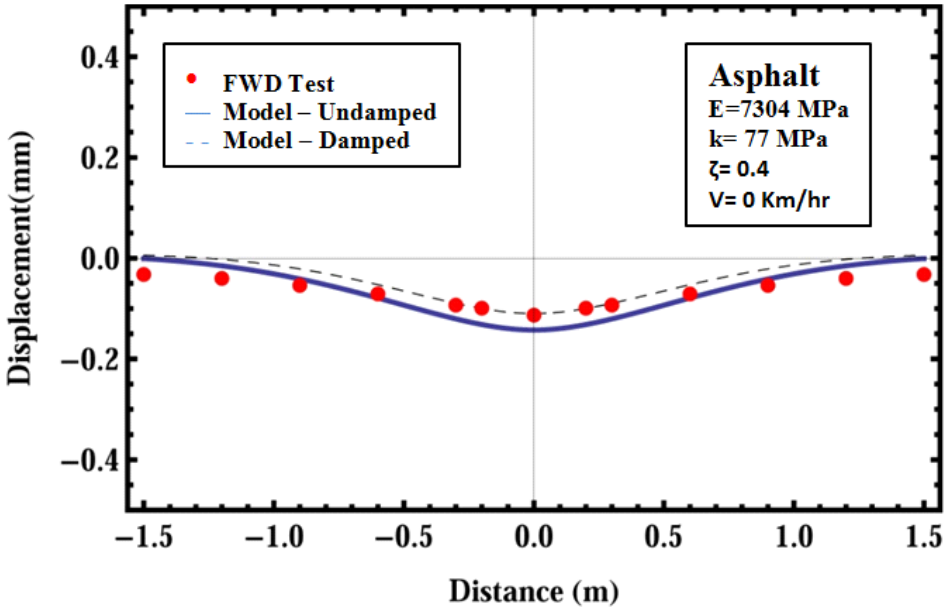

Figure 4-11: FWD test versus model prediction of the deflection basin for an asphalt section.

4.5 Parameter Relations

Having calibrated and validated the model to calculate all material parameters of our model and the pavement response, it is necessary to investigate the relationship between the model material parameters (E, k, ζ) and structural parameters (h) to assure they are uncorrelated. Here, the relationships between top layer elastic modulus (E), subgrade modulus (k), top layer thickness (h), and the damping ratio (ζ) are considered.

4.5.1 Elastic Moduli and Pavement Thickness

To assure accuracy of the calibration sequence described in Section 4.3, the top layer elastic modulus E, the subgrade modulus k, and top layer thickness h have to be uncorrelated. Thus, these cross-plots show that no correlation exists between these parameters. Figure 4-12 shows the relationship between the subgrade modulus k and the top layer elastic modulus E for the asphalt and concrete sections. Also, the relationship between the top layer thickness h with the elastic modulus E is investigated for both pavement types and shown in Figure 4-13.

4.5.2 Elastic Moduli and Damping Ratio

The damping ratio ζ, an ever-present term in the subgrade soil, is used within the model as the sole free parameter to improve the predicted model deflection. Hence, its relationship with the top layer elastic modulus E and the subgrade modulus k is of high importance and is investigated for the 5,643 datasets considered to determine whether damping is correlated with other material properties. Figure 4-14 shows that there is no relationship between the elastic modulus of flexible and rigid pavements with the damping ratio; while Figure 4-15 shows that the subgrade modulus and the damping ratio are also uncorrelated for asphalt and concrete sections. Otherwise said, the three model material parameters (E, k, ζ) along with thickness (h) represent a minimum set of material and structural properties to represent accurately the dynamic response of pavements to vehicle load. This justifies a posteriori the choice of the simple pavement model considered here.

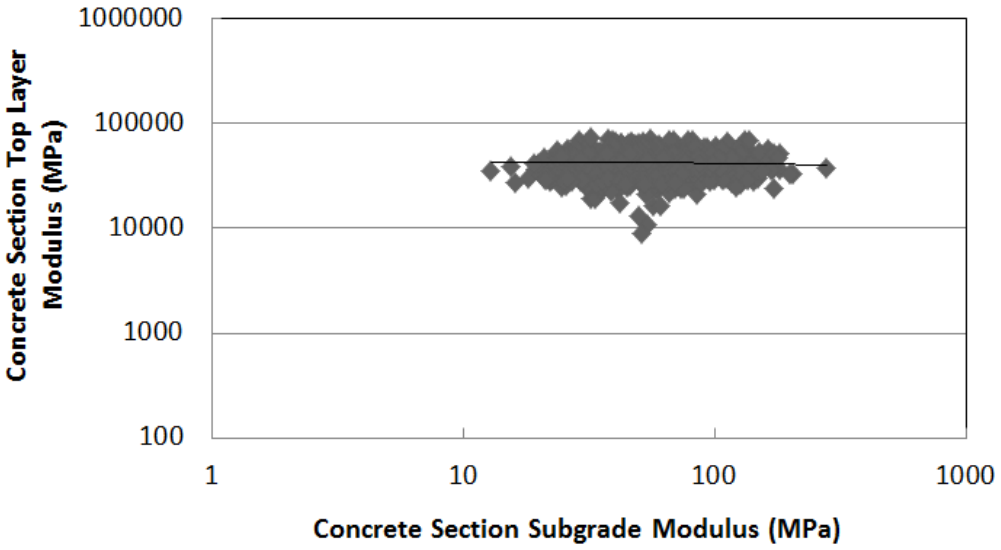

(a)

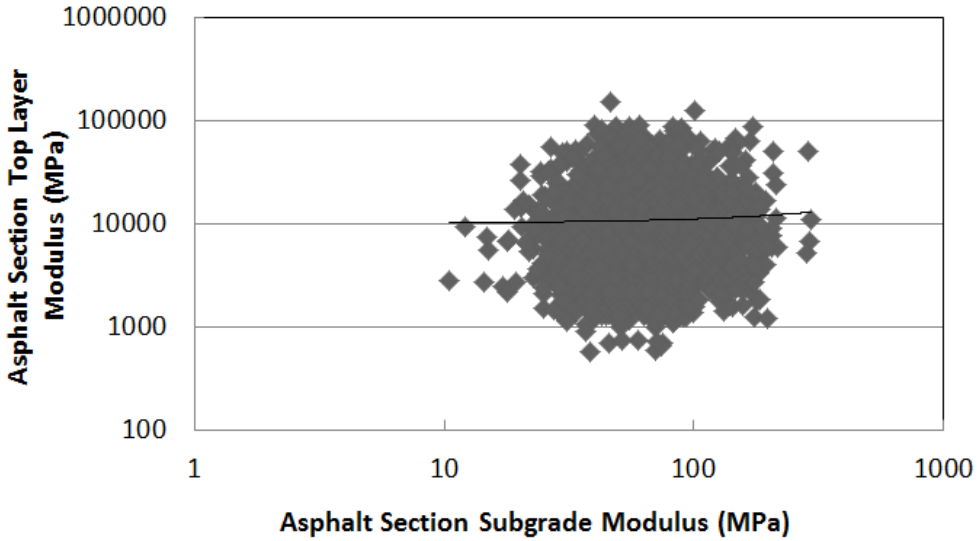

(b)

Figure 4-12: Cross-plot of top layer modulus E vs. subgrade modulus k for (a) concrete and (b) asphalt sections, showing no correlation between the two elements.

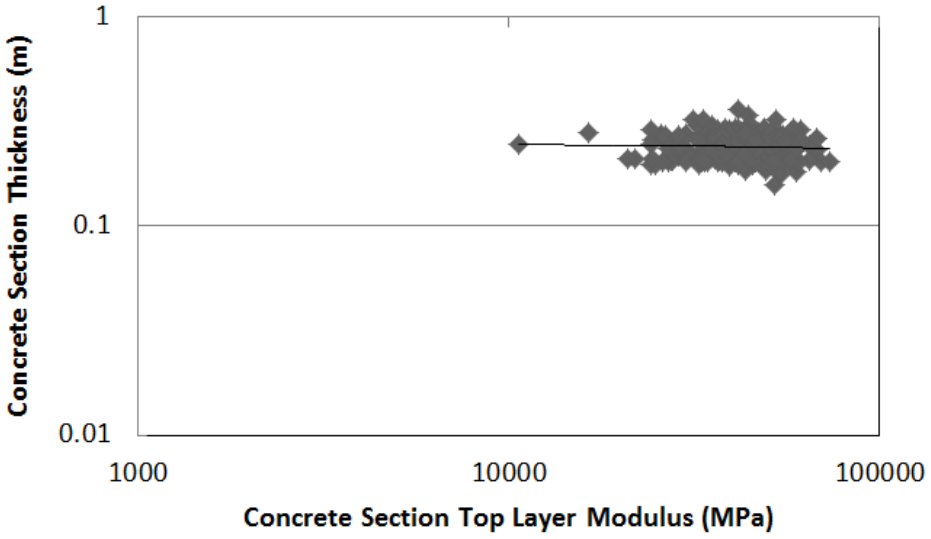

(a)

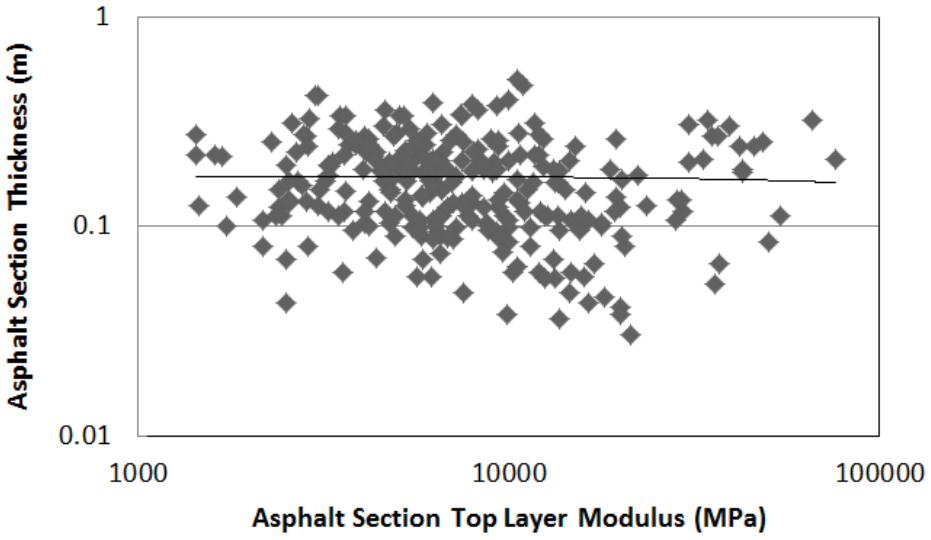

(b)

Figure 4-13: Cross-plot of top layer modulus E vs. top layer thickness h for (a) concrete and (b) asphalt sections, showing no correlation between the two elements.

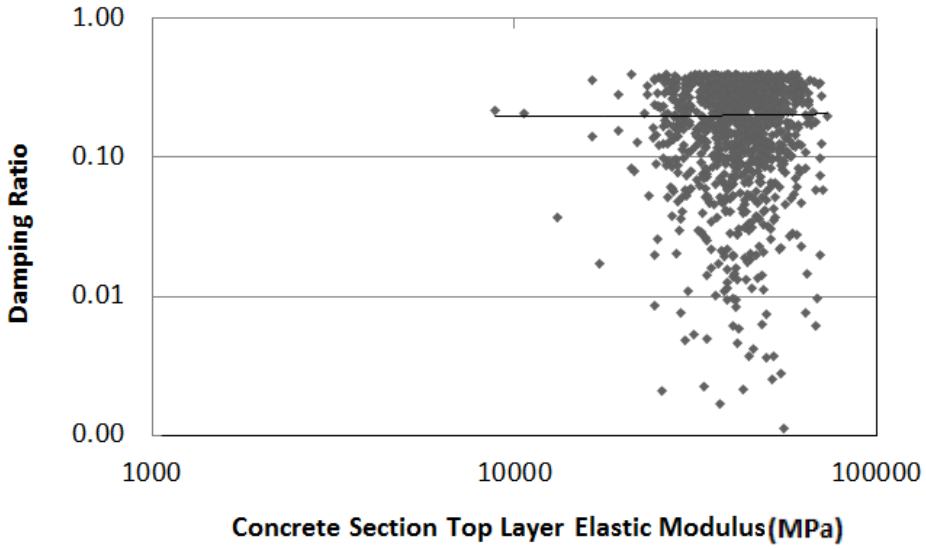

(a)

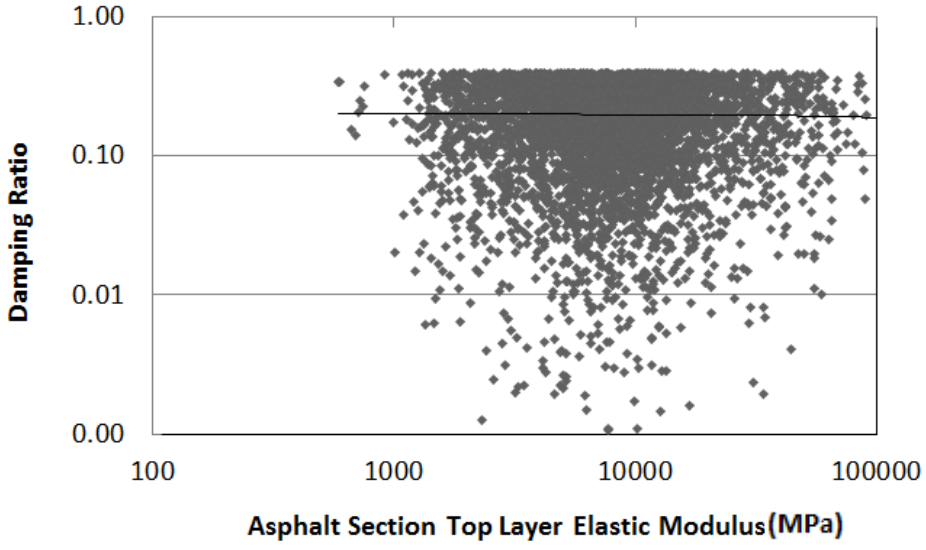

(b)

Figure 4-14: Cross-plot of the damping ratio ζ vs. top layer elastic modulus E of (a) concrete (b) asphalt sections showing no correlation between the two elements.

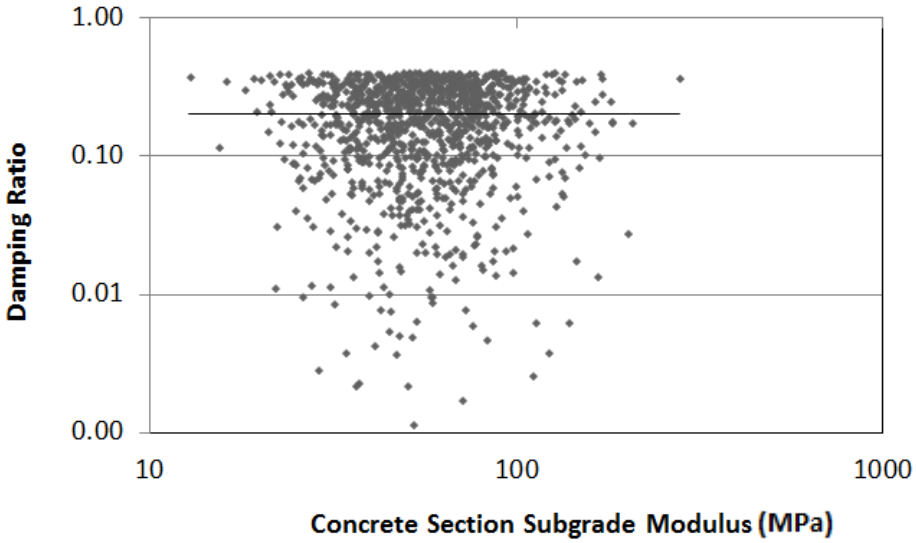

(a)

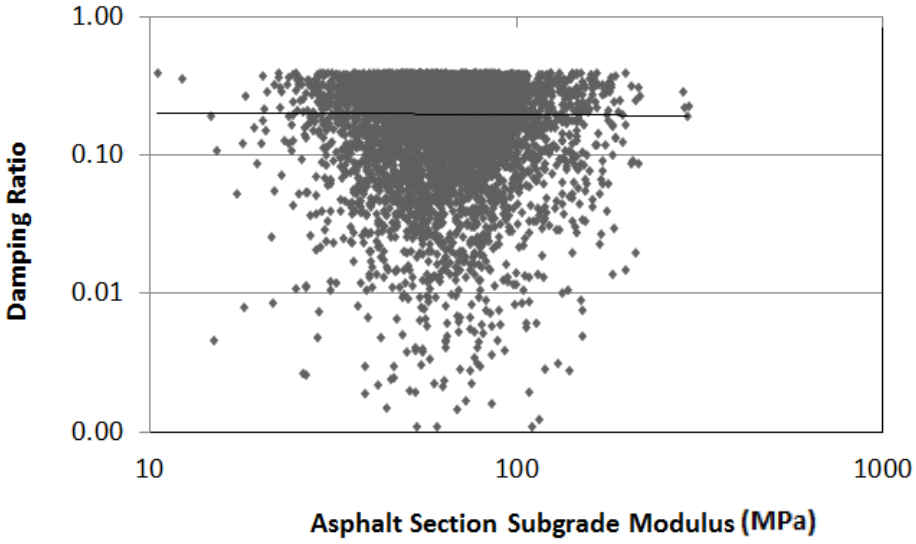

(b)

Figure 4-15: Cross-plot of the damping ratio ζ vs. subgrade modulus k of (a) concrete (b) asphalt sections showing no correlation between the two elements.

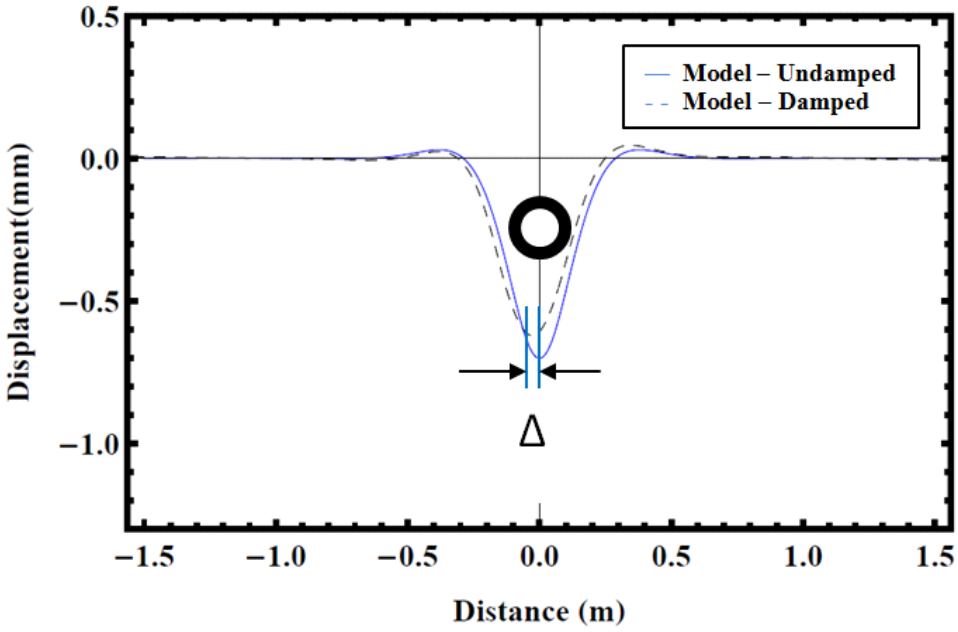

Figure 4-16: Effect of damping at vehicle velocity greater than zero. Figure represents a pavement with EI=2.3 kN.m^2, k=68.9 MPa, m=48.2 kg/m, q=-70 kN/m, a=0.075 m, V=9.525 m/s, and ζ=0.3.

4.6 Effect of Damping

Since damping was selected as a free variable to enhance the model's output and the subgrade always has damping, it is important to understand its role within the model. Here, the effect of subgrade damping on deflection for a moving load is investigated.

As shown in Figures 4-10 and 4-11, as damping increases, the maximum deflection at the loading point decreases. However, these figures correspond to the vehicle velocity of zero (V=0) for comparison to FWD test results. Figure 4-16 shows the effect of damping at the speed of V= 9.52 m/s (35 km/hr, 21 mi/hr). It is shown that with presence of damping and velocity, a distance lag Δ is created between the loading point and the point of maximum deflection. The tire, represented by a black ring, is therefore forced to travel uphill during vehicle movement, on a grade that is directly related to the structural and material properties of the pavement. This relationship, along with the impact of the added grade is further discussed in Chapter 5.

It is hence interesting to investigate the combined effect of damping and vehicle velocity as

predicted by the model. By making use of the model, a relationship can be drawn between the damping ratio ζ, the vehicle velocity V, and the changes in pavement deflection. Figure 4-17 shows this effect: at a highway speed of 100 km/hr (62 mi/hr) the influence of the damping ratio ζ on the pavement deflection is of second order. Yet, it is worth differentiating between the impact of damping on deflection and its impact on the distance lag Δ. Even though damping does not influence the deflection of the pavement as much as material and structural factors do, its impact within the model and within pavement-vehicle interaction is significant and non-negligible. In fact, the combined effect of damping and vehicle velocity creates the distance lag Δ which puts the vehicle on a slope. This slope increases with added damping and velocity, as shown in Figure 4-18. In this figure, the distance lag Δ is normalized with regard to the characteristic wavelength L_s of the beam on a viscoelastic foundation, as described in Section 3.2[2].

4.7 Chapter Summary

This chapter focused on model calibration and validation through implementing the FWD databases provided by FHWA's Long-Term Pavement Performance program. Over 5,500 datasets were used to evaluate the model's capabilities in deflection prediction, parameter interaction, calibration, and validation. The first-order deflection model predicts the pavement response with high accuracy. It was also shown that model material and structural parameters are uncorrelated; and the impact of damping within the model was investigated. With the model in place, and the FWD databases evaluated, the analysis on the impact of pavement deflection on fuel consumption can be performed on the LTPP network scale.

It is important to note that both pavement types are modeled elastic and the time dependent behavior of flexible pavements is not considered. Moreoever, the pavement system is modeled as a beam on a viscoelastic subgrade and the impact of the base layer on pavement performance is not included. However, the damping term is utilized to minimize the difference between the model predicted deflection and the measured deflection from FWD tests.

[2]The characteristic wavelength L_s of the beam on viscoelastic foundation is calculated as $L_s = (4d/k)^{1/4}$ where $d = EI$ is the rigidity of the beam, E is the top layer modulus, I is the moment of inertia of the beam, and k is the subgrade modulus.

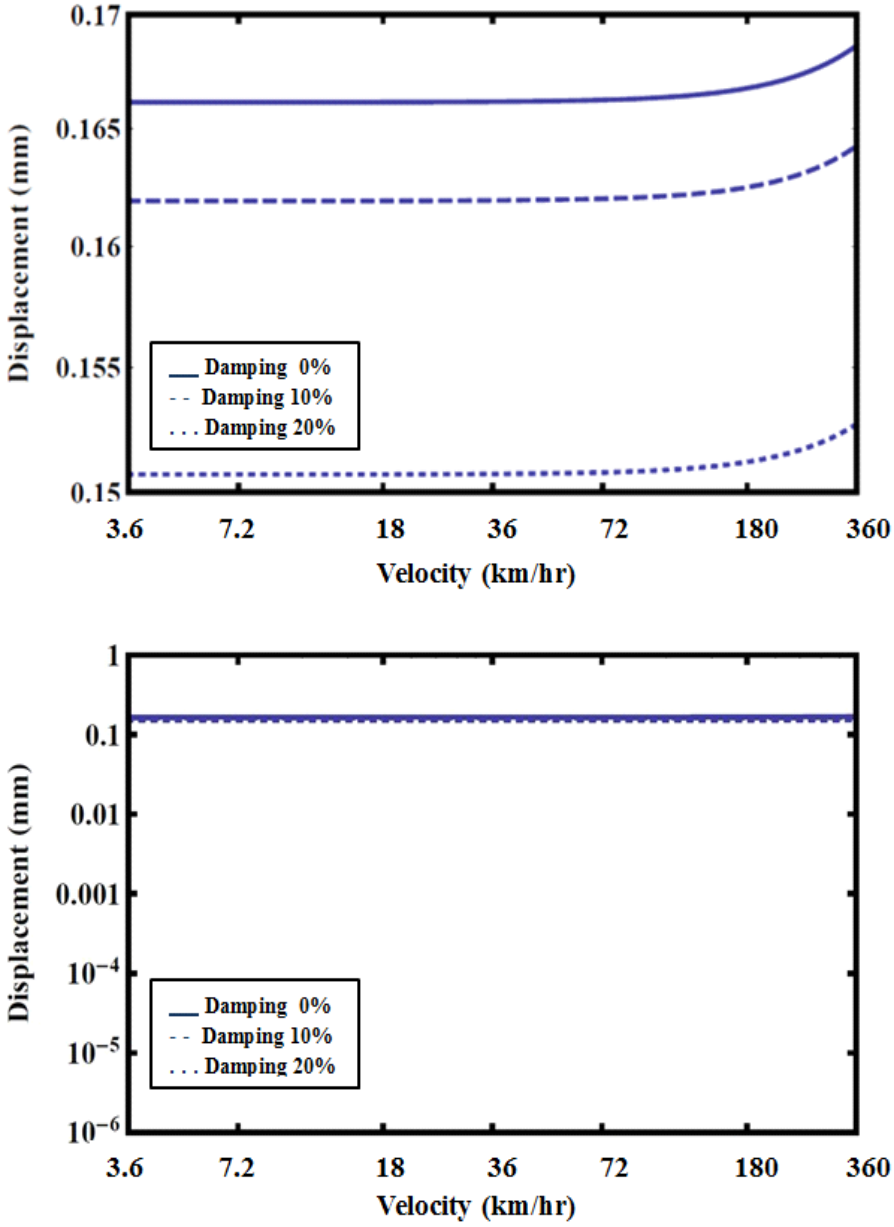

Figure 4-17: Relationship between the damping ratio ζ, velocity V, and pavement deflection at two vertical scales showing the second-order effect of damping on deflection. Figure represents a pavement with EI=2.3 kN.m^2, k=68.9 MPa, m=48.2 kg/m, q=-70 kN/m, a=0.075 m.

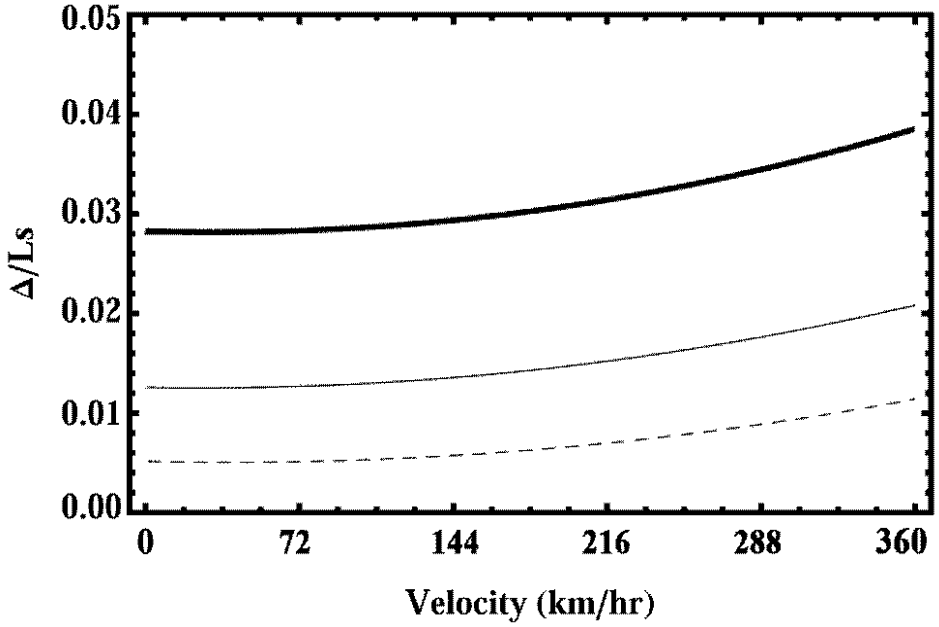

Figure 4-18: The combined effect of vehicle velocity V and damping ratio ζ on the normalized distance lag Δ in regards to the characteristic wavelength L_s. Figure represents a pavement with EI=2.3 kN.m^2, k=68.9 MPa, m=48.2 kg/m, q=-70 kN/m, a=0.075 m.

Chapter 5

Scaling of Pavement Parameters

Now that the model has been calibrated and validated, it is necessary to obtain the importance of different parameters that affect fuel consumption due to the deflection of a pavement. To achieve this goal, this chapter presents scaling relationships between structural and material parameters that affect pavement deflection within PVI.

5.1 Reminder: Bernoulli-Euler Beam Model

The Bernoulli-Euler beam on a viscoelastic foundation presented in Chapter 3 and calibrated and validated in Chapter 4 is an idealized model that allows first-order understanding of the importance of different input parameters and their impact on pavement deflection. From Chapter 3, we recall Eq. (3.13):

$$y(\eta) = \frac{q}{k} \times \Pi \left(\overline{\eta} = \frac{\eta}{(d/k)^{1/4}}; \zeta = \frac{c}{c_{crit}}; \overline{V} = \frac{V}{V_{os}} \right) \tag{5.1}$$

where $y(\eta)$ is the key output of the model, the beam deflection profile, and q is the applied external load. We recognize the characteristic wavelength of the beam model in Eq. (5.1), illustrated in Figure 5-1:

$$L_s \sim (d/k)^{1/4} \tag{5.2}$$

The dimensionless quantity of subgrade damping ratio ζ is the ratio of the damping coefficient c to the critical damping coefficient of the substrate $\zeta = \frac{c}{c_{crit}}; c_{crit} = 2\sqrt{mk}$; and $\overline{V}$ is

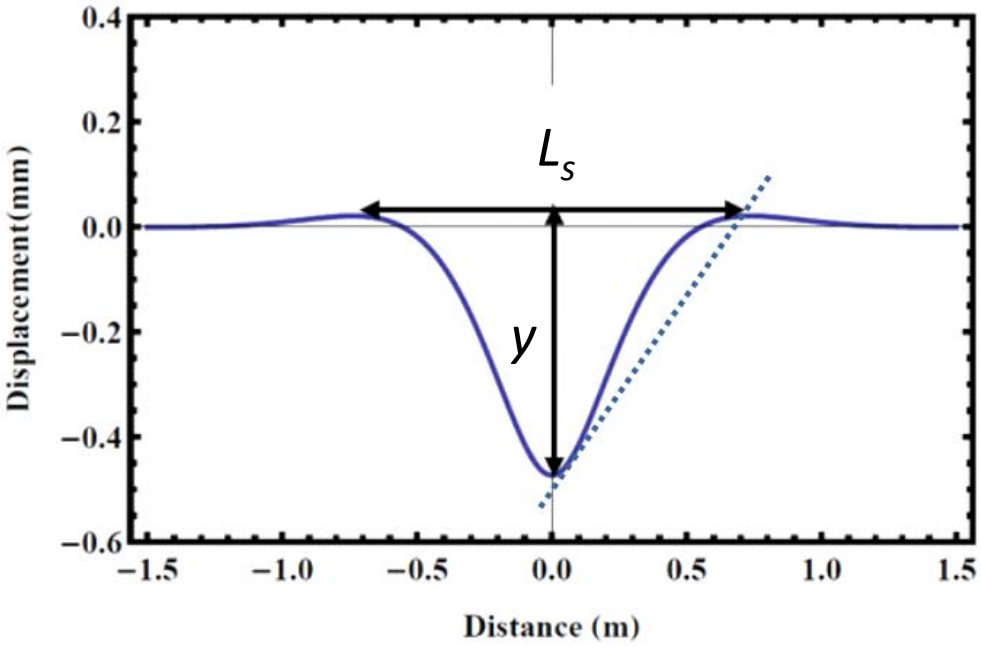

Figure 5-1: Representation of maximum pavement deflection y under load and characteristic wavelength L_s.

the velocity ratio relative to the oscillation velocity $\overline{V} = \frac{V}{V_{os}}; V_{os} = (d/k)^{1/4}(k/m)^{1/2}$. Also, $d = EI$ is the rigidity of the beam where $I = h^3/12$. These parameters correspond to the pavement structural and material properties of top layer elastic modulus E, subgrade modulus k, top layer thickness h, and mass per unit length m.

Figure 5-1 shows a deflected pavement with two characteristic quantities: y is the maximum deflection under the load for $y(0)$, and L_s is the characteristic wavelength (width) of the deflection basin. While damping has a second order effect on pavement deflection (see section 4.6), the combination of the ever present soil damping and vehicle velocity creates a distance lag Δ which locates the maximum pavement deflection behind the direction of motion. This distance lag causes the moving load, here the vehicle wheels, to move uphill during travel.

As shown in Figure 5-2, the approach slope varies throughout the deflection basin, and depends on the damping ratio ζ. In order to avoid these variations, an average slope GR is defined using the characteristic wavelength L_s and the maximum deflection y as the change in

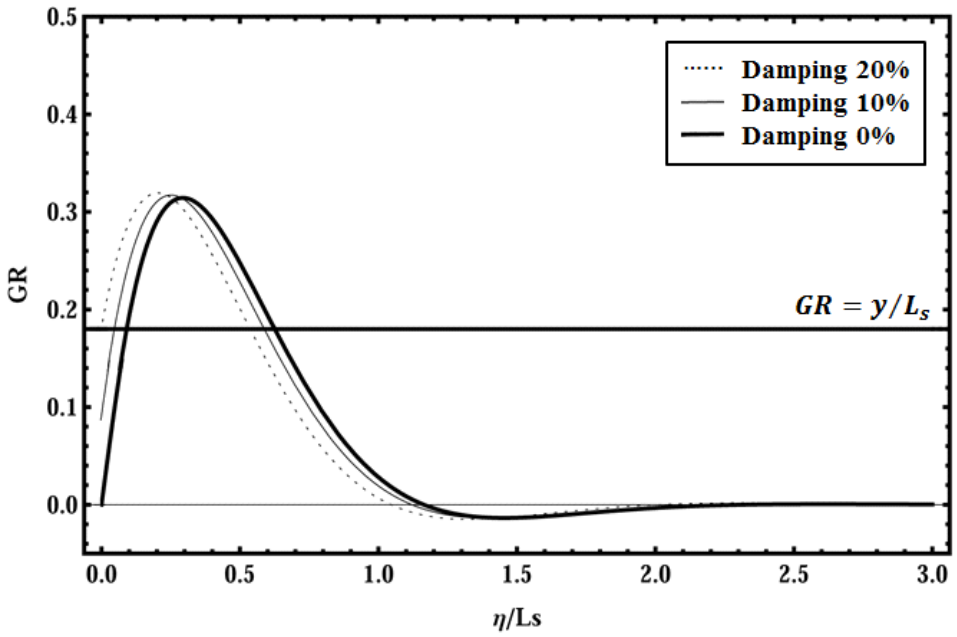

Figure 5-2: Effect of the damping ratio ζ on deflection basin approach slope GR. Figure represents a pavement with EI=2.3 kN.m^2, k=68.9 MPa, m=48.2 kg/m, q=-70 kN/m, a=0.075 m, V=9.525 m/s.

the pavement's grade compared to that of a pavement with no deflection as:

$$GR = \frac{w}{L_s} \tag{5.3}$$

In what follows, each of the main parameters of external load q, top layer modulus E, subgrade modulus k, and top layer thickness h and their effects on PVI are discussed.

5.2 Scaling of Weight q

To illustrate the scaling approach we consider first the external load q. Because of the linear elastic nature of the model, the magnitude of deflection y is linearly related to this load. Figure 5-3 illustrates the relationship between load and deflection, considering q equal to that of a passenger vehicle (axle load of 8 kN), a truck with a dual tire configuration (axle load of 80 kN), and one with a wide-base tire (axle load of 110 kN) [9]. It is interesting to note from the model that the characteristic wavelength L_s is not related to the load, as shown in Figure 5-3. From Eq. (5.1) we write:

$$y\left(q = \lambda q_0\right) = \frac{q}{k} \times \Pi\left(\overline{\eta} = \frac{\eta}{(d/k)^{1/4}}; \zeta = \frac{c}{c_{crit}}; \overline{V} = \frac{V}{V_{os}}\right) = \lambda^1 y(q_0) \tag{5.4}$$

where $\lambda \in \mathbb{R}^+$ is a non-negative scalar. Furthermore, from Eq. (5.2) we readily recognize that:

$$L_s\left(q = \lambda q_0\right) = \lambda^0 L_s(q_0) \tag{5.5}$$

Thus, from Eq. (5.3) to Eq. (5.5):

$$GR(q = \lambda q_0) = \frac{y(q = \lambda q_0)}{L_s(q = \lambda q_0)} = \frac{\lambda^1 y(q_0)}{\lambda^0 L_s(q_0)} = \lambda^1 GR(q_0) \tag{5.6}$$

Thus, as expected, the slop GR scales linearly with the weight:

$$GR(q) \sim q^1 \tag{5.7}$$

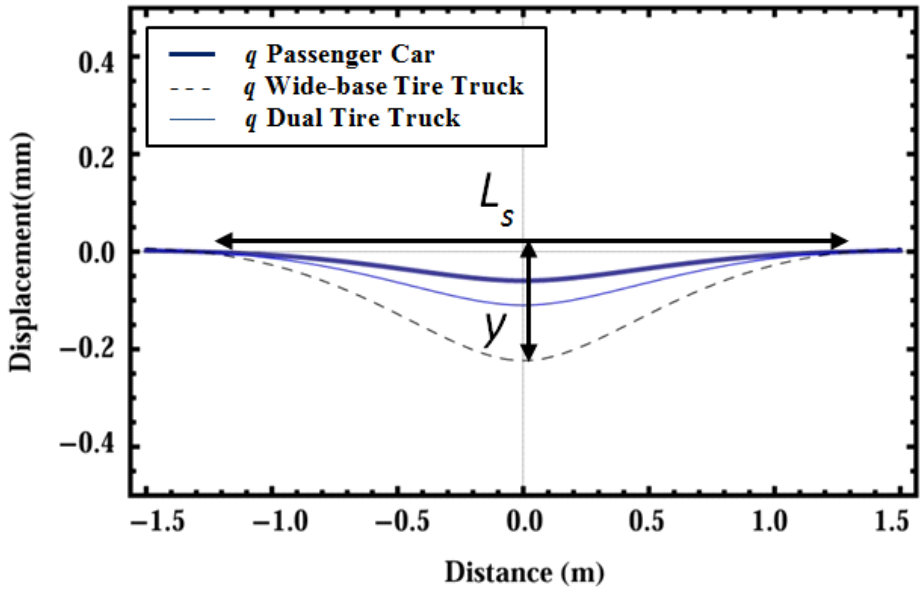

Figure 5-3: Sensitivity of maximum pavement deflection y and characteristic wavelength L_s to load weight q.

We will use this scaling approach for all other model parameters.

5.3 Scaling of Top Layer Modulus E

An important parameter of rigid and flexible pavements is the elastic modulus. Rigid pavements generally have a higher modulus (E) value compared to that of flexible pavements. Figure 5-4 shows the sensitivity of the maximum deflection y and the characteristic wavelength L_s to changes in the top layer modulus E, as calculated from the model. It is observed that as E increases, the deflection y decreases, however, the characteristic wavelength of the deflection basin L_s increases, too.

Then using Eq. (5.1) and Eq. (5.2) as before, we find that:

$$y\left(E=\lambda E_0\right)=\frac{q}{k}\times\Pi\left(\overline{\eta}=\frac{\eta}{(d/k)^{1/4}};\zeta=\frac{c}{c_{crit}};\overline{V}=\frac{V}{V_{os}}\right)=\lambda^{-1/4}y(E_0) \tag{5.8}$$

$$L_s\left(E=\lambda E_0\right)=\lambda^{+1/4}L_s(E_0) \tag{5.9}$$

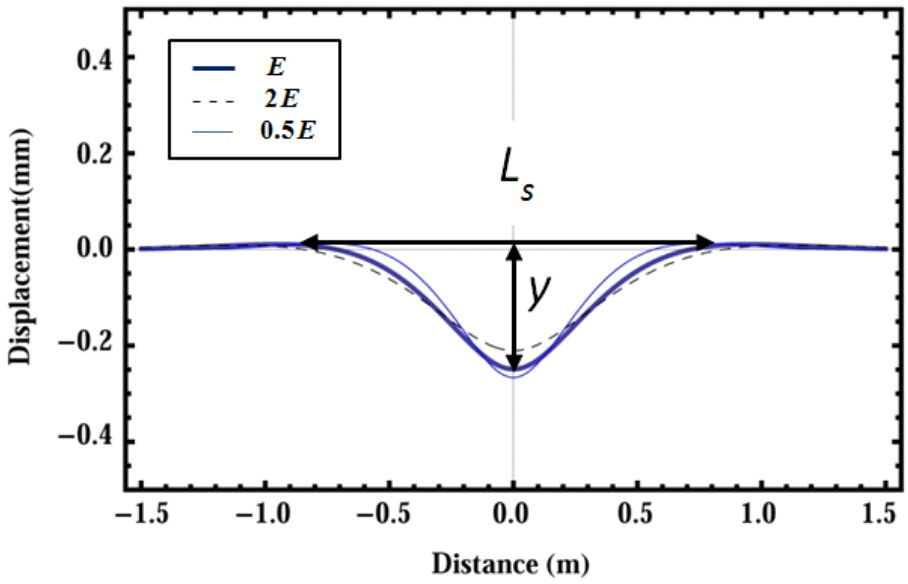

Figure 5-4: Sensitivity of maximum pavement deflection y and characteristic wavelength L_s to top layer modulus E.

From Eq. (5.3), we thus obtain:

$$GR(E = \lambda E_0) = \frac{y(E = \lambda E_0)}{L_s(E = \lambda E_0)} = \frac{\lambda^{-1/4} y(E_0)}{\lambda^{+1/4} L_s(E_0)} = \lambda^{-1/2} GR(E_0) \tag{5.10}$$

Therefore, the grade scales with the top layer modulus as:

$$GR(E) \sim E^{-1/2} \tag{5.11}$$

5.4 Scaling of Subgrade Modulus k

Another factor that can have an influence on both deflection and width of the deflection basin is the subgrade modulus k. Unlike in the case of the top layer modulus, as k increases, the deflection y and the characteristic wavelength L_s decrease, as shown in Figure 5-5. From Eq.

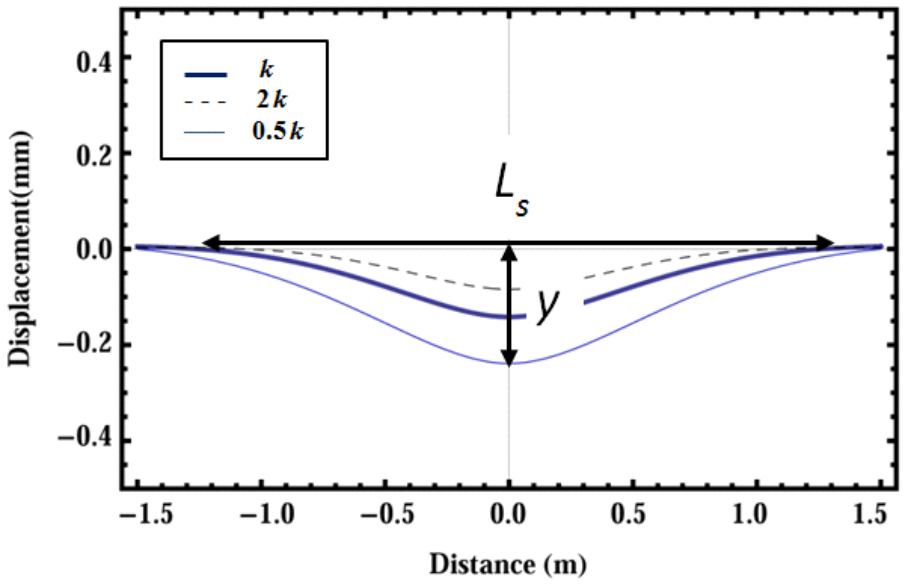

Figure 5-5: Sensitivity of maximum pavement deflection y and characteristic wavelength L_s to subgrade modulus k.

(5.1) through Eq. (5.3), we find that:

$$y\left(k=\lambda k_0\right)=\frac{q}{k}\times\Pi\left(\overline{\eta}=\frac{\eta}{(d/k)^{1/4}};\zeta=\frac{c}{c_{crit}};\overline{V}=\frac{V}{V_{os}}\right)=\lambda^{-3/4}y(k_0) \tag{5.12}$$

$$L_s\left(k=\lambda k_0\right)=\lambda^{-1/4}L_s(k_0) \tag{5.13}$$

$$GR(k=\lambda k_0)=\frac{y(k=\lambda k_0)}{L_s(k=\lambda k_0)}=\frac{\lambda^{-3/4}y(k_0)}{\lambda^{-1/4}L_s(k_0)}=\lambda^{-1/2}GR(k_0) \tag{5.14}$$

Thus, GR scales with the subgrade modulus as:

$$GR(k)\sim k^{-1/2} \tag{5.15}$$

5.5 Scaling of Top Layer Thickness h

Top layer thickness h is an important criterion for design, and plays a major role in the scaling relationships. This element, much like the top layer modulus, affects the maximum deflection

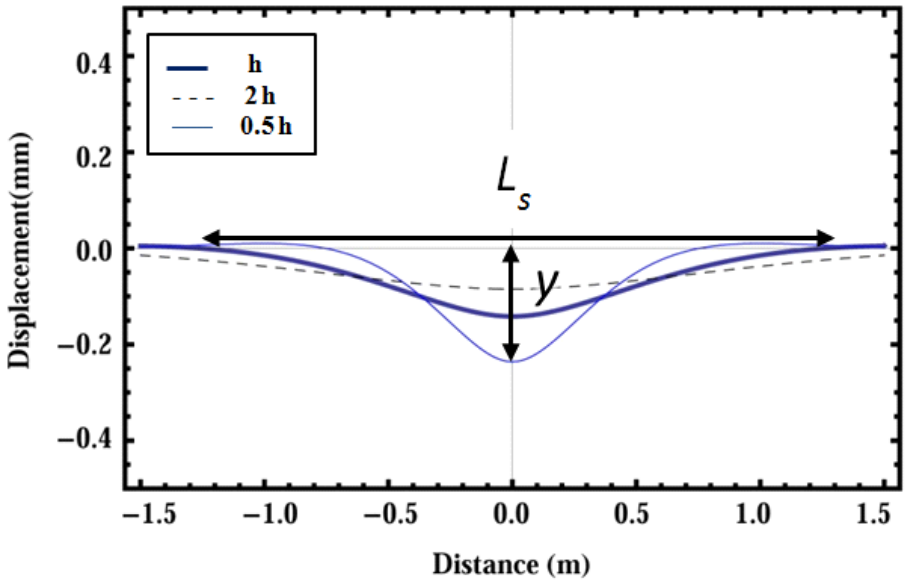

Figure 5-6: Sensitivity of maximum pavement deflection y and characteristic wavelength L_s to top layer thickness h.

y and the characteristic wavelength L_s. As shown in Figure 5-6, with increase in the value of h the maximum deflection decreases; however, the characteristic wavelength increases.

Noting $d = EI$ the rigidity of the beam and $I = h^3/12$, from Eq. (5.1) and Eq. (5.2) we write:

$$y\left(h = \lambda h_0\right) = \frac{q}{k} \times \Pi\left(\overline{\eta} = \frac{\eta}{(d/k)^{1/4}}; \zeta = \frac{c}{c_{crit}}; \overline{V} = \frac{V}{V_{os}}\right) = \lambda^{-3/4} y(h_0) \tag{5.16}$$

$$L_s\left(h = \lambda h_0\right) = \lambda^{+3/4} L_s(h_0) \tag{5.17}$$

Thus, substituting Eq. (5.16) and Eq. (5.17) in Eq. (5.3) gives:

$$GR(h = \lambda h_0) = \frac{y(h = \lambda h_0)}{L_s(h = \lambda h_0)} = \frac{\lambda^{-3/4} y(h_0)}{\lambda^{+3/4} L_s(h_0)} = \lambda^{-3/2} GR(h_0) \tag{5.18}$$

This means that GR scales with the top layer thickness as:

$$GR(h) \sim h^{-3/2} \tag{5.19}$$

5.6 Combined Scaling of All Parameters

Scaling relationships between maximum pavement deflection (y) and characteristic wavelength (L_s) have been established with the structural and material pavement parameters (h, E, k) along with the external load (q). These relationships were illustrated in Figures 5-3 through 5-6, and were developed from the model for all cases. By combining the effect of each parameter on the deflection y and the characteristic wavelength L_s, the following scaling relation is obtained:

$$GR \sim q \times E^{-1/2} k^{-1/2} h^{-3/2} \tag{5.20}$$

This scaling relationship shows the importance of the external load q, along with that of material parameters E and k, and structural component h. It is observed that the pavement thickness h is of higher importance for reduction of the impact of deflection within PVI compared to the other parameters.

5.7 Chapter Summary

The Bernoulli-Euler beam on a viscoelastic foundation allows the derivation of scaling relationships for the material and structural properties of pavements and their impacts on pavement deflection and grade. It was shown that the combination of soil damping and moving load creates a distance lag between the maximum deflection and the load location. This phenomenon creates a slope resisting the motion of vehicles. The maximum deflection under load and the characteristic wavelength of the deflection basin are used to scale the added slope to the pavement's profile. We will use these scaling relations in the next chapter for pavement-vehicle interaction predictions of added fuel consumption.

Part III

Model-Based PVI Prediction

Chapter 6

Pavement-Vehicle Interaction and Fuel Consumption

The scaling relationships of the Bernoulli-Euler beam on a viscoelastic foundation provide a means to link material parameters (top layer modulus E, subgrade modulus k), structural parameters (top layer thickness h), and the external load q to the added pavement slope GR due to deflection. In this chapter, the pavement deflection scaling relationships, obtained from the model, are combined with the empirical fuel consumption relations introduced in Chapter 2. Calibration outputs for all LTPP datasets from Chapter 4 are integrated with the deflection model to estimate the change in fuel consumption through a statistical analysis of all E and k values for both rigid and flexible pavements. Finally, using Monte Carlo simulations we estimate the change in fuel consumption due to pavement deflection at the Network scale.

6.1 Scaling of Fuel Consumption

It was shown in Table 2-1 and Table 2-2, that the fuel consumption of a vehicle is in direct relationship with the resisting forces that it has to overcome to travel on a pavement (Aerodynamic forces F_a, Gradient forces F_g, Curvature forces F_c, Rolling resistance forces F_r, Inertial forces F_i). Furthermore, the combined effect of damping and vehicle velocity creates a resistive force by putting the vehicle on an uphill slope (see Figure 5-2). This slope adds to the vehicle resistive forces through the Gradient Force F_g and is related to the instantaneous fuel

consumption (IFC) through Eq. (2.1):

$$F_g = q \times GR \times g \sim IFC \tag{6.1}$$

where q is the external load, GR is the gradient, and g is the gravity. It was shown in the last chapter that the gradient GR scales with pavement material and geometric properties (see Eq. (5.20)):

$$GR \sim q \times E^{-1/2} k^{-1/2} h^{-3/2} \tag{6.2}$$

Thus combining Eq. (6.1) with (6.2), a link can be established between IFC and the pavement parameters:

$$\text{IFC} \sim GR \times q \times g = q^2 \times E^{-1/2} k^{-1/2} h^{-3/2} \tag{6.3}$$

Equation (6.3) shows that the instantaneous fuel consumption and the external load scale as IFC$\sim q^2$. This is due to the impact of the external load q on the deflection induced grade (Eq. (6.2)) and the Gradient Force F_g itself. From Figure 2-1 we recall that the majority of empirical studies measured statistically significant changes in fuel consumption for trucks, while the disagreement in fuel consumption readings were higher for passenger vehicles. Moreover, the magnitude of change in fuel consumption of trucks were generally higher than that of passenger cars. For instance, Zabaar and Chatti [51] suggest a change in fuel consumption of 1 liter/100km for trucks, but observe no change in fuel consumption for passenger vehicles. Although the limited data from these empirical studies does not allow a statistical analysis, it is evident that the scaling relationship between fuel consumption and the external load of IFC$\sim q^2$ captures exactly this trend.

Scaling relationship (6.3) allows comparison of different pavement scenarios in terms of PVI in order to guide pavement design. The importance of such scaling relationship can be illustrated through various examples, of which two are presented in this section.

6.1.1 Comparative Analysis

Assuming two pavement scenarios, where the ultimate goal is an environmental design with regard to change in fuel consumption, both pavements can be designed so that the change in

IFC due to pavement deflection is equivalent. Consider an asphalt (A) and a concrete (C) pavement to be designed for the same load. If the same instantaneous fuel consumption due to deflection is pursued, the thickness ratio of the two pavements can be calculated from Eq. (6.3):

$$\frac{\text{IFC(A)}}{\text{IFC(C)}} = \frac{q^2 \times E_a^{-1/2} k_a^{-1/2} h_a^{-3/2}}{q^2 \times E_c^{-1/2} k_c^{-1/2} h_c^{-3/2}} = 1 \tag{6.4}$$

$$\frac{h_a}{h_c} = \sqrt[3]{\frac{E_c}{E_a} \times \frac{k_c}{k_a}} \tag{6.5}$$

Designing the two pavement scenarios for the same subgrade moduli under the same loading conditions, and assuming a modulus of elasticity of $E_a = 5,000$ MPa for the asphalt section and $E_c = 20,000$ MPa for the concrete section, Eq. (6.5) would give:

$$\frac{h_a}{h_c} = \sqrt[3]{\frac{20,000}{5,000}} = 1.6 \tag{6.6}$$

Equation (6.6) shows that the asphalt top layer needs to be 1.6 times thicker than the concrete top layer to maintain the same instantaneous fuel consumption caused by deflection of the pavement for the two pavement scenarios considered.

6.1.2 Comparative Analysis Generalization

The scaling example of Section 6.1.2 can be expanded to include a wider range of pavements scenarios, with varying top layer moduli E, subgrade moduli k, and thicknesses h. As before, IFC(A) and IFC(C) represent the instantaneous fuel consumption of an asphalt (A) and a concrete (C) pavement. Using the same notations of Eq. (6.4) and setting the ratio of these two quantities equal to X gives:

$$\text{X} = \frac{\text{IFC(A)}}{\text{IFC(C)}} = \frac{q^2 \times E_a^{-1/2} k_a^{-1/2} h_a^{-3/2}}{q^2 \times E_c^{-1/2} k_c^{-1/2} h_c^{-3/2}} = \sqrt{\frac{E_c}{E_a} \times \frac{k_c}{k_a} \times \left(\frac{h_c}{h_a}\right)^3} \tag{6.7}$$

From Eq. (6.7) the instantaneous fuel consumption on an asphalt pavement IFC(A) is:

$$\text{IFC(A)} = \text{IFC(C)} \times \text{X} \tag{6.8}$$

As shown in Chapter 2, most empirical studies that focus on the impact of pavement deflection on fuel consumption, report the change in fuel consumption as a quantity relative to that of a concrete pavement (since vehicles are shown to consume more fuel on asphalt pavements). Therefore, writing Eq. (6.8) in the same manner leads to:

$$\text{IFC(A)} - \text{IFC(C)} = (\text{X} - 1) \times \text{IFC(C)} \tag{6.9}$$

Absolute changes in fuel consumption are not of interest when developing a scaling relationship. Therefore, the change in fuel consumption shown in Eq. (6.9) can be normalized against the instantaneous fuel consumption on the concrete pavement IFC(C) to demonstrate the advantages and disadvantages of the asphalt pavement compared to that of the concrete pavement in percentages:

$$\frac{\text{IFC(A)} - \text{IFC(C)}}{\text{IFC(C)}} = (\text{X} - 1) \times 100 \tag{6.10}$$

By assuming same external loading q and same subgrade moduli k for the asphalt and concrete pavement cases, Eq. (6.7) and (6.10) are used to calculate the advantages and disadvantages of different pavement designs with regard to pavement vehicle interaction.

Table 6-1 shows the values of X calculated for a range of top layer modulus ratios (E_c/E_a) and a range of thickness ratios (h_c/h_a) between a concrete and an asphalt pavement. Eq. (6.8) shows that when X has a value larger than 1, the instantaneous fuel consumption is greater for the asphalt pavement than the concrete pavement (shaded region). Using Eq. (6.10) the percentage change in the impact of PVI on fuel consumption is calculated and shown in Table 6-2 for the same modulus and thickness ratios as before. The values in each cell represent the added advantage to fuel consumption of a concrete pavement to an asphalt pavement with their corresponding designs. The shaded cells are where fuel consumption due to deflection is lower for the concrete pavement than the asphalt pavement. Figure 6-1 shows the values of Table 6-2 graphically; positive values on the vertical axis denote combinations of top layer modulus and thickness ratios where fuel consumption on the concrete pavement is lower than that of the asphalt pavement.

E_c/E_a Range	h_c/h_a Range								
	X	1.4	1.2	1.1	1	0.9	0.8	0.7	0.6	0.5
	10	5.2	4.2	3.6	3.2	2.7	2.3	1.9	1.5	1.1
	9	5.0	3.9	3.5	3.0	2.6	2.1	1.8	1.4	1.1
	8	4.7	3.7	3.3	2.8	2.4	2.0	1.7	1.3	1.0
	7	4.4	3.5	3.1	2.6	2.3	1.9	1.5	1.2	0.9
	6	4.1	3.2	2.8	2.4	2.1	1.8	1.4	1.1	0.9
	5	3.7	2.9	2.6	2.2	1.9	1.6	1.3	1.0	0.8
	4	3.3	2.6	2.3	2.0	1.7	1.4	1.2	0.9	0.7
	3	2.9	2.3	2.0	1.7	1.5	1.2	1.0	0.8	0.6
	2	2.3	1.9	1.6	1.4	1.2	1.0	0.8	0.7	0.5

Table 6.1: Calculated multiplying factor X in Eq. (6.8) for a range of top layer modulus and thickness ratios. Values greater than 1 represent cases where IFC is higher on the asphalt pavement compared to that of a concrete pavement.

E_c/E_a Range	h_c/h_a Range								
	1.4	1.2	1.1	1	0.9	0.8	0.7	0.6	0.5
10	424 %	316 %	265 %	216 %	170 %	126 %	85 %	47 %	12 %
9	397 %	294 %	246 %	200 %	156 %	115 %	76 %	39 %	6 %
8	369 %	272 %	226 %	183 %	141 %	102 %	66 %	31 %	0 %
7	338 %	248 %	205 %	165 %	126 %	89 %	55 %	23 %	-6 %
6	306 %	222 %	183 %	145 %	109 %	75 %	43 %	14 %	-13 %
5	270 %	194 %	158 %	124 %	91 %	60 %	31 %	4 %	-21 %
4	231 %	163 %	131 %	100 %	71 %	43 %	17 %	-7 %	-29 %
3	187 %	128 %	100 %	73 %	48 %	24 %	1 %	-20 %	-39 %
2	134 %	86 %	63 %	41 %	21 %	1 %	-17 %	-34 %	-50 %

Table 6.2: Calculated advantage/disadvantage of a concrete pavement to an asphalt pavement for a range of top layer modulus and thickness ratios in percent. Values above zero represent cases where concrete pavements perform better than asphalt pavements in regards to PVI.

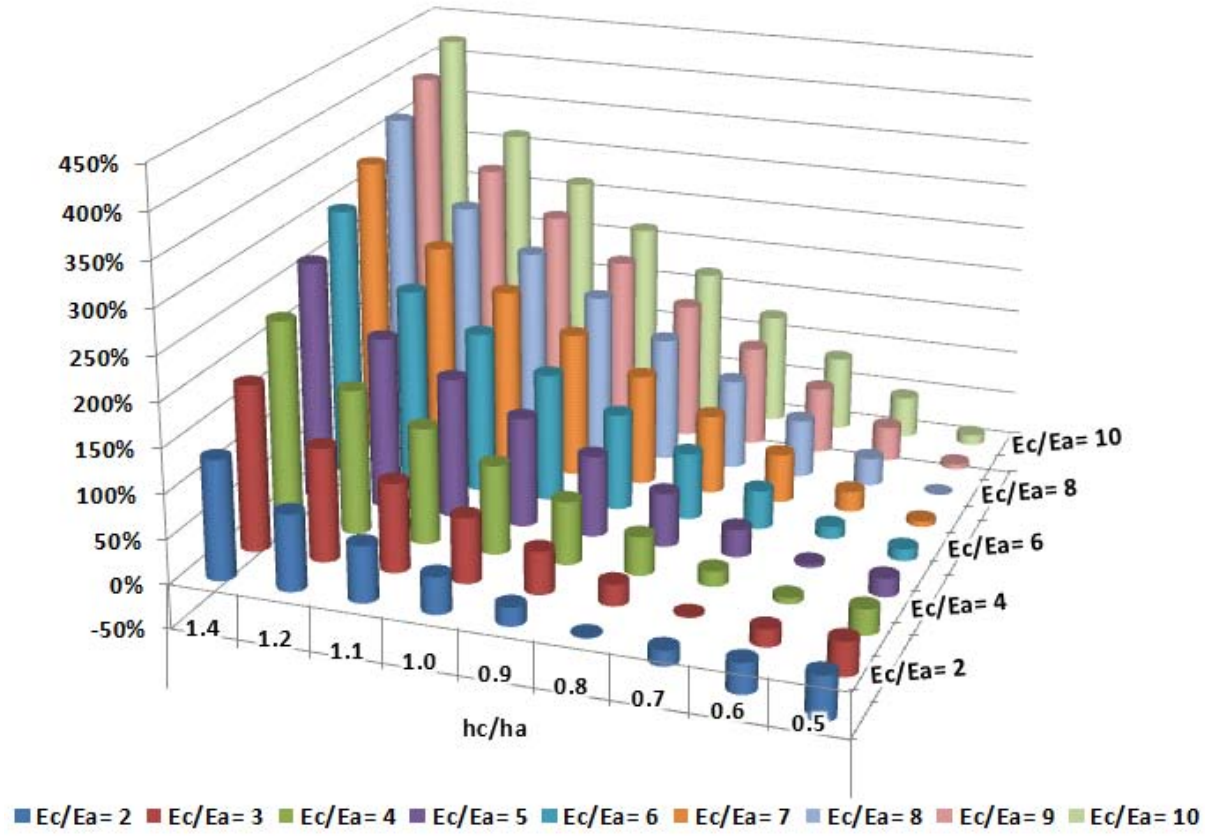

Figure 6-1: Graphical representation of the calculated advantage/disadvantage of a concrete pavement to an asphalt pavement for a range of top layer modulus and thickness ratios in percent. Values above zero on the vertical axis represent cases where concrete pavements perform better than asphalt pavements with regard to PVI.

Pavement Type	μ (MPa)	μ (psi)	σ (MPa)	σ (psi)
Flexible	8212	1.19E+06	4234	6.14E+05
Rigid	43914	6.37E+06	8957	1.30E+06

Table 6.3: Mean and standard deviation of top layer elastic modulus for flexible and rigid pavements.

6.2 PVI on LTPP Sections

The extent of Falling Weight Deflectometer tests (FWD) conducted by the Long-Term Pavement Performance program was discussed in Chapter 4. By using the proposed calibration method, values of the top layer elastic modulus E and the subgrade modulus k were calculated for all asphalt and concrete sections. Here, a statistical analysis is performed using these values, along with that of the pavement thickness h (extracted from tables MON_DEFL_FLX_BAKCAL_LAYER and MON_DEFL_RGD_BAKCAL_LAYER [28]). In total, 1,079 datasets for rigid pavements and 4,564 datasets for flexible pavements are included in the statistical analysis. Monte Carlo simulations are performed to estimate the resulting deflection and added fuel consumption for both pavement types due to variations in the input parameters.

6.2.1 Top Layer Modulus E

Using FWD time history datasets, top layer elastic modulus values are calculated separately for flexible and rigid pavements. Figure 6-2 shows the top layer elastic modulus E of flexible and rigid pavements in a logarithmic-normal distribution. A log-normal distribution is the continuous probability distribution of a random variable whose logarithm is normally distributed: if X is a random variable with a log-normal distribution, then Y=log(X) is normally distributed. Moreover, the mean μ and standard deviation σ of the log-normal distribution X are that of its natural logarithm, Y. The probability density function of a log-normal distribution is:

$$f_x(x;\mu,\sigma) = \frac{1}{x\sigma\sqrt{2\pi}} e^{-\frac{(\ln x-\mu)^2}{2\sigma^2}}, x > 0 \tag{6.11}$$

Table 6-3 shows the mean μ and standard deviation σ for both distributions. It is observed that the rigid sections have a dominating higher modulus value compared to the flexible sections, as well as a much tighter distribution.

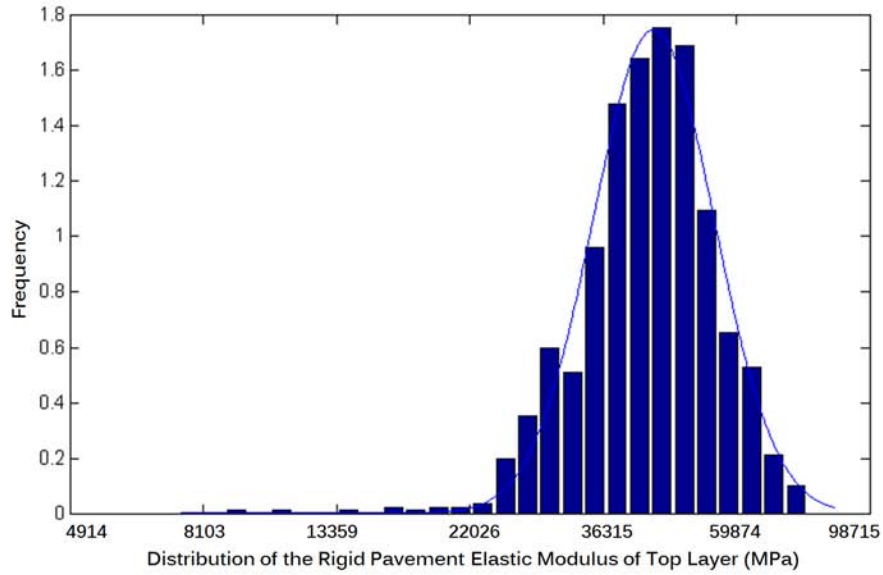

(a)

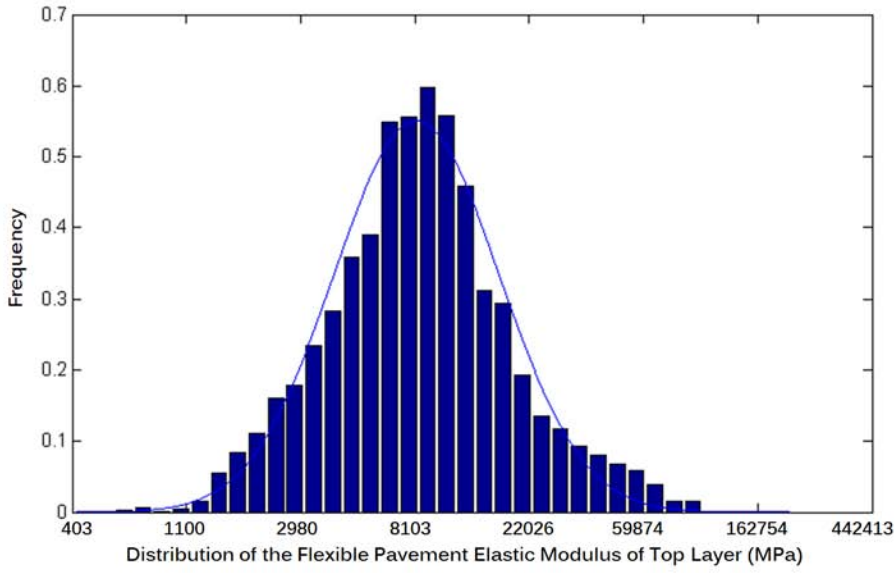

(b)

Figure 6-2: Histogram of top layer elastic modulus E of all (a) rigid and (b) flexible sections within the LTPP databases, presented with a log-normal distribution.

Pavement Type	μ (MPa)	μ (psi)	σ (MPa)	σ (psi)
Flexible	65.9	9.56E+03	20.5	2.97E+03
Rigid	59.9	8.69E+03	20.1	2.91E+03

Table 6.4: Mean and standard deviation of subgrade elastic modulus for flexible and rigid pavements.

Pavement Type	μ (m)	μ (in)	σ (m)	σ (in)
Flexible	0.15	5.9	0.05	1.96
Rigid	0.24	9.44	0.03	1.18

Table 6.5: Mean and standard deviation of top layer thickness for flexible and rigid pavements.

6.2.2 Subgrade Modulus k

The same methodology as above is used to determine the probability distribution of the subgrade modulus k, as a log-normal distribution. Figure 6-3 shows the probability distribution of flexible and rigid pavement subgrades and Table 6-4 summarizes their mean μ and standard deviation σ values. As expected, it is observed from these values that the subgrade modulus of flexible and rigid pavements are fairly similar. This is mainly due to the fact that pavement subgrade is independent of pavement top layer material properties (see Section 4.5.1).

6.2.3 Top Layer Thickness h

The probability distribution of the top layer thickness h in a log-normal space for flexible and rigid pavements is presented in Figure 6-4. Table 6-5 summarizes the mean μ and standard deviation σ of the top layer thickness h for flexible and rigid sections. It is observed from Figure 6-4, along with Table 6-5, that rigid pavements mainly have a greater thickness compared to flexible pavements. It is important to keep in mind that as presented in the scaling relationships in Section 5.6, thickness has the greatest effect on pavement deflection induced slope compared to the other parameters since $GR \sim q \times E^{-1/2} k^{-1/2} h^{-3/2}$.

6.2.4 External Load q

The applied external load q within the Network is dependent on the weight of each vehicle class travelling on the roadway, but also on the distance of their travel. The Federal Highway Administration publishes data on vehicle classes and their travel distance per year within the

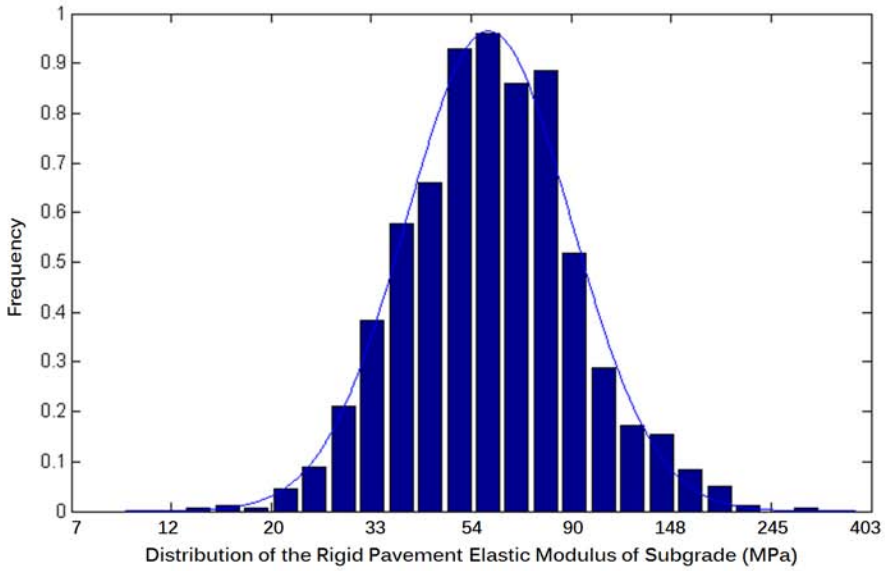

(a)

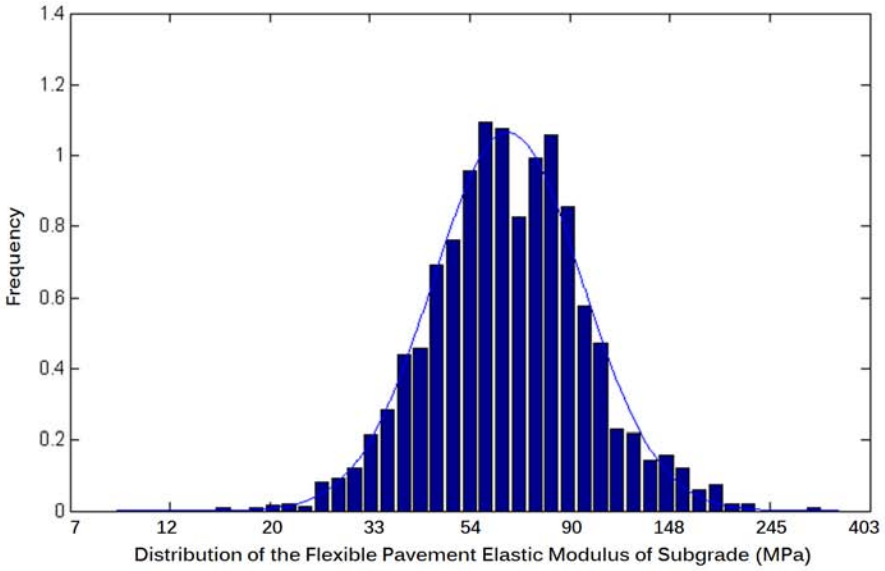

(b)

Figure 6-3: Histogram of subgrade modulus k of all (a) rigid and (b) flexible sections within the LTPP databases, presented with a log-normal distribution.

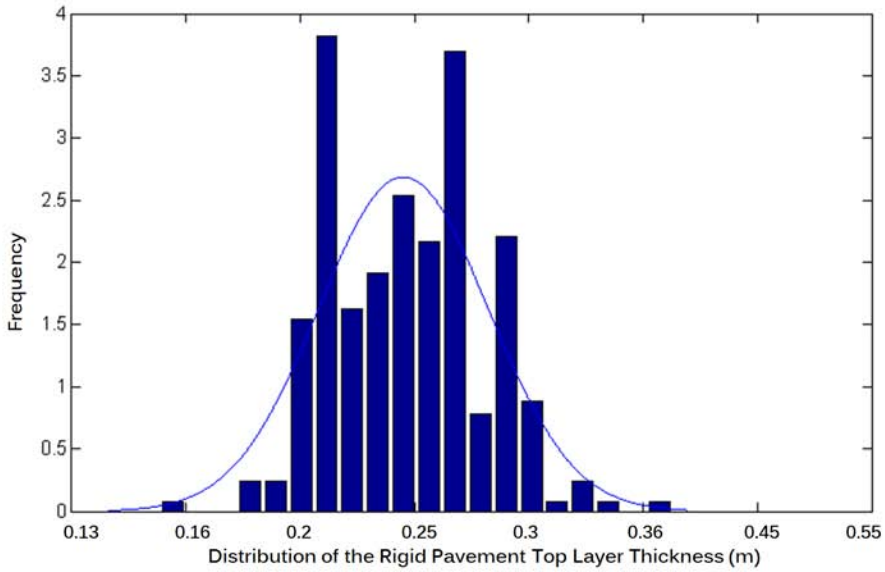

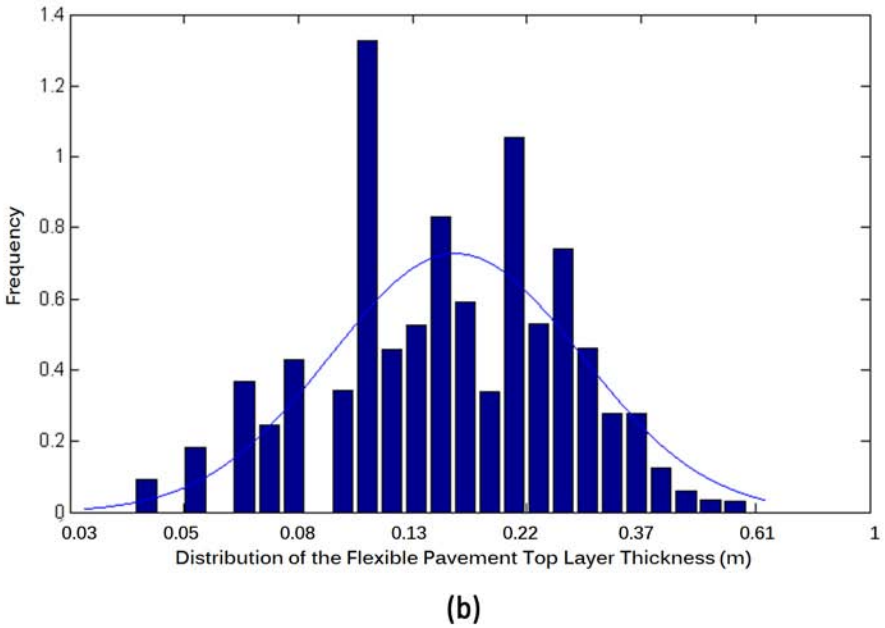

Figure 6-4: Histogram of top layer thickness h of all (a) rigid and (b) flexible sections within the LTPP databases, presented with a log-normal distribution.

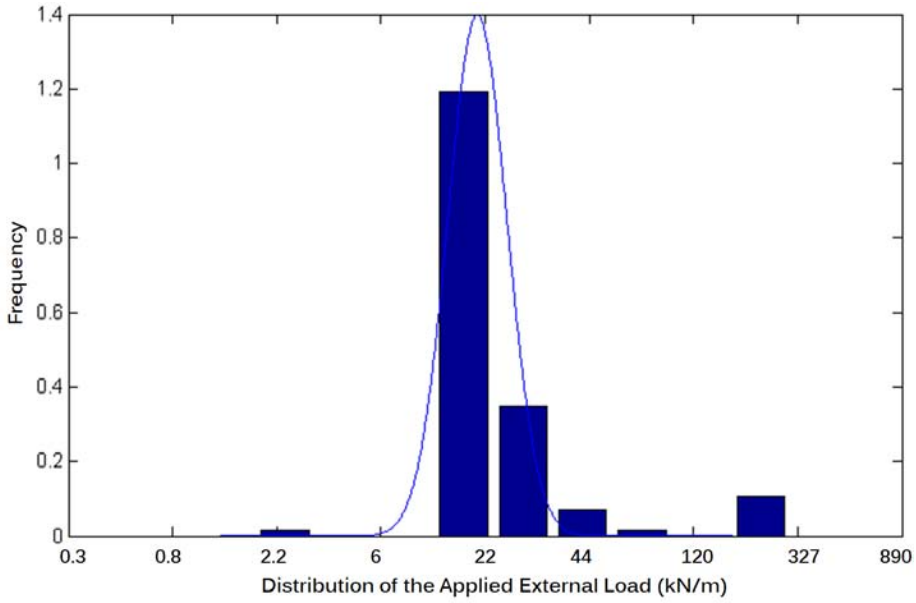

Figure 6-5: Histogram of external load q as suggested by FHWA [17] presented with a log-normal distribution.

	μ (kN/m)	μ (kip/ft)	σ (kN/m)	σ (kip/ft)
External Load q	18.5	1.03	4.38	0.3

Table 6.6: Mean and standard deviation of top layer thickness for flexible and rigid pavements.

Highway Statistics Manual [17]. Figure 6-5 shows the log-normal probability distribution of the external load q within the Network, extracted from Table VM-1 [17]. It is observed that passenger vehicles, due to their high volume, dominate througout the data. Table 6-6 summarizes the mean μ and standard deviation σ of the external load q within the Network.

6.2.5 Monte Carlo Simulation of Deflection y

Using the distributions for E, k, and h, Monte Carlo simulations are performed to determine an estimate for the average and standard deviation of pavement deflection within the network. Monte Carlo simulations sample probability distribution for each variable to produce a large number of possible outcomes; the Monte Carlo procedure is illustrated in Figure 6-6. Here, 1,000 iterations are performed and the probability distributions for deflection y along with

Pavement Type	μ (mm)	μ (mil)	σ (mm)	σ (mil)
Flexible	0.27	10.62	0.16	6.22
Rigid	0.11	4.33	0.06	2.36

Table 6.7: Mean and standard deviation of estimated pavement deflection through a Monte Carlo simulation for rigid and flexible pavements in log space and transformed.

the corresponding characteristic wavelength L_s are obtained for flexible and rigid pavements. Figure 6-7 shows the probability distribution of deflection for rigid and flexible pavements in a log-normal space. Table 6-7 shows the evaluated mean and standard deviations for both cases. The deflection distribution and the characteristic wavelengths are used to calculate the added grade GR and its impact on fuel consumption.

6.3 Comparison with Field Data

As stated earlier, the added fuel consumption due to pavement deflection is an effect of added grade to the roadway caused by the combination of soil damping and vehicle velocity (see Section 4.6) . Studies by Zabaar and Chatti [51], Park and Rakha [33], Boriboonsomsin and Barth [6], and Goodyear [19] have investigated the impact of roadway grades on vehicle fuel consumption; both for passenger vehicles and for trucks. For example, Goodyear [19] reports that a change in grade of 0.1% can lead to a change in fuel consumption of 10% for trucks; whereas Boriboonsomsin and Barth [6] suggest a change in fuel consumption of 3% for the same change in grade. Here, impacts of pavement deflection within PVI on passenger vehicle and truck fuel consumption are considered. The relationship between fuel consumption with roadway grade for passenger cars and trucks are drawn from [6] and [19] respectively:

$$\mathrm{FC}_{\mathrm{Cars}} = 2.94 \times GR + 12.22 \tag{6.12}$$

$$\mathrm{FC}_{\mathrm{Trucks}} = 361.8 \times GR + 36.18 \tag{6.13}$$

where FC is fuel consumption of passenger cars and trucks in liters/100km.

The weight of passenger cars and trucks are equal to 1.2 tons and 41.2 tons, respectively. It is important to remember from Section 6.1 that IFC$\sim q^2$, and to verify that the relationships in Eq. (6.12) conform with the scaling of weight q. Figure 6-8 shows fuel consumption from Eq.

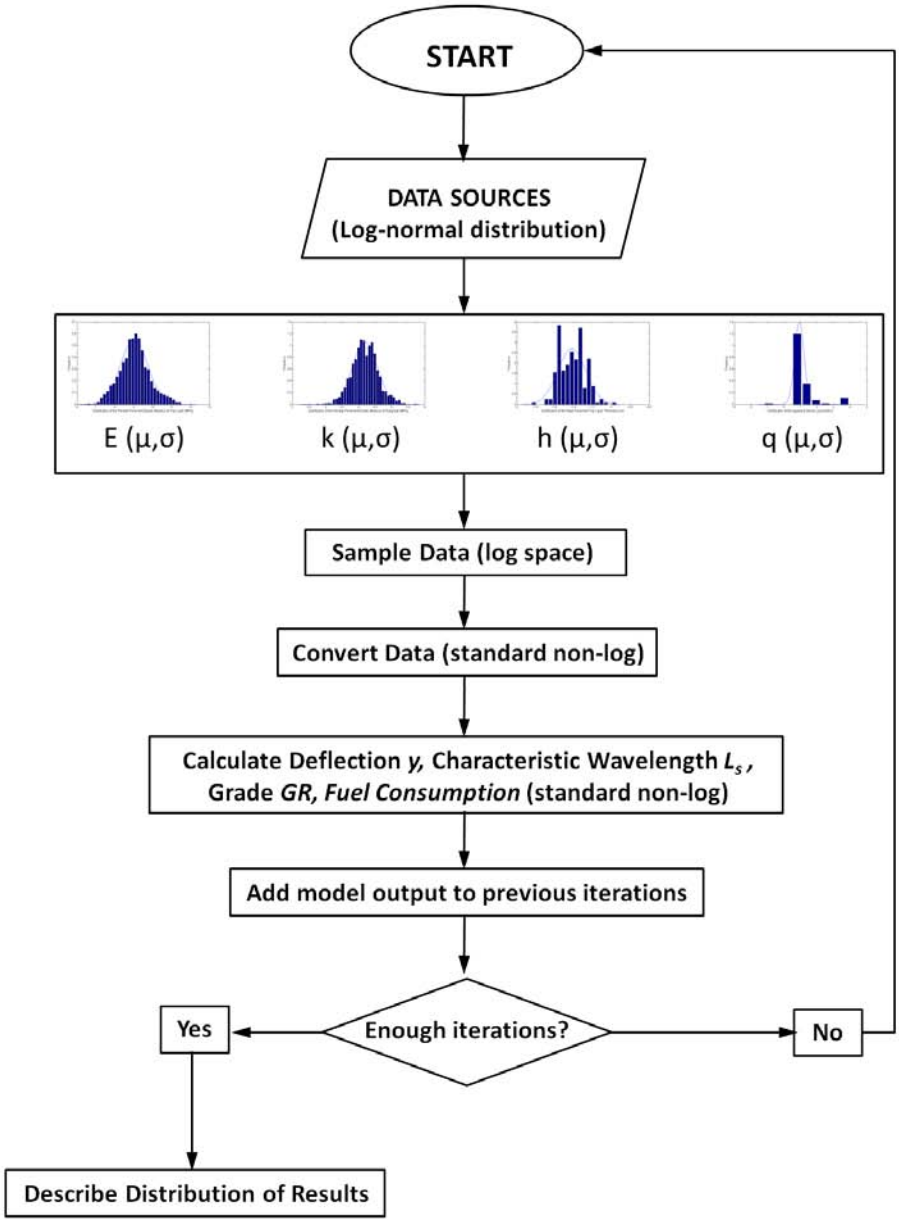

Figure 6-6: Flow chart illustrating the Monte Carlo procedure in the logarithmic space.

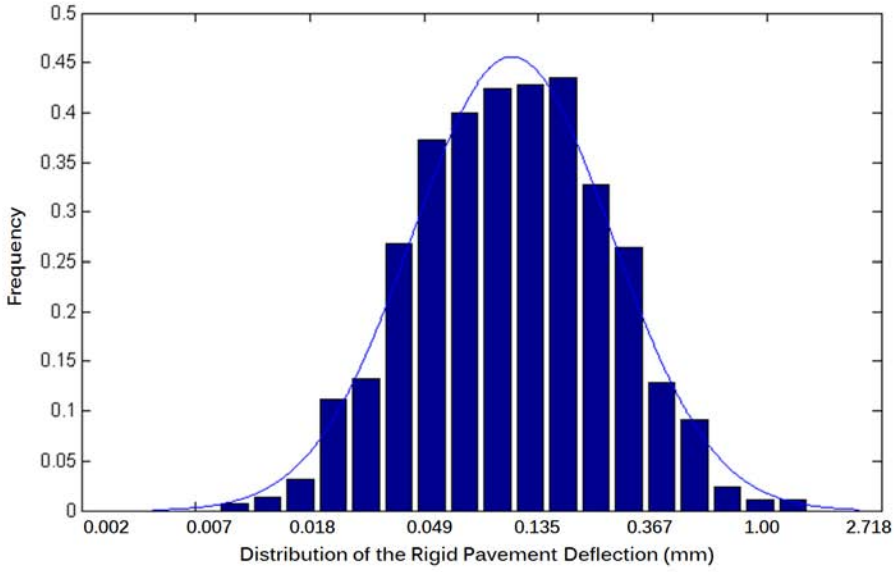

(a)

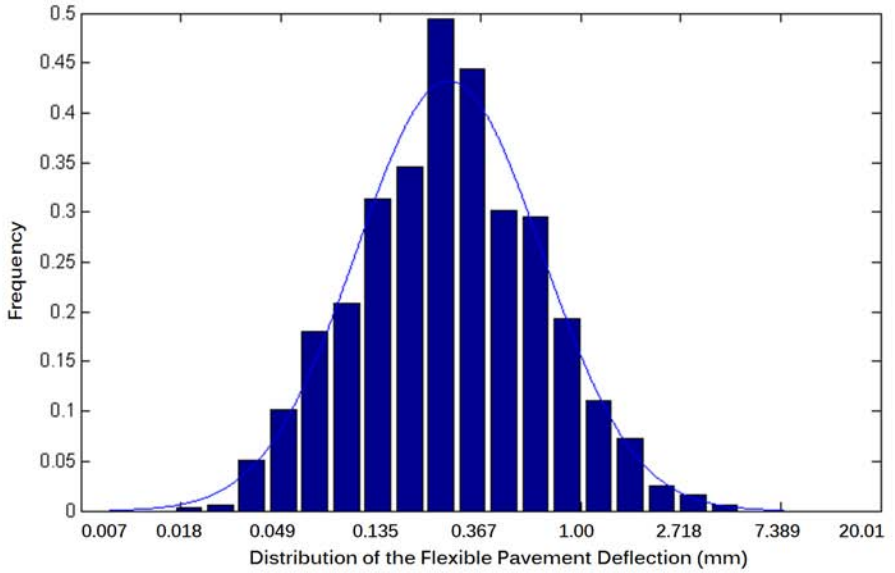

(b)

Figure 6-7: Histogram of pavement deflection y of all (a) rigid and (b) flexible sections calculated through Monte Carlo simulations, presented with a log-normal distribution.

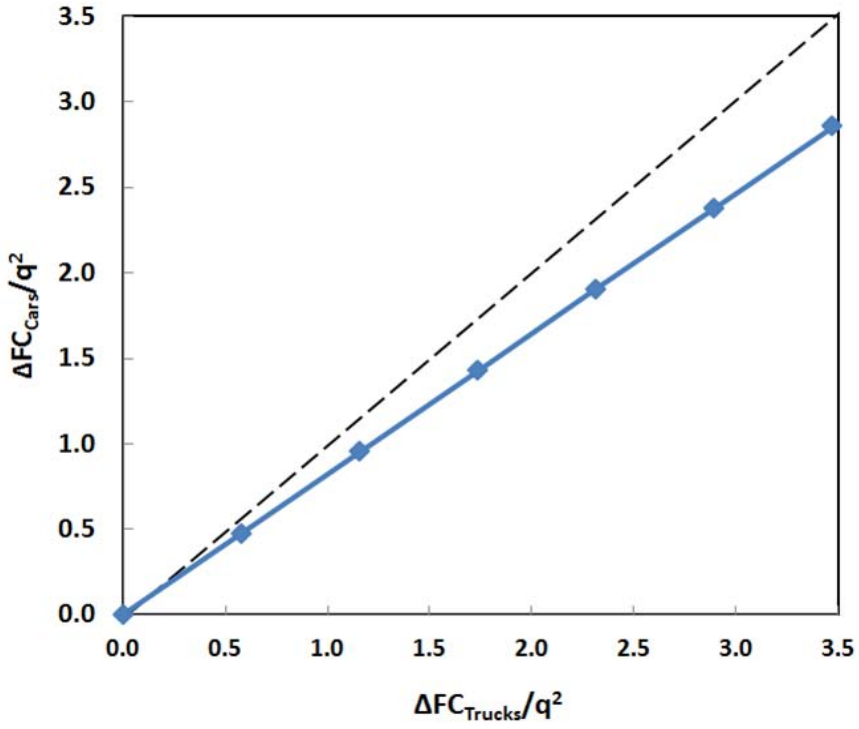

Figure 6-8: Fuel consumption with respect to the square of load of passenger vehicles versus trucks.

(6.12) normalized to q^2 (FC/q^2) of passenger cars versus trucks. It is seen that the normalized fuel consumption of passenger cars and trucks obey the scaling relationship of IFC (Eq. (6.3)), however, the normalized fuel consumption of trucks is slightly higher than that of passenger cars; possibly due to higher aerodynamic forces exerted on trucks.

Using deflection, characteristic wavelength, and grade distributions obtained from the Monte Carlo simulations (Figure 6-7), the change in fuel consumption due to pavement deflection is calculated for passenger vehicles and trucks on concrete and asphalt sections. Table 6-7 presents the change in fuel consumption due to deflection of the pavement. This change in fuel consumption is for a pavement that undergoes a deflection and is relative to a flat pavement. It should be noted that the values suggested in these tables are calculated for all FWD test datasets considered in Chapter 4.

In Table 6-8, the mean μ and standard deviation σ for change in fuel consumption for

	Concrete		Asphalt	
	μ (l/100km)	σ (l/100km)	μ (l/100km)	σ (l/100km)
Passenger cars	0.002	0.0016	0.012	0.009
Truck	0.013	0.012	0.077	0.06

Table 6.8: Impact of deflection on fuel consumption modeled as added grade to the roadway for the deflection distribution calculated with the Monte Carlo analysis.

the 1,079 concrete sections and 4,564 asphalt sections are reported. The influence of vehicle weight is clear, with trucks having significantly larger changes in fuel consumption compared to passanger cars. Figure 6-9 shows the distribution of change in grade GR on asphalt and concrete pavements, and Figures 6-10 and 6-11 show the log-normal distribution of change in fuel consumption on these pavements, corresponding to the values of Table 6-8.

It is interesting to compare the calculated change in fuel consumption (Figures 6-10 and 6-11) to previously performed empirical studies (Figure 2-1). However, the empirical studies mentioned in Section 2.3 report change in fuel consumption on asphalt pavements compared to concrete pavements. It is necessary to first determine the distribution of change in fuel consumption on asphalt pavements relative to concrete pavements from Figures 6-10 and 6-11. If X and Y are independent random variables that are normally distributed (the log-normal distribution behaves as a normal distribution in log space, see Section 6.2.1), then their sum is also normally distributed if:

$$X \sim N(\mu_X, \sigma_X^2) \tag{6.14}$$

$$Y \sim N(\mu_Y, \sigma_Y^2) \tag{6.15}$$

$$Z = X + Y \tag{6.16}$$

then [31]:

$$Z \sim N(\mu_X + \mu_Y, \sigma_X^2 + \sigma_Y^2) \tag{6.17}$$

Hence, the sum of independent normally distributed random variables is normal, with its mean μ equal to the sum of the means and its standard deviation σ equal to the sum of the standard deviations. Figure 6-12 shows the distribution of change in fuel consumption on asphalt sections relative to that of concrete sections for passenger cars and trucks; and Table 6-9 shows the

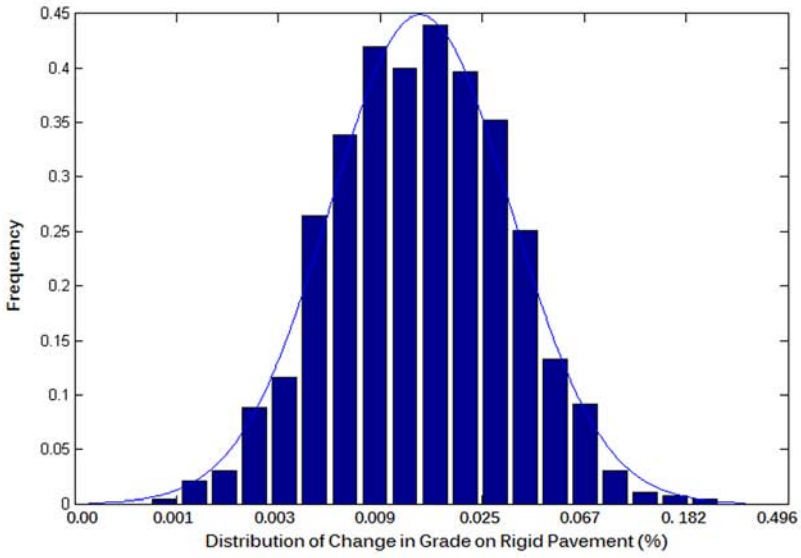

(a)

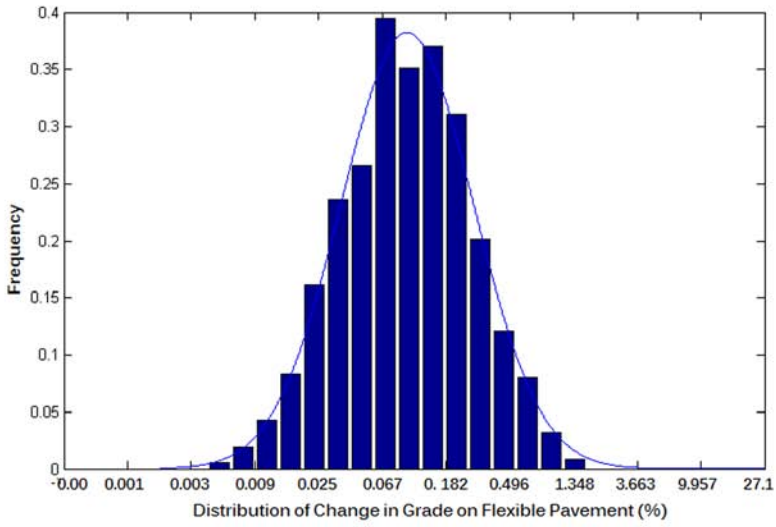

(b)

Figure 6-9: Histograms of change in roadway grade on (a) rigid and (b) flexible pavement as seen from LTPP datasets, presented with a log-normal distribution.

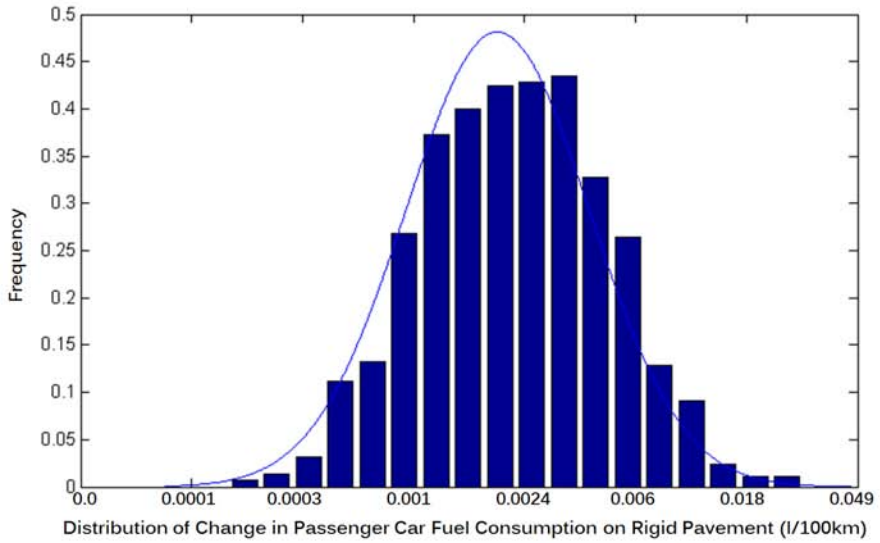

(a)

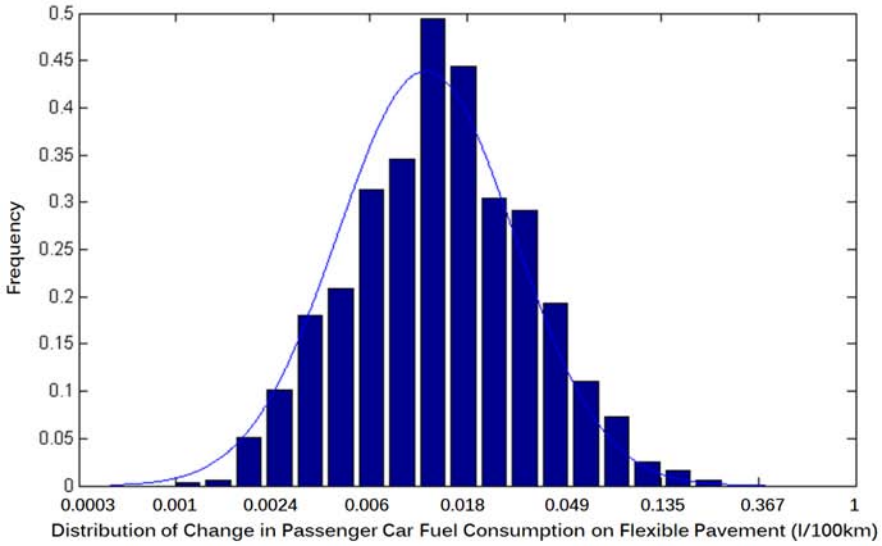

(b)

Figure 6-10: Histograms of change in fuel consumption of passenger cars on all LTPP (a) rigid and (b) flexible pavement datasets presented with a log-normal distribution.

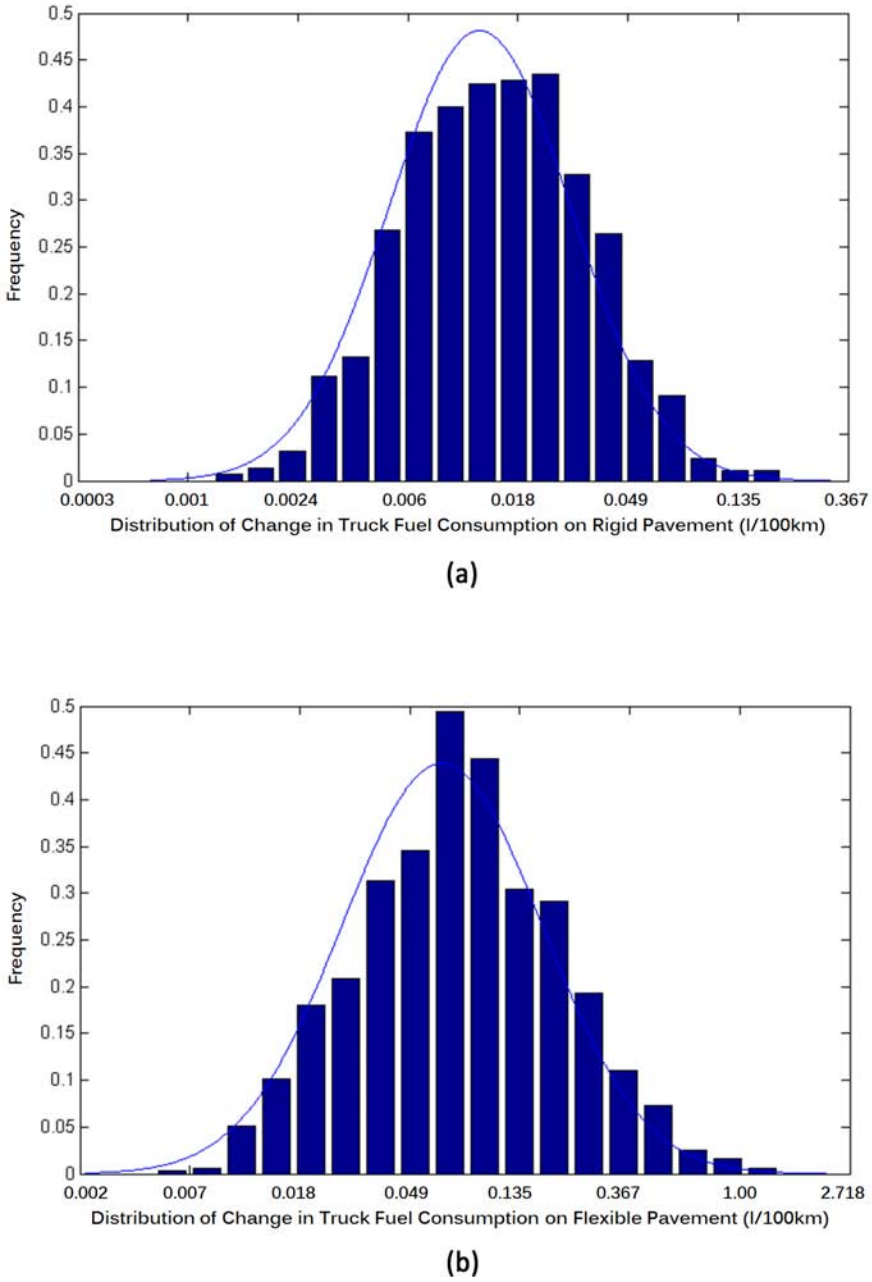

Figure 6-11: Histograms of change in fuel consumption of trucks on all LTPP (a) rigid and (b) flexible pavement datasets presented with a log-normal distribution.

	Asphalt	
	μ (l/100km)	σ (l/100km)
Passenger cars	0.011	0.007
Truck	0.061	0.042

Table 6.9: The average and standard deviation from the distribution of the change in fuel consumption of passenger cars and trucks on the asphalt sections compared to that of the concrete sections from Figure 6-11.

average μ and standard deviation σ corresponding to this figure.

The distributions of Figure 6-12 are plotted against the empirical studies of Section 2.3 and shown in Figure 6-13 and Figure 6-14 for passenger cars and trucks. These figures show that the model suggests changes in fuel consumption due to pavement deflection on the same order of magnitude as those proposed by some of the more recent studies. The change in fuel consumption on these figures, similar to Figure 2-1, is relative to that of the concrete sections. It is necessary to note, however, that even though the change in fuel consumption suggested by this study are on the same order of magnitude as the previous empirical measurements, the main contribution of this work is creating the relationship between pavement material and structural properties with the change in fuel consumption from a predictive mechanistic perspective.

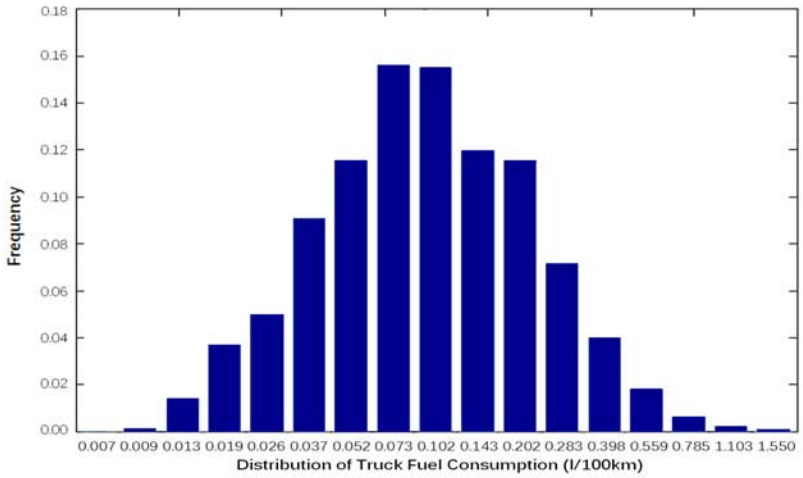

(a)

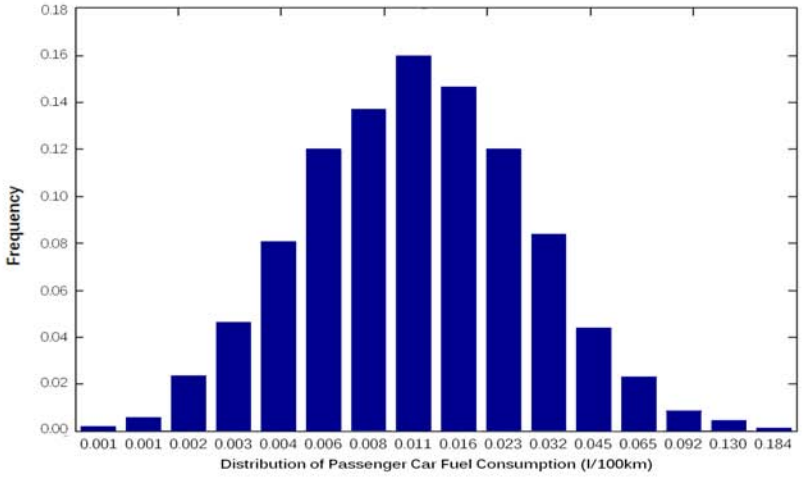

(b)

Figure 6-12: Log-normal distribution of the change in fuel consumption of (a) trucks and (b) passenger cars on the asphalt sections compared to that of the concrete sections, calculated from Figures 6-10 and 6-11.

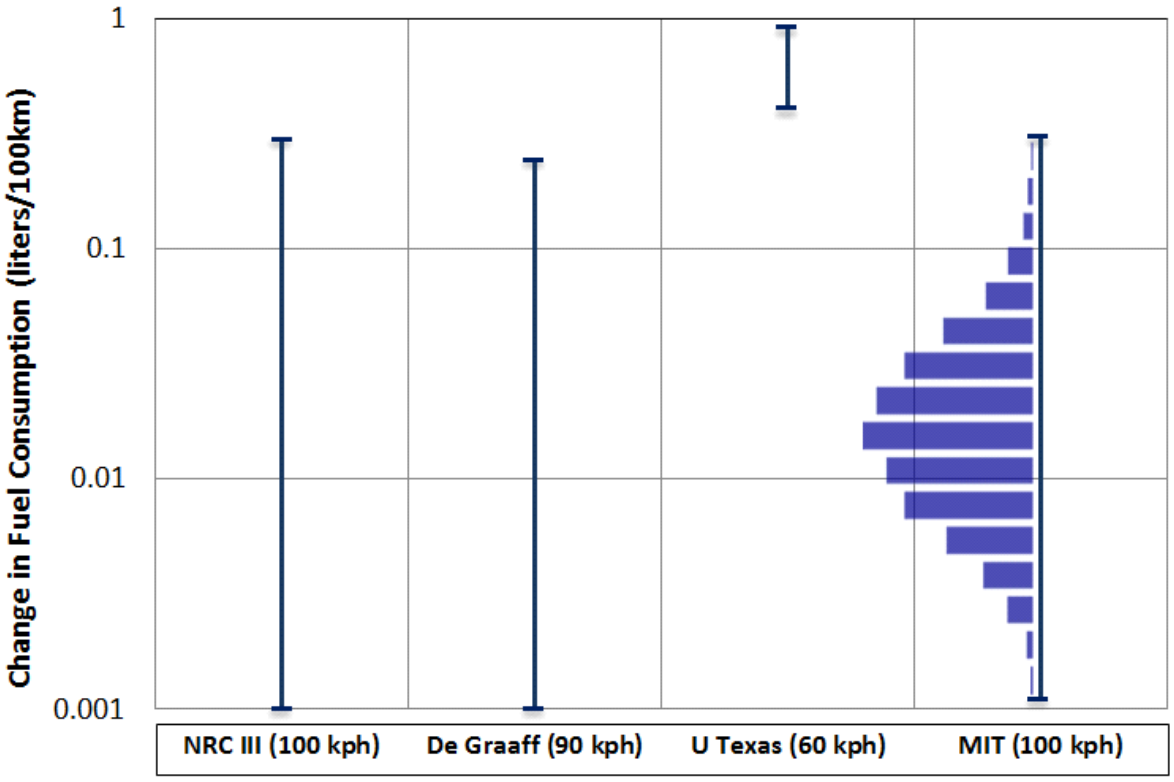

Figure 6-13: Comparison of the suggested change in fuel consumption from the model outputs to previous empirical studies for change in fuel consumption of passenger cars on asphalt pavements compared to that of concrete pavements in log-scale.

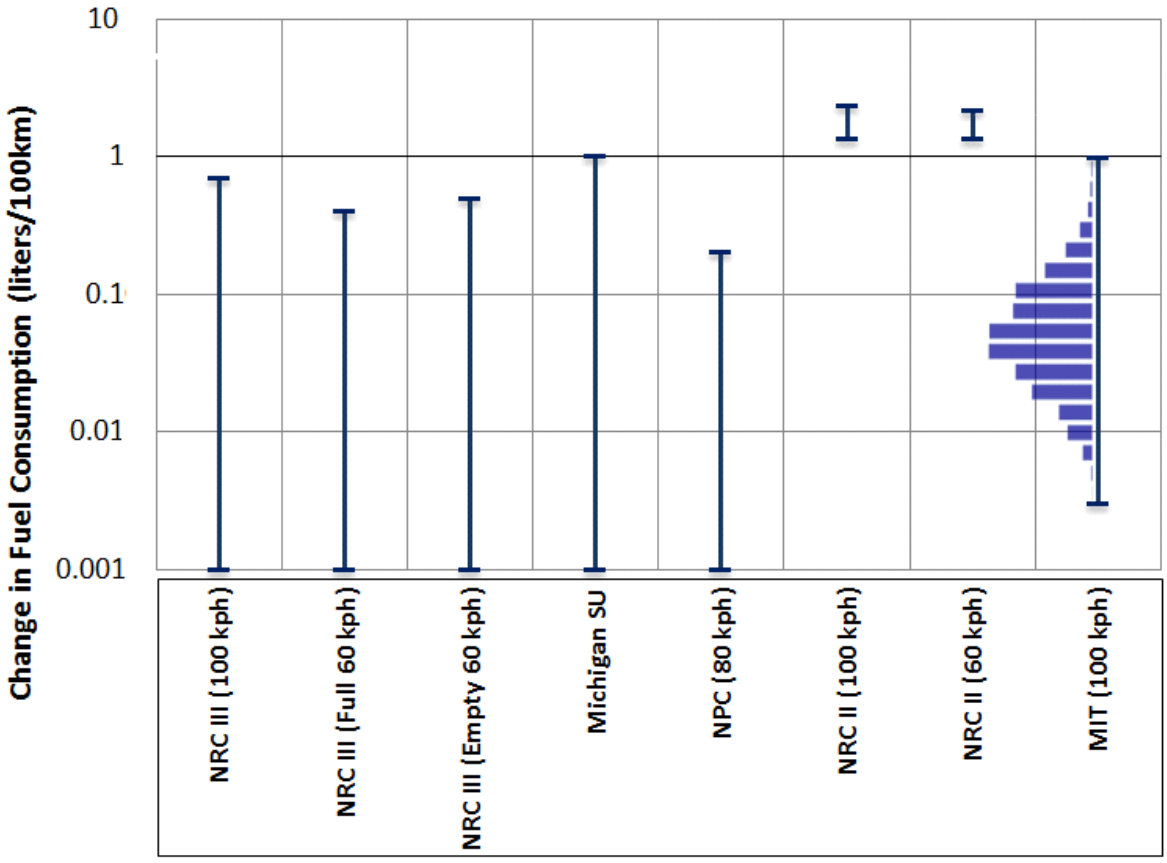

Figure 6-14: Comparison of the suggested change in fuel consumption from the model outputs to previous empirical studies for change in fuel consumption of trucks on asphalt pavements compared to that of concrete pavements in log-scale.

6.4 Chapter Summary

In this chapter, three main topics were discussed. First, the importance and capabilities of the fuel consumption scaling model was presented. It was shown that this model is capable of guiding pavement design by aiding the comparison of pavements with regard to the impact on vehicle fuel consumption due to deflection induced PVI. Second, a statistical analysis of all LTPP falling weight deflectometer databases was performed for parameters of E, k, and h; and through a Monte Carlo simulation, deflection estimates, slope GR, and the change in fuel consumption FC for the U.S. roadway network was conducted. Third, the results of this analysis were related to change in fuel consumption due to deflection through empirical relationships and a network-wide estimate for change in fuel consumption was presented. Moreoever, comparison of the calculated changes in fuel consumption at the network scale with previous empirical studies shows good agreement. In return, the strength of this model compared to previous empirical studies is its ability to relate changes in fuel consumption to structural and material properties of the pavement. Also, unlike previous works, this model compares both asphalt and concrete pavements to an ever-flat surface and allows for a model-based comparative analysis.

It should be noted that this study presents a simplified model which rationalizes PVI in first order and does not capture all phenomena involved. For instance, this model assumes that both asphalt and concrete pavements are continuous (i.e., no joints). Moreover, the impacts of aging of the pavement such as cracking, rutting, faulting etc., which mainly affect the pavement performance and roughness, are not taken into account. It is also important to note that the changes in fuel consumptions suggested by the model are conservative both for concrete and asphalt sections, and impacts of the aforementioned phenomena will increase changes in fuel consumption.

Chapter 7

Use in Life-Cycle Assessment Model

So far, the PVI deflection model and its relationship with fuel consumption have been established. The change in fuel consumption on a network level was calculated using the LTPP FWD data for the considered flexible and rigid sections and it was shown that on the network level, higher fuel consumption is expected for the flexible sections. This change in fuel consumption, even though small for one vehicle, has a major aggregated impact within the U.S. road network due to the extent of vehicle travel on the road network. In order to understand the impact of change in vehicle fuel consumption for a pavement section, the life-cycle assessment (LCA) framework is employed and the environmental impacts of the pavement and the change in fuel consumption of vehicles over the pavement life are investigated.

7.1 Life Cycle Assessment

Life-cycle assessment, also known as life-cycle analysis, is a method to assess environmental impacts, energy consumption, material use, etc. throughout the life-time of a product. LCA comprehensively quantifies and evaluates material and energy flows within a product from cradle to grave: raw material extraction, material processing, manufacturing, distribution, use, repair and maintenance, and disposal or recycling are the main phases that need to be included in a comprehensive LCA.

The impacts throughout the phases of the life-cycle are evaluated in order to draw conclusions and guide decision making. The International Organization for Standardization (ISO)

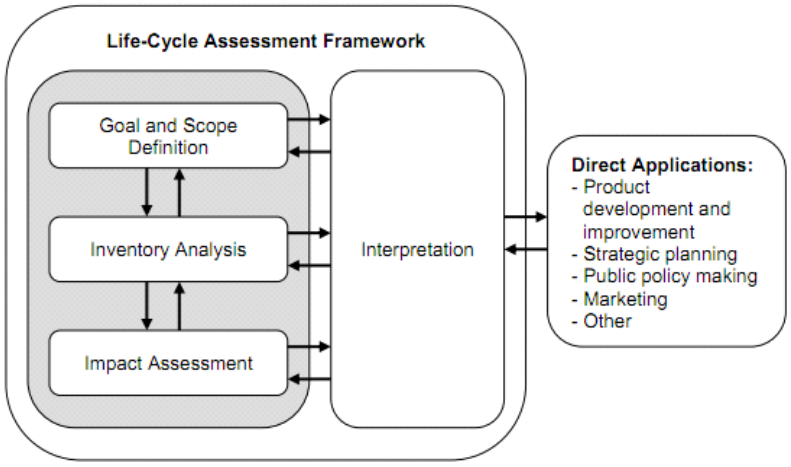

Figure 7-1: LCA framework, including the relationships among the assessment stages and the outcomes.

provides guidelines for the LCA framework under ISO-14040 and defines LCA with four major principles: goal and scope definition, inventory analysis, impact assessment, and interpretation. These principles are depicted in Figure 7-1, which shows the iterative process of life-cycle assessment.

The goal and scope definition entails determining the phases and processes that are included in the LCA study, and creating system boundaries. Then, material and energy flows for each process is collected through an inventory analysis of datasets and captured for the entire system. After processing the material and energy flow data, an impact assessment is performed, in which the influence of the product on the environment, people, the ecosystem, etc. is determined. A major impact category of LCAs is greenhouse gas (GHG) emissions which relate the environmental footprint of products to equivalent CO_2 emissions, denoted by CO_2e.

7.2 LCA of Pavements

A major hurdle in LCA studies is the lack of fundamental understanding of elements within each of the major phases. Since LCA practitioners are mainly consultants for products or companies, this fundamental understanding is lacking in many areas. Within the pavement LCA, the use-phase elements become highly challenging especially for a comparative LCA between asphalt

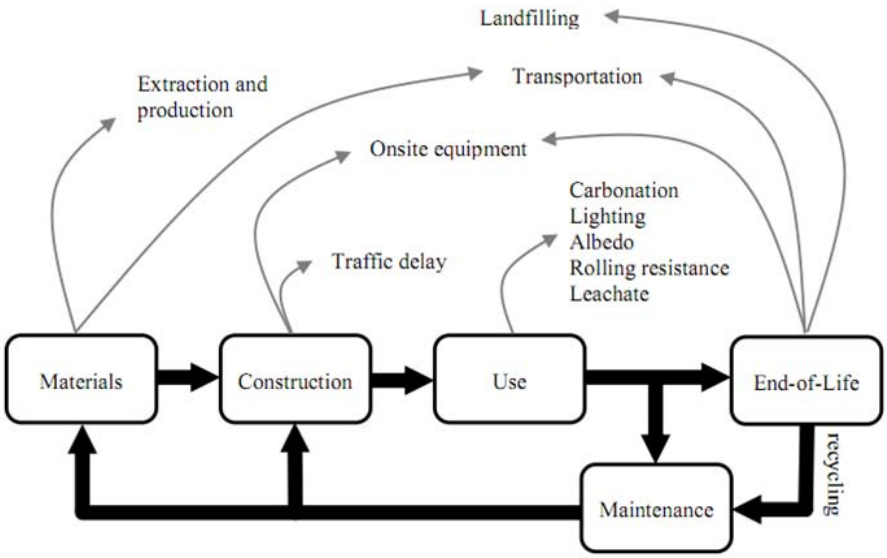

Figure 7-2: Suggested system boundaries (including life-cycle phases and components) for pavement LCA [39].

and concrete pavements. Figure 7-2 shows the main phases and processes that are necessary for a comprehensive life-cycle assessment of concrete pavements [39].

A clear example of a knowledge gap is the impact of PVI on fuel consumption of vehicles. Although existence of the impact of pavements on vehicle fuel consumption has been known for decades (see Section 2.3), the lack of a true understanding of this phenomenon has stopped the pavement LCA community from implementing this element within the use phase of pavements.

7.3 PVI within Life Cycle Assessment

Thus far, the impact of pavement deflection within PVI and its impact on fuel consumption have been established. In order to illustrate the importance of such changes on fuel consumption, LCA of two scenarios are presented in this section. Since a comprehensive LCA is outside the scope of this study, the environmental impact of change in fuel consumption due to PVI is compared to that of pavement production and maintenance throughout the pavement life-time.

Scenario Name (CBR 3)	GHG: Production+M&R (tons CO_2e)	Design Life (years)	Traffic Volume (AADT)	Functional Unit
High Vol. – Concrete	688	50	50,000	2 lane-km
High Vol. – Asphalt	738	50	50,000	2 lane-km
Arterial – Concrete	554	50	15,000	2 lane-km
Arterial - Asphalt	555	50	15,000	2 lane-km

Table 7.1: Main assumptions of the Athena study on GHG emissions and energy consumption of asphalt and concrete pavements [2].

7.3.1 Scenario Definition

The pavement scenarios considered are for high-volume and low-volume roadways, with an asphalt and a concrete pavement for each case. These scenarios are extracted from the Athena study of 2006 [3] where the pavement design life, structural designs, traffic scenarios, and the associated production, maintenance and rehabilitation (M&R) greenhouse gas (GHG) emissions are provided.

The Athena report on the GHG emissions and energy consumption of asphalt and concrete pavements presents their assumptions with high transparency. Table 7-1 summarizes the main assumptions and input parameters of the considered pavement designs. The scenarios used from the Athena study are that of the "Canadian High Volume Highway CBR 3" and the "Canadian Arterial Highway CBR 3", where CBR is the California Bearing Ratio (CBR) of the subgrade. Traffic volumes for the high volume and arterial roadways are 50,000 and 15,000 annual average daily traffic (AADT) respectively; both with 10% annual average daily truck traffic (AADTT). The functional units for both scenarios are two lane-kilometers with 50 year analysis periods.

As seen in Table 7-1, the GHG emissions associated with the asphalt and concrete section production, maintenance, and rehabilitation for both pavement classifications are almost identical. The authors of the Athena report did not consider any use phase elements, mainly the impacts of PVI, within their results. It is shown here that consideration of this phenomenon has significant influence on results and conclusions.

7.3.2 LCA Implementation

To illustrate the influence of PVI deflection and the resulting change in fuel consumption, the distributions of change in fuel consumption for passenger vehicles and trucks on asphalt

Fuel Type	GHG (kg CO_2e/liter)	GHG (lb CO_2e/gallon)
Passenger Car Gasoline	2.32	19.36
Truck Diesel	2.67	22.28

Table 7.2: GHG emissions associated with 1 liter (gallon) of fuel [39].

and concrete pavements are used from Figures 6-10 and 6-11. Table 7-2 shows the CO_2e emissions from 1 liter (gallon) of gasoline and diesel fuel, used to relate fuel consumption to GHG emissions.

Using the embodied GHG emissions from Table 7-1, the distribution of change in fuel consumption from Monte Carlo simulations (Figures 6-10 and 6-11), and the CO_2e factors for passenger car and truck fuel from Table 7-2, a partial LCA of the two pavement scenarios (high volume and low volume) is performed over a 50 years lifetime. According to the principle of ergodicity, a dynamic system such as the road Network has the same behavior averaged over time as averaged over space. Since the databases used to calculate the impact of deflection on fuel consumption represent various aging states within the Network, they also represent a pavement's condition throughout its lifetime.

In this analysis, the impact of deflection within PVI is reported at the 95% confidence bounds for each scenario. The bounds of the lognormal distribution are calculated using the inverse of the Fisher information matrix, which provides the variance of the parameter $Var(\mu)$. The confidence bounds on the parameters are then calculated by:

$$\text{Lower Bound} = \mu \exp\left[-(z_{\alpha/2}/\mu)\sqrt{Var(\mu)}\right] \tag{7.1}$$

$$\text{Upper Bound} = \mu \exp\left[(z_{\alpha/2}/\mu)\sqrt{Var(\mu)}\right] \tag{7.2}$$

where μ is the mean value of the parameter, $\alpha = 1 - C$, where C is the confidence level, and $z_{\alpha/2}$ is the inverse of the standard normal cumulative distribution for $\alpha/2$ [31].

Figure 7-3 shows the production, maintenance and rehabilitation values from Table 7-1 for both high volume and arterial roadways in blue; the impact of change in fuel consumption due to deflection (aggregated for trucks and cars) for the asphalt and concrete pavements are shown at 95% confidence intervals in red.

As expected, due to the multiplying factor of vehicle traffic, the impact of PVI is more

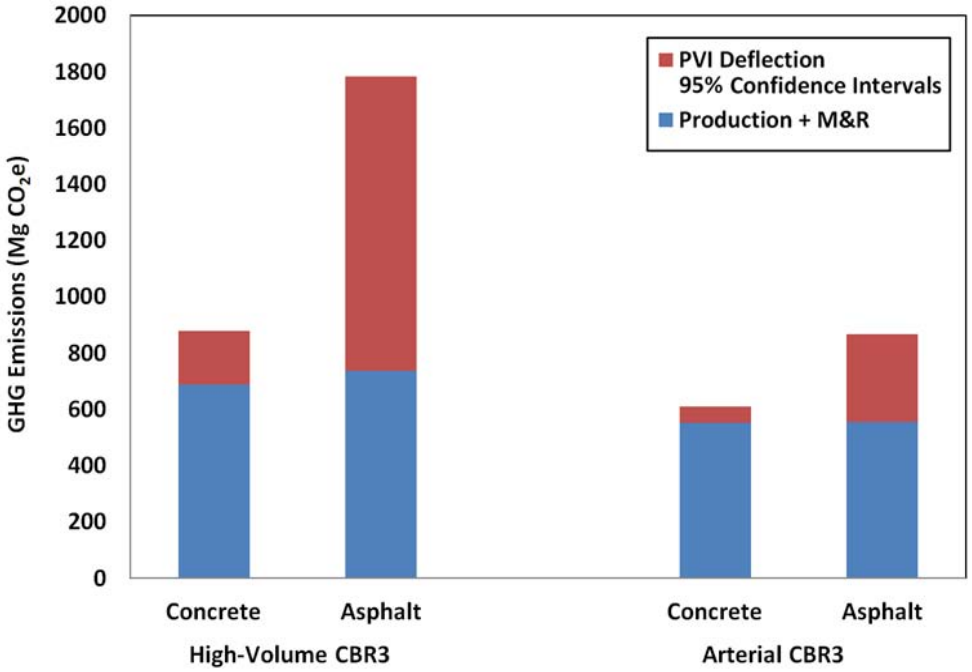

Figure 7-3: Use of model predicted values in an LCA. Production and M&R values are extracted from [3]. Impact of PVI deflection is shown for 50 years lifetime at the 95% confidence interval.

significant for the high-volume highway than for the low-volume arterial. It is observed from Figure 7-3 that in the case of the high-volume asphalt pavement, the impact of PVI-related emissions through the pavement lifetime can be equivalent to that of the embodied emissions.

It is useful to remember that pavement-vehicle interaction is due to two major components: pavement deflection and pavement roughness (Section 2.3). The focus of this work was on understanding the impact of pavement deflection on fuel consumption, and the effect of pavement roughness on fuel consumption was not considered.

It is necessary to note that the Athena study uses an annual average daily traffic (AADT) of 50,000 on the high-volume roadway for two-way traffic with two lanes in each direction. This traffic volume corresponds to values suggested in section 13.2.1 of the highway statistics manual [17] for the average AADT of 13,355 per lane on urban interstates. Hence, the high-volume scenario used in this section is not that of an extremely high volume highway and the impact of pavement vehicle interaction on highways with greater number of users (AADT per lane) would be further magnified.

7.4 Chapter Summary

This chapter briefly described the LCA framework, and discussed difficulties of conducting a comprehensive pavement life-cycle assessment. To understand the impact of pavement deflection within PVI, the distribution of change in fuel consumption, as calculated in Section 6.3, along with the impact factor of fuels were used to perform a LCA. The pavement embodied emissions, and design criteria were taken from the Athena study [3] for two high-volume and two low-volume sections. It was shown that in the case of high-volume roadways, the impact of PVI is much more significant so that it can surpass the embodied emissions from pavement construction, maintenance and rehabilitation. This phenomenon may still be magnified when adding IRI-related PVI, which have not been considered in this study.

Chapter 8

Conclusion

The accuracy and comprehensiveness of any pavement LCA is limited by the ability of the supporting science to quantify the environmental impacts. Pavement-vehicle interaction (PVI) represents a significant knowledge gap that has important implications for many pavement LCA studies. The development of the model, here proposed, provides insight into the importance of deflection-related PVI, and the parameters. It will ultimately help guide pavement design for reduction of vehicle emissions associated with pavement structural and material properties.

8.1 Main Findings

This study presents a first-order mechanistic model that rationalizes the impact of deflection on pavement-vehicle interactions. The model has been calibrated and validated against 5,643 falling weight deflectometer time histories, previously recorded by the FHWA's LTPP program. Statistical analysis of this data is used in Monte Carlo simulations to develop a relationship between vehicle weight q, material (top layer modulus E, subgrade modulus k), and structural parameters (thickness h) with deflection induced vehicle fuel consumption at the network level. This relationship provides realistic estimates of change in fuel consumption due to deflection when compared to previously-performed empirical studies.

It was shown that the scaling of input parameters is critical, as it provides a quantitative link between pavement design and its impact on pavement-vehicle interaction. Such relationships demonstrate the level of importance of each parameter on the final impact within a LCA, and

can guide pavement design for reduction of PVI related emissions.

The model provides a first-order estimate of the importance of various factors that affect vehicle fuel consumption. The impact of pavement deflection on fuel consumption is magnified within a LCA of a high-volume roadway, and can exceed the impacts from materials, construction, and maintenance phases of the pavement life-cycle. As such a model matures to include more aspects of PVI, it can be implemented into design procedures and tools such as the mechanistic-empirical pavement design guide (MEPDG) [29].

8.2 Current Limitations and Future Perspectives

The goal of this work has been to create a first-order understanding of the impact of deflection within pavement-vehicle interaction and the effect of structural and material properties on fuel consumption. Even though more accurate models and solution strategies for calculation of pavement deflection exist, a beam on an elastic damped foundation is used to create scaling relationships between structural and material properties of the pavement with changes in fuel consumption. This solution strategy proved to be sufficiently accurate for calculation of the change in fuel consumption and its order of magnitude.

In order to create a more refined understanding of the impact of pavement deflection on fuel consumption, more components can be added to the model to represent discontinuities, loading location, aging, temperature effects, refined damping model, and other phenomena that can affect the pavement response. Also, the calibration model can be improved by use of dynamic backcalculation procedures, and the pavement deflection model can be refined by including the impact of pavement sub-layers within the analysis. Moreover, the combined effects of roughness and unevenness of the pavement with deflection need to be accounted for in order to capture pavement-vehicle interaction and all its components within the model. This study has not included the impact of roughness in PVI within its scope. Addition of roughness induced fuel consumption to PVI will lead to a greater impact of this element within the pavement LCA.

Lastly, the new modeling approach to PVI defines a baseline for fuel consumption of pavement structures in function of the relevant material and geometrical design parameters. The accuracy of the model relates to the mechanical model assumptions, such as straight pave-

ment, neglecting of joints, aging, and other factors, thus warranting further validation through extensive field measurements, particular for pavements designed according to MEPDG.

Bibliography

[1] Achenbach, J.D., 1987. Wave Propagation in Elastic Solids. North Holland Pub. Co. The University of California.

[2] Ardekani, S. and Sumitsawan, P. 2009. Effect of Pavement Type on Fuel Consumption and Emissions in City Driving. 2010 Concrete Sustainability Conference. National Ready Mixed Concrete Association.

[3] Athena. 2006. A Life Cycle Perspective on Concrete and Asphalt Roadways: Embodied Primary Energy and Global Warming Potential. Ottawa, Ontario: Athena Institute.

[4] Bennett, C. R., Greenwood, I. D. 2003. Modeling Road User and Environmental Effects in HDM-4. Version 3.0. International Study of Highway Development and Management Tools (ISOHDM), World Road Association (PIARC), Cedex, France.

[5] Beskou, N. D., and Theodorakopoulos, D. 2010. Dynamic Effects of Moving Loads on Road Pavements: A Review. Soil Dynamics and Earthquake Engineering: 547-567.

[6] Boriboonsomsin, K., and Barth, M. 2009. Impacts of Road Grade on Fuel Consumption and Carbon Dioxide Emissions Evidenced by Use of Advanced Navigation Systems. Journal of the Transportation Research Board. Transportation Research Record: 21-30.

[7] Buckingham, E. 1914. On physically Similar Systems; illustrations of the Use of Dimensional Equations. Physical Review 4(4):345376.

[8] Chatti K., Lei L. 2012. “Forward Calculation of Subgrade Modulus Using Falling Weight Deflectometer Time Histories and Wave Propagation Theory". GeoCongress 2012: State of the Art and Practice in Geotechnical Engineering.

[9] Daehyeon K, Rodrigo S., Altschaeffl A. 2005. Effects of Supersingle Tire Loadings on Pavements. Journal of Transportation Engineering. ASCE.

[10] De Graaff. 1999. Dutch report: Rolling resistance of Porous Asphalt - a pilotstudy. The Netherlands: Report nr. M+P.MVM.97.2.1 rev. 2 M+P, 1999.

[11] Descornet, G. 1990. Road-Surface Influence and Tire Rolling Resistance, in Surface Characteristics of Roadways. International Research and Technologies, 401-415.

[12] Du Plessis, H. W. 1990. Fuel Consumption of Vehicles as Affected by Road Surface Characteristics. Surface Characteristics of Roadways: International Research and Technologies, 480-496.

[13] Edil, T., Benson, C., Bin-Shafique1, M., Tanyu1, B.,Kim, W., Senol, A. 2002. Field Evaluation of Construction Alternatives for Roadways over Soft Subgrade. Transportation Research Record: Journal of the Transportation Research Board. Volume 1786. 36-48.

[14] Enegefoto testing device. 2011. Web address: "http://www.engefoto.com.br/content/ upload/conteudo/image/Transp_Aval_3.jpg"

[15] EPA. 2009. 2009 U.S. Greenhouse Gas Inventory Report. Environmental Protection Agency. [Online] Available at: http://www.epa.gov/climatechange/emissions/downloads09/GHG2007entire_report-508.pdf [Accessed February 2010].

[16] FHWA, H. F. 2004. Significant Findings from Full-Scale Accelerated Pavement Testing. National Cooperative Highway Research Program and Transportation Research Board.

[17] FHWA. 2008. Highway Statistics 2008. [Online] Availalble at: http://www.fhwa.dot.gov/policyinformation/statistics/2008/ [Accessed July 2011].

[18] FHWA. 2011. INVEST: Infrastructure Voluntary Evaluation Sustainability Tool. Federal Highway Administration. [Online] Available at: https://www.sustainablehighways.org/ [Accessed July 2011].

[19] Goodyear. 2011. Fuel Economy Information. [Online] Available at: http://www.goodyeartrucktires.com/resources/factors-fuel-economy.aspx [Accessed January 2011].

[20] Greenroads. 2011. The Greenroads Rating System. [Online] Available at: http://www.greenroads.us/ [Accessed July 2011].

[21] Greenwood, I. Riaz Ul-Islam, 2007. Opus International Consultants, Review of the Adequacy of Current Pavement Information.

[22] G.W. Taylor Consulting. 2002. Additional Analysis of the Effect of Pavement Structure on Truck Fuel Consumption. Ottawa: Cement Association of Canada.

[23] Holtz, K., & Eighmy, T. T. 2000. Scanning European Advances in the Use of Recycled Materials in Highway Construction. Public Roads.

[24] Kim, S.-M. and Roesset, J.M. 2003. Dynamic response of a beam on a frequency independent damped elastic foundation to moving load. Canadian Journal of Civil Engineering. 30(2) 460–467.

[25] Laganier, R., & Lucas. 1990. The Influence of Pavement Evenness and Macrotexture on Fuel Consumption, in Surface Characteristics of Roadways. International Research and Technologies, 454-459.

[26] Lenngren, C.A., and Faldner, L. 2011. Fuel Cost Consideration Regarding Truck Rolling Resistance on Different Pavement Types. Swedish Road and Transport Research Institute, VTI.

[27] Long-Term Pavement Performance program. 2003. Information Management System Pavement Performance. Database User Reference Guide. U.S. Department of Transportation, Federal Highway Administration.

[28] Long-Term Pavement Performance program. 2011. [Online] Available at: http://www.fhwa.dot.gov/research/tfhrc/programs/infrastructure/pavements/ltpp/ [Accessed 2011].

[29] MEPDG. 2011. Mechanistic-Emripical Pavement Design Guide. [Online] Available at: www.trb.org/mepdg [Accessed 2011].

[30] NPC. 2002. VEROAD® Calculations. Maximum energy dissipation when driving on asphalt pavement versus driving on rigid cement concrete. Netherlands: Netherlands Pavement Consultants.

[31] O'Connor, P.D.T., Kleyner, A. 2012. Practical Reliability Engineering. John Wiley & Sons, Ltd.

[32] Office of Infrastructure, R&D. 2000. Long-Term Pavement Performance Team, Manual for Falling Weight Deflectometer Measurements. Operational Field Guidelines.

[33] Park, S., Rakha, H. 2005. "Energy and Environmental Impacts of Roadway Grades." Transportation Research Board 06-0628.

[34] RMA. 2010. Rubber Manufacturers Association. [Online] Available at: http://www.rma.org/ [Accessed July 2010].

[35] Roesset J. M. Kenneth H. Stokoe II, and Chia-Ray Seng. 1995. "Determination of depth to bedrock from Falling weight Deflectometer Test Data" Transportation Research Record 1504, pp. 68-78.

[36] Salt, G., Stevens, D., and McLeod, R. 2002. Pavement Structural Evaluation: Production Level FWD Back-Analysis Using the Full Time History. Proceedings of the 6th International Conference on the Bearing Capacity of Roads and Airfields, Portugal.

[37] Sandberg. 1990. Road Macro- and Megatexture Influence on Fuel Consumption. Surface Characteristics of Roadways: International Research and Technologies, 460-479.

[38] Santero, N. and Horvath, A. 2009. Global Warming Potential of Pavements. Environmental Research Letters. 4(3). 034011.

[39] Santero, N., Masanet, E. and Horvath, A. 2011. Life-cycle assessment of pavements. Part I: Critical review. Resources, Conservation, and Recycling. 55(9–10): 801–809.

[40] Sayers, M.W. 1990. Profiles of Roughness. Transportation Research Record 1260, Transportation Research Board, National Research Council, Washington, D.C.

[41] Sun, L. and Deng, X. 1998. Dynamic analysis of infinite beam under the excitation of moving line loads. Applied Mathematics and Mechanics, Vol. 19, No.4, 1998, 367-373.

[42] Sun, L. 2001. A Closed-Form Solution of a Bernoulli-Euler Beam on a Viscoelastic Foundation Under Harmonic Line Loads. Sound and Vibration. 242(4): 619–627.

[43] Sun, L. 2001. Dynamic response of beam-type structures to moving line loads. International Journal of Solids and Structures, Vol. 38, No. 48-49, 2001, 8869-8878.

[44] Sun, L. and Luo, F. 2008. Steady-state dynamic response of a Bernoulli-Euler beam on a viscoelastic foundation subject to a platoon of moving dynamic loads. Journal of Vibration and Acoustics, ASME, Vol. 130, No. 5.

[45] Taylor, G. W., Marsh, P, and Oxelgren. 2000. Effect of Pavement Surface Type on Fuel Consumption: Seasonal Tests. Portland Cement Association.

[46] Taylor, G. W., Patten, J. D. 2006. Effects of Pavement Structure on Vehicle Fuel Consumption - Phase III. Ontario: NRC-CNRC.

[47] U.N. Florida, J. N. 2004. An Evaluation of the Relationship Between Fuel Consumption and Pavement Roughness. Jacksonville, FL: Universtiy of North Florida.

[48] US DOT. 2008. Transportation Statistics Annual Report. Washington, DC: United States Department of Transportation.

[49] Von Quintus, H., Simpson, A. 2002. Back-Calculation of Layer Parameters for LTPP Test Sections, Volume II: Layered Elastic Analysis for Flexible and Rigid Pavements. FHWA Report No. FHWA-RD-01-113.

[50] Yoshimoto, T., Kazato, T., and Hayakawa, I. 2010. Effect of Pavement Type on Rolling Resistance and Fuel Consumption of Heavy-Duty Vehicles. Japan Cement Association. Nippon Expressway Research Co. Ltd. Narita International Airport Co. Ltd.

[51] Zaabar, I., Chatti, K. 2010. "Calibration of HDM-4 Models for Estimating the Effect of Pavement Roughness on Fuel Consumption for U.S. Conditions." Transportation Research Record: Journal of the Transportation Research Board: 105-116.

[52] Zabaar, I. 2010. Effect of Pavement Conditions on Vehicle Operating Costs Including Fuel Consumption, Vehicle Durability, and Damage to Transported Goods. Ph.D. Dissertation. Michigan State University.

[53] Zaniewski, J. P., Butler, B. C., Cunningham, G. E., Elkins, G. E., Paggi, M. S.k, and Machemehl., R. 1982. Vehicle Operating Costs, Fuel Consumption, and Pavement Type and Condition Factors. Washington D.C.: U.S. Department of Transportation, Federal Highway Administration.